Manuscript Details

Manuscript number	DYPI_2017_1059_R2
Title	New series of non-toxic DNA intercalators, mitochondria targeting fluorescent dyes
Article type	Research paper

Abstract

Five novel benzoxazolium and benzothiazolium derived asymmetric dicationic monomethine cyanine dyes, bearing a thioester group have been synthesised via condensation of quaternary nitrogen containing heterocyclic salts in various anhydrides. Their chemical structures were evaluated by NMR, ESI/MS, IR spectroscopy, and melting point temperatures. Photophysical studies on the title compounds were performed in methanol solutions. The longest wavelength absorption maxima λmax of the studied dyes are in the region 453-508 nm. The corresponding fluorescence maxima λfl were registered within the 489-553 nm. Further spectroscopy and calorimetric techniques including circular dichroism (CD), UV-Vis, fluorescence, thermal denaturation and isothermal titration calorimetry have been applied to the studied dyes in the presence of biopolymers, in order to evaluate their staining ability as fluorescent markers. In aqueous solution the compounds exhibit no intrinsic fluorescence, however upon binding to dsDNA and dsRNA they show considerable enhancement of fluorescence intensity. Binding constants Ks of the complexes [dye–polynucleotide] have been evaluated from fluorescence spectral titrations. Although the intercalation is the predominant binding mode, the compounds show little or no effect on the cell proliferation. Upon fast cell internalization the compounds accumulate in the mitochondrial space.

Keywords	monomethine cyanine dyes; DNA/RNA; circular dichroism; binding parameters; mitochondria; isothermal titration calorimetry

Corresponding Author	Ivo Crnolatac
Corresponding Author's Institution	RBI
Order of Authors	Iva Orehovec, Atanas Kurutos, Ana Tomašić Paić, Ivo Crnolatac, Lucija Horvat, Nikolai Gadjev, ivo Piantanida, Todor Deligeorgiev
Suggested reviewers	Hans-Jorg Schneider, Enrique García-España, Marijana Hranjec

Submission Files Included in this PDF

File Name [File Type]

Cover D&P revision.doc [Cover Letter]

comments final.docx [Response to Reviewers]

Highlights.docx [Highlights]

graph abs.tif [Graphical Abstract]

rev Final D&P no synthesis.docx [Manuscript File]

Supp Info-with synt.doc [e-Component]

To view all the submission files, including those not included in the PDF, click on the manuscript title on your EVISE Homepage, then click 'Download zip file'.

Dear Editor,

Please find enclosed revised manuscript entitled "**New series of non-toxic DNA intercalators, mitochondria targeting fluorescent dyes**", written by Atanas Kurutos[α], Iva Orehovec[α], Ana Tomašić Paić, Ivo Crnolatac[*], Lucija Horvat, Nikolai Gadjev, Ivo Piantanida[*] and Todor Deligeorgiev, which I am submitting for a publication as a research article in Dyes and Pigments**.** Please note that we have included one co-author (Lucija Horvat).

One of the comments of the reviewer 3 was to move the whole synthesis part in the supporting information. This was done, but I would rather await your decision on the matter, taking into consideration the scope and targeted readers of Dyes and Pigments.

Kindest regards,

Ivo Crnolatac

Laboratory for Study of Interactions of Biomacromolecules
Division of Organic Chemistry and Biochemistry
Ruđer Bošković Institute
Bijenička 54, 10000 Zagreb, Croatia
Fax: +385 1 46 80 195
E-mail: icrnolat@irb.hr

Reviewer 1

1. In Table 3, “binding ratios n indicated ([bound compound]/ [polynucleotide])”, it seems incorrect. The n should indicate ([bound compound]/ [nucleotide]). The same question in “r = [dye] / [polynucleotide]”, “r[dye]/[DNA] < 0.3 ” etc.

corrected

2. Figure 4, the name of Y axis is missed.

corrected

3. Line1095 Error! Reference source not found.

corrected

4.Do these compounds bind nucleic acids in mitochondria? Why the fluorescence light up in mitochondria?

Since they exhibit fluorescence they are bound to something, most probably DNA, but we do not know for sure, we also do not know whether they enter into mitochondria or stay bound to the inner mitochondrial membrane.

Reviewer 2

In this paper, series novel benzoxazolium and benzothiazolium derived asymmetric dicationic monomethine cyanine dyes, bearing a thioester group were synthesised and well characterized, and their staining ability as fluorescent markers were well studied.

1. The cyanine dyes with “the bulky substituents on the long arm” were designed and synthesized to “limits the damage envoked by the interaction with DNA/RNA”. However, the author didn’t discuss the effect of bulky substituents in details.

This is from our experience, the reference is added where such conclusion has been put forward.

2. The authors mentioned that fluorimetric response of the dye/polynucleotide complexes is strongly dependent on the dye structure. But they didn’t explain the reason. Is it possible to explain the phenomenon from the structures of dyes and polynucleotide complexes?

Due to the quite complex pattern of physical events involved in fluorescence increase upon binding to DNA, the microenvironment of the dye, geometry of the binding pocket, existence of the fluorescence quenching water molecules in the binding pockets, the strength of the emission increase could not be directly correlated to binding affinity.

3. In addition, there are some spelling errors, and format is not uniform in some places, which need to be revised.

Spell check, format check done, hopefully it is OK now

This paper can be accepted after minor revision.

Reviewer 3

Th authors present interesting results. But there is requirement of a major revision.

1. All synthetic portion should be removed from the main text and put as electronic supplementary material.

Done, but we would like to have the final decision by the editor, taking into the consideration the scope and targeted audience of D&P

2. The motivation behind this work is to be mentioned clearly in the introduction.

Mentioned clearly in the introduction: There are numerous mitochondrial dyes and mitochondrial membrane potential probes available on the market, however they all exhibit serious drawbacks related to their use in vitro/in cellulo. Respiration inhibition, inhibition of mitochondrial ATPase, general cytotoxicity, photobleaching and sensitivity issues are problems which are reported [4],[5],[6]. Inspired by our previously reported specific mitochondrial fluorescent probes [7],[8], we prepared novel cyanine dyes, lipophilic di-cations which should: a) Have affinity towards DNA/RNA; b) Have limited or no effect on cell proliferation; c) Aim the mitochondria.

3. There is no equilibrium in the binding. The reason is not clear

Added in the text: Thermodynamic equilibrium is reached within a minute of polynucleotide addition to dye and 2-3 min incubation time was maintained through all the experiments.

4. The binding affinity values must be presented as "K"in M-1 and not as log K. How was this estimated and what are the errors?

K corrected

Previous data was replaced by K values obtained from ITC experiments, with the errors fot the fit presented.

5.A titration calorimetric study would have provided direct K and also the thermodynamic values?

Done

6. The thermodynamic parameters including K should be presented in italics throughout.

corrected

7. The differences in the CD change for DNAs and that of the induced CD of the dyes in the presence of the DNAs needs detailed interpretation and elaboration.

done

8. Does the concentration used in the studies here lead to aggregation? How was it verified.

Chosen concentration range was checked for linear dependence of the absorption vs concentration (supp. Info). Aggregation would lead to non-linearity.

9. What is the difference in selectivity for DNA and RNA for these dyes. Please slaborae

Elaborated in the text: The particular reason for intriguing DNA vs. RNA ICD band selectivity at low ratios r>0.2 could be attributed to particular property of RNA major groove, which being deep and narrow (width 3.8A, depth 13.5A) allows better accommodation of dye aggregates in comparison to DNA minor groove (width 5.7A, depth 7.5A). Because of this, ***A1-7*** *dyes prefer to intercalate into DNA, while in ds-RNA there is competitive aggregation taking place.*

Highlights

- 5 novel benzoxazolium and benzothiazolium derived dicationic monomethine cyanine dyes
- Interaction with DNA/RNA: Intercalation with dsDNA; groove binding with dsRNA
- No antiproliferative activity on cell cultures
- Fluorescence emission in the mitochondrial space upon cellular uptake

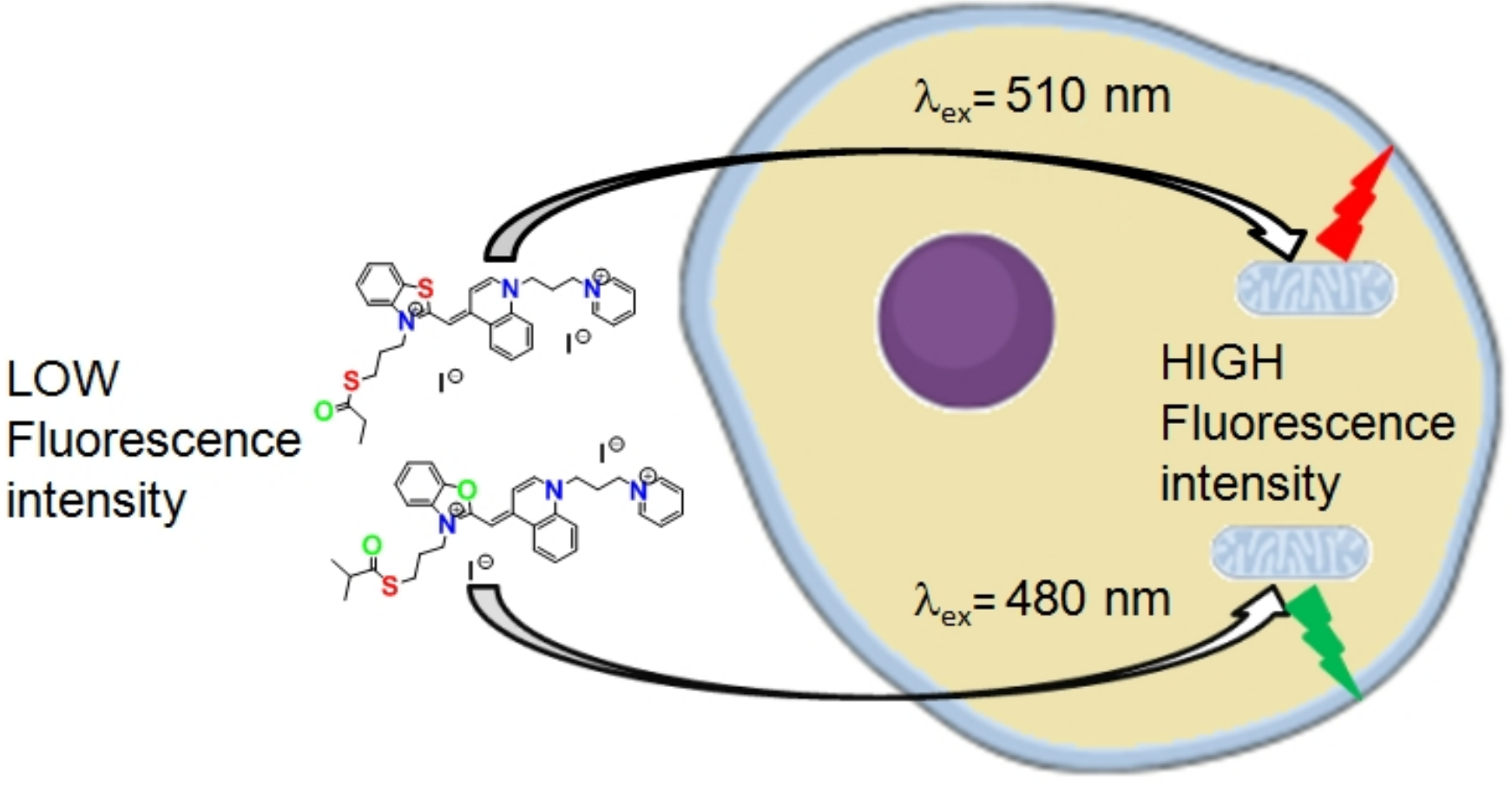
LOW
Fluorescence
intensity
λex= 510 nm
HIGH
Fluorescence
intensity
λex= 480 nm

New series of non-toxic DNA intercalators, mitochondria targeting fluorescent dyes

Atanas Kurutos[a, b†], Iva Orehovec[c†], Ana Tomašić Paić[c], Ivo Crnolatac[c*], Lucija Horvat[d], Nikolai Gadjev[b], Ivo Piantanida[c*], Todor Deligeorgiev[b]

[a] *Institute of Organic Chemistry with Centre of Phytochemistry, Bulgarian Academy of Sciences, Acad. G. Bonchev str., bl. 9, 1113 Sofia, Bulgaria*

[b] *Department of Pharmaceutical and Applied Organic Chemistry, Faculty of Chemistry, University of Sofia, 1164 Sofia, Bulgaria*

[c] *Laboratory for Biomolecular Interactions and Spectroscopy, Division of Organic Chemistry and Biochemistry, Ruđer Bošković Institute, Bijenička c. 54, 10000 Zagreb, Croatia*

[d] *Laboratory for Molecular Plant Biology and Biotechnology, Division of Molecular Biology, Ruđer Bošković Institute, Bijenička c. 54, 10000 Zagreb, Croatia*

[*]**corresponding author:**

E-mail: icrnolat@irb.hr**;** tel: +38514571326; fax: +38514680195

E-mail: pianta@irb.hr**;** tel**:** +38514571326; fax: +38514680195

[†] Authors share equal contribution to the first position.

Abstract: Five novel benzoxazolium and benzothiazolium derived asymmetric dicationic monomethine cyanine dyes, bearing a thioester group have been synthesised via condensation of quaternary nitrogen containing heterocyclic salts in various anhydrides. Their chemical structures were evaluated by NMR, ESI/MS, IR spectroscopy, and melting point temperatures. Photophysical studies on the title compounds were performed in methanol solutions. The longest wavelength absorption maxima λ_{max} of the studied dyes are in the region 453-508 nm. The corresponding fluorescence maxima λ_{fl} were registered within the 489-553 nm. Further spectroscopy and calorimetric techniques including circular dichroism (CD), UV-Vis, fluorescence, thermal denaturation and isothermal titration calorimetry have been applied to the studied dyes in the presence of biopolymers, in order to evaluate their staining ability as fluorescent markers. In aqueous solution the compounds exhibit no intrinsic fluorescence, however upon binding to dsDNA and dsRNA they show considerable enhancement of

fluorescence intensity. Binding constants *Ks* of the complexes [dye–polynucleotide] have been evaluated from fluorescence spectral titrations. Although the intercalation is the predominant binding mode, the compounds show little or no effect on the cell proliferation. Upon fast cell internalization the compounds accumulate in the mitochondrial space.

Keywords: monomethine cyanine dyes; DNA/RNA; ITC; circular dichroism; binding parameters; mitochondria

Highlights: DNA intercalators, mitochondria markers, non-toxic

1. Introduction

Within the last two decades design of small molecules that are able to recognize DNA/RNA by non-covalent interaction often combines two or more non-covalent binding modes (intercalation, groove binding, or electrostatic sugar-phosphate backbone binding) [1],[2]. Such dyes selectively report on structural differences of DNA and RNA secondary structure. Furthermore their subcellular positioning and fate can be in that way manipulated. Lipophilic di-cations usually target mitochondria, namely the mitochondrial matrix space due to the permeability of the outer mitochondrial membrane and the inner mitochondrial membrane potential $\Delta\psi_{mito}$. After passing the plasma membrane, where this potential is not so prominent ($\Delta\psi_{cell}$ = 30-60 mV), accumulation in the mitochondrial matrix is enabled by the driving force of $\Delta\psi_{mito}$ = 150-180 mV [3]. Although the cationic charge increases affinity for the mitochondrial matrix, it should be dispersed over a large surface area to enable easier passage through the phospolipid bilayers. There are numerous mitochondrial dyes and mitochondrial membrane potential probes available on the market, however they all exhibit serious drawbacks related to their use *in vitro/in cellulo.* Respiration inhibition, inhibition of mitochondrial ATPase, general cytotoxicity, photobleaching and sensitivity issues are problems which are described [4],[5],[6]. Inspired by our previously reported specific mitochondrial fluorescent probes [7],[8], we prepared novel cyanine dyes, lipophilic di-cations which should: a) Have affinity towards DNA/RNA; b) Have limited or no effect on cell proliferation; c) Aim the mitochondria.

The probes are benzothiazole and benzooxazole based cyanine dyes carrying additional mitochondria targeting cationic charge. Previously, we used triphenylphosphonium cation which targets mitochondria *in vitro* and *in vivo* [9, 10], this series of compounds bear pyridinium ion,

also known to facilitate mitochondrial uptake [11]. To avoid problems related to general cytotoxicity and anti proliferative activity we attached the bulky substituents on the long arm of the cyanine dyes, which by our experience limits the damage caused by the interaction with DNA/RNA [12].

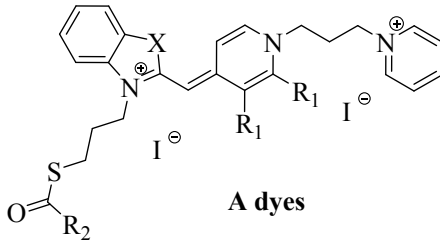

A dyes

Dye	X	R_1	R_2
A1	O	-CH=CH-CH=CH-	$-(CH_3)_2CH$
A2	S	H	$-CH_3$
A3	S	H	$-(CH_3)_2CH$
A4	S	-CH=CH-CH=CH-	$-C_2H_5$
A7	O	-CH=CH-CH=CH-	$-C_5H_{11}$

Figure 1 Studied compounds **A1-7**.

2. Materials and methods

2.1 Study of DNA/RNA interactions

2.1.1 UV/Visible Spectrophotometry, circular dichroism (CD) and fluorescence spectroscopy

The UV/Vis spectra were recorded on a Varian Cary 100 Bio spectrophotometer, fluorescence spectra on a Varian Cary Eclipse fluorescence spectrophotometer and CD spectra were collected with a Jasco J-810 spectropolarimeter at 25°C using 1 cm path quartz cuvettes.

The polynucleotides: $p(dAdT)_2$, $p(dGdC)_2$, pApU, and *calf thymus* (*ct*)-DNA (Sigma-Aldrich, St.Louis, USA) were dissolved in sodium cacodylate buffer, I = 0.05 mol dm^{-3}, pH=7, calf thymus (*ct*-) DNA was additionally sonicated and filtered through a 0.45 μm filter. Aqueous solutions of compounds were buffered to pH=7 (sodium cacodylate buffer, I = 0.05 mol×dm^{-3}). The polynucleotide concentration was determined as the concentration of phosphates by UV absorption [13]. Spectrophotometric and titrations were performed at pH = 7.0 (sodium cacodylate buffer, I = 0.05 mol dm^{-3}) by adding portions of polynucleotide solution into the solution of the studied compound. Thermodynamic equilibrium is reached within a minute of polynucleotide addition to dye and 2-3 min incubation time was maintained through all the experiments.

In fluorescence spectroscopy experiments the excitation wavelength above 450 nm (λ_{exc} > 450 nm) was used to avoid the possible inner filter effect caused by increasing absorbance of the

polynucleotide. The emission spectra were collected in the range λ_{em}= 460 – 650 nm. The CD experiments were performed by adding aliquots of the aqueous solutions of compounds into the buffered solution of polynucleotide.

2.1.2 Thermal denaturation experiments

Thermal melting curves for $p(dAdT)_2$, pApU and ct-DNA and their complexes with studied compounds were determined by following the change in the absorption at 260 nm as a function of temperature. The absorbance of the ligands was subtracted from each curve and the absorbance scale was normalized. *T*m values are the midpoints of the transition curves, determined from the maximum of the first derivative and checked graphically by the tangent method. The Δ*T*m values were calculated subtracting *T*m of the free nucleic acid from *T*m of the complex. The Δ*T*m values (with the instrumental error ± 0.5 °C) reported are the average of at least duplicate measurements.

2.1.3 Isothermal titration calorimetry (ITC)

Titrations were performed on MicroCal VP-ITC (Malvern, UK), the polynucleotide solutions (ctDNA, $p(dAdT)_2$, $p(dGdC)_2$ prepared as in Section 2.1.1. Origin 7.5 software, supplied by the manufacturer was used for data analysis. Due to multifaceted binding interactions of all the compounds with pApU, the fitting procedure did not yield satisfactory results and those were omitted. The reference cell was filled with ultrapure water. In the experiments, one aliquot of 2 μL five aliquots of 5 μL and 24 aliquots of 10 μL of the compound **A1**, **A2**, **A3**, **A4** or **A7** were injected from a rotating syringe (220 rpm) into the isothermal cell, equilibrated at 25.0 °C, containing 1.4406 mL of the polynucleotide (C= 20 □ 30 × 10^{-6}mol dm^{-3}).

The spacing between each injection was in the range 240–300 s. The initial delay before the first injection was 2000 s in all experiments. All solutions used in ITC experiments were degassed prior to use under vacuum (0.64 bar, 10 min) to eliminate air bubbles.

Microcalorimetric experiment, after fitting procedure, using built in Origin 7.5 software and one set of sites mode, directly gave three parameters: reaction enthalpy change (*ΔH*), binding constant (K_s) and stoichiometry (N). The value of *ΔG* was calculated from the binding constant ($\Delta G = -RT \ln K_s$) and the reaction entropy change was calculated from the binding enthalpy and Gibbs energy ($\Delta S = (\Delta H - \Delta G)/T$).

2.2 Biological assays

2.2.1 Subculturing of cells

Adherent cell lines (**MCF-7**, **H460**, **HEK293** and **HeLa**) growing as monolayers on the surface of T-25 flasks (Sigma) were used. Dulbecco's Modified Eagle's medium (DMEM) (Sigma-Aldrich) containing amino acids and vitamins, as well as additional supplementary components were used for cell growth. The primary cell culture media spent was removed and discarded from the culture flask. Cells were rinsed with 5 ml of the pre-warmed phosphate-buffered saline (PBS) to remove protease inhibitors, and 0.1% trypsin solution to detach the cells from the substrate. Flask was further placed back in an incubator at 37ºC. The progress of the enzyme treatment was checked with an inverted phase contrast microscope. As the cells have rounded up and detach from the surface, 5 ml of growth medium was added to the cell suspension and cells were vigorously washed. Suspended cells were further centrifuged (100xg for 5 minutes) and trypsin containing medium was replaced with the fresh one. Cells were counted using Neubauer chamber under inverted phase contrast microscope. Considering the required dilutions, the amount of the cells in fresh medium was transferred to new flasks.

2.2.2 Anti-proliferative activity evaluation by MTT assay

This test was performed with MCF-7 and H460 cells. Tested compounds, (AK-A1, AK-A2, AK-A3, AK-A4 and AK-A7) were prepared as stock solutions (4 x 10^{-2}M moldm^{-3}) in dimethylsulfoxide (DMSO), and working solutions (10^{-4}-10^{-8} moldm^{-3}) were prepared in DMEM medium accordingly. Cells were seeded in a 96 micro well flat bottom plates at the concentration 1 x 10^4 cells/l and incubated overnight allowing them to attach to the plate surface. 72 h after incubation with tested compounds, growth medium was discarded and 5 mgml^{-1} of MTT was added. After 4h incubation at 37°C water insoluble MTT-formazan crystals were dissolved in DMSO. Absorbance was measured at 570 nm on a microplate reader (Multiskan EX, ThermoFisher Scientific). Control cells were grown under the same conditions. The experiments were performed in tetraplicates. The IC_{50} value, defined as compound concentration leading to cellular viability reduction by 50%, was calculated and used as a comparison parameter.

2.2.3 Flow cytometry analysis of the **A1-7** dyes cell accumulation kinetics

The cells ($1x10^6$/ml) were incubated in 1 ml culture medium containing respective dyes for indicated amount of time in the dark at 37°C. Flow cytometry was carried out on a Becton Dickinson FACSCalibur model equipped with a 488 nm Argon laser and a 635 nm red diode laser. The collected data was analysed using BD CellQuest or FlowJo software version 7.2.5 for Microsoft (TreeStar, San Carlos, CA, USA). The cells were gated and discriminated from background based on light scattering properties and PI exclusion.

2.2.4 Transient transfection of **HeLa** cells with *pECFP*-Mito vector

pECFP-Mito vector is designed for fluorescent labelling of mitochondria in living cells and for co-localization experiments. Expression vector encodes monomeric enhanced cyan fluorescent protein (ECFP) fused to mitochondrial leader sequence (ECFP-Mito) derived from the subunit VIII of human cytochrome C oxidase. The resulting CFP has an absorption maximum at 458 nm and emits cyan fluorescence centred at 480 nm. Vector pECFP-Mito was purified from *E. coli* with Plasmid Midi Kit (Promega) according to manufacturer's protocol and stored at -20ºC in water. pECFP-Mito vector was transiently transfected into the mammalian HeLa cells and the signal was received 24 hours after transfection. A *pECFP*-Mito vector containing CFP gene was provided by Dr. Oliver Vugrek (Ruđer Bošković Institute, Zagreb, Croatia). For each transfection with Lipofectamine 2000, 8 x 10^4 cells/ml were distributed in glass bottom petri dish moulds (35 mm dish with 20 mm bottom well, In Vitro Scientific, USA) and incubated for 16-24 h in 5% CO_2 at 37°C. Transfections were performed according to manufacturer′s instructions with 7,5 μl lipofectamine 2000 and 3 μg of *pECFP*-Mito vector. Reagent/DNA was incubated within the cells for minimum 24 h at 37°C, and the wells were then washed and replenished with fresh DMEM medium.

2.2.5 Confocal Laser Scanning Microscopy (CLSM)

Leica SP8X FLIM was used for complex fluorescence experiments in live-cell imaging. The images were processed in LAS X Leica Microsystems and ImageJ (Wayne Rasband, NIH, USA) software packages.

2.2.6 Colocalization study

ImageJ was used for colocalization studies to obtain the Pearson correlation coefficients (PCC) (JACoP plugin for ImageJ) based on pixel-by-pixel summation of the products of the intensities

of two fluorophores [14]. To correct for noise we use the replicate based noise corrected correlation (RBNCC), as suggested by Adler et. al. [15]. Both PCC and RBNCC are explained in more detailed way in supporting info.

3. Results and discussion

3.1 Synthesis and structural analysis of AK-A dyes.

A series of unsymmetrical dicationic cyanine dyes were obtained via condensation reaction of equimolar amounts of N-quaternary benzazolium salts and various quinolinium or pyridinium derivatives possessing a methyl group (Supp info). The 1-(3-bromopropyl)pyridin-1-ium bromide **2**, which was used as a building block for the dicationic chromophores **4a** and **4b**, was obtained in 91% yield via mono N-quarterisation of the pyridine, using a 5-fold excess of 1,3-dibromopropane. This synthetic approach was used in order to avoid the formation of bis-N-quaternary side product, which is typically formed when using lower ratios. The N-quaternary benzothiazolium derivatives **6a** and **6b** were isolated in high yields by a cyclization of 2-thiomethyl benzothiazole / 2-thiomethyl benzoxazole and an excess of 1,3-dibromopropane in a solvent free reaction. For the final synthetic step, where the condensation of the two chromophores **4** and **6** takes place, N-Ethyldiisopropylamine was used as a basic reagent. The reaction was carried out using several different anhydrites which contributed to the formation of thioesters. With respect to the reaction duration in this final step, only 15 minutes of reflux followed by stirring for further 5 hours at room temperature, were required for the formation of the target **A1-7** dyes. In order to exchange the anion, the dyes were dissolved in methanol and precipitated in an aqueous solution of potassium iodide. The cyanines were isolated with moderate to high yields. The chemical structures of the target products, were elucidated by ^{1}H NMR, ^{13}C NMR, APT NMR spectroscopy, ESI mass spectrometry, IR spectroscopy and melting point temperatures (Supp info). The synthetic strategy was focused on the variation of both the aliphatic and aromatic parts of the molecule aiming to alter both the electronic and steric properties, which could potentially lead to specific types of non-covalent interaction, and eventually express selectivity towards certain biomolecules.

*3.2 Interactions of **A1-7** dyes with ds-DNA and ds-RNA.*

The UV/vis spectra of the dyes aqueous solutions are proportional to their concentration up to 0.1 mM concentrations and solution thermal stability upon heating to 95 °C was excellent. Molar extinction coefficients are given in Table 1. Dye solutions in buffer do not exhibit fluorescence emission.

Table 1. Electronic absorption data of **A1, A2, A3, A4** and **A7** determined from data on Figure 1.

	λ_{max} / nm	$\varepsilon \times 10^3$ / mmol^{-1} cm^2
A1	483	52.325
A2	453	75.647
A3	453	66.089
A4	510	53.496
A7	484	64.637

Addition of any ds-DNA/RNA to studied dyes resulted in pronounced hypochromic effect and minor bathochromic shifts in the UV/Vis spectra (Figure 2, Supp. Info.). Particularly interesting was change observed only for **A4** / pApU (Figure 2), where intriguingly strong hypochromicity was accompanied by change in absorbance ratio between absorption maxima at 510 nm/478 nm. Such change could be ascribed to intensive aggregation of dye into H-type of aggregate typical for instance for perylene bisimide dyes [16, 17], in this case induced by RNA binding.

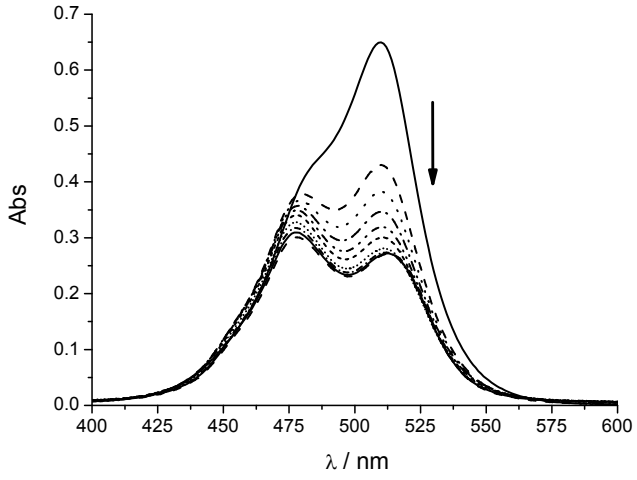

Figure 2 Changes in UV/Vis spectrum of **A4** (c= 1.00 × 10^{-5} M) upon titration with pApU; at pH 7.0, sodium cacodylate buffer, I = 0.05 M.

Intrinsically non-fluorescent, aqueous dye solutions became strongly fluorescent upon DNA/RNA addition (Figure 3 Figure 4).

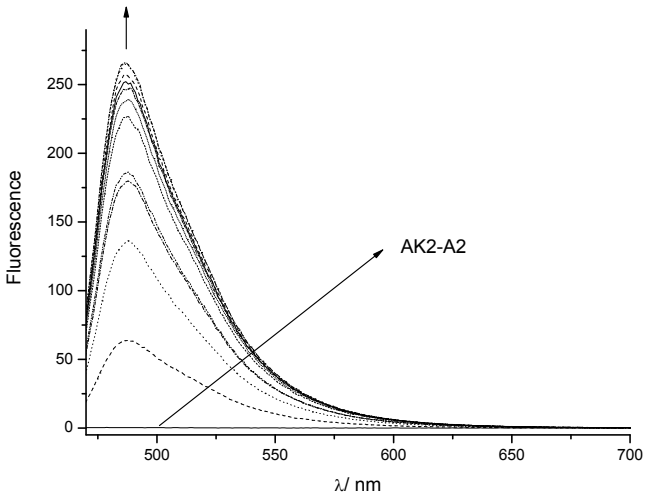

Figure 3 Changes in fluorescence spectrum of **A2** (c= 1.00 × 10^{-6} M) upon titration with pApU; at pH 7.0, sodium cacodylate buffer, I = 0.05 M.

However, the intensity of fluorescence response was dependent on the dye structure as well as on the differences between DNA/RNA structures (Figure 4). For instance, **A3** showed strong fluorimetric selectivity toward AU-RNA (also **A4** but less pronounced), while **A1** was selective toward AT-DNA, **A2** and **A7** fluorescence response was almost identical for all ds-DNA/RNA. Due to the complexity of physical events involved in fluorescence increase upon binding to DNA/RNA, the microenvironment of the dye (existence of water molecules in the binding pockets, aggregates formation) geometry of the binding pocket, the magnitude of the emission increase could not be directly correlated to binding affinity.

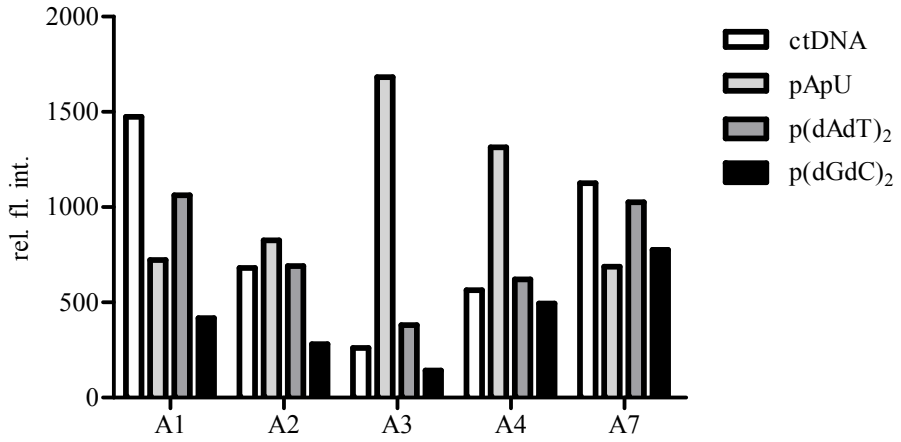

Figure 4. The increase of the fluorescence intensity upon addition of the polynucleotide (ctDNA, pApU, $p(dAdT)_2$ and $p(dGdC)_2$) to the dye solutions ($c=1 \times 10^{-6}$ M, 50 mM Na cacodylate, pH7). The increase was calculated by subtraction of the intrinsic dye fluorescence intensity from the maximal calculated intensity of the formed complex [dye-polynucleotide].

Such pronounced differences in emission selectivity within series of very close structural analogues required more detailed structural analysis of dye-polynucleotide binding mode. For that purpose we applied CD spectropolarimetry, as a highly sensitive method for the elucidation of conformational changes in the secondary structure of polynucleotides [18]. Moreover, the DNA/RNA complexes with the dyes, could acquire induced (I)CD bands (coinciding with the UV/Vis absorption bands of the dyes, far from the CD bands of DNA/RNA), which could be helpful in determination of the binding mode (intercalation, groove binding, agglomeration, etc.)[19].

Addition of studied dyes to ds-DNA at ratios r[dye]/[nucleotide] < 0.3 resulted in negative ICD band within 450-550 nm range accompanied by decrease of DNA CD bands (230-290 nm); both changes characteristic for the intercalative binding mode (Figure 5 LEFT, Supp. Info). At higher ratios r (r>0.3) dye is in the excess of intercalative binding sites, according to the "neighbour exclusion principle"[20]. In such situations some dye/DNA combinations exhibit secondary binding event, represented by bisignate CD signals at 450-550 nm, which indicates excitonic coupling of dye aggregates [21]. However, the addition of dyes to AU-RNA even at r<0.3 yielded exclusively bisignate CD signals in 450-550 nm range (Figure 5 RIGHT, Supp. Info), thus indicating the dye aggregation (most likely within RNA major groove) as dominant binding mode of **A1-7** dyes to ds-RNA. For most of the studied dyes, observed bisignate ICD signal was characterised by isoelliptic point for the whole range of dye/nucleotide ratio (r=0-0.7),

supporting formation of only one type of aggregate. Only **A7** showed change in shape of ICD response for r>0.3, indicating rearrangement of the dye molecules (Supp. info.). Furthermore, the intensity of bisignate CD signals was strongly dependent on the dye structure, **A4** showed the strongest ICD response (Figure 5), which could be correlated to peculiar UV/Vis spectra changes upon **A4** titration with RNA (Figure 2). The ICD intensity increase was proportional to ratio r[dye]/[nucleotide] up to saturation at about r=0.5, marking the saturation of all available binding sites.

The particular reason for intriguing DNA vs. RNA ICD band selectivity at low ratios r>0.2 could be attributed to particular property of RNA major groove, which being deep and narrow (width 3.8A, depth 13.5A) allows better accommodation of dye aggregates in comparison to DNA minor groove (width 5.7A, depth 7.5A). Because of this, **A1-7** dyes prefer to intercalate into DNA, while in ds-RNA there is competitive aggregation taking place.

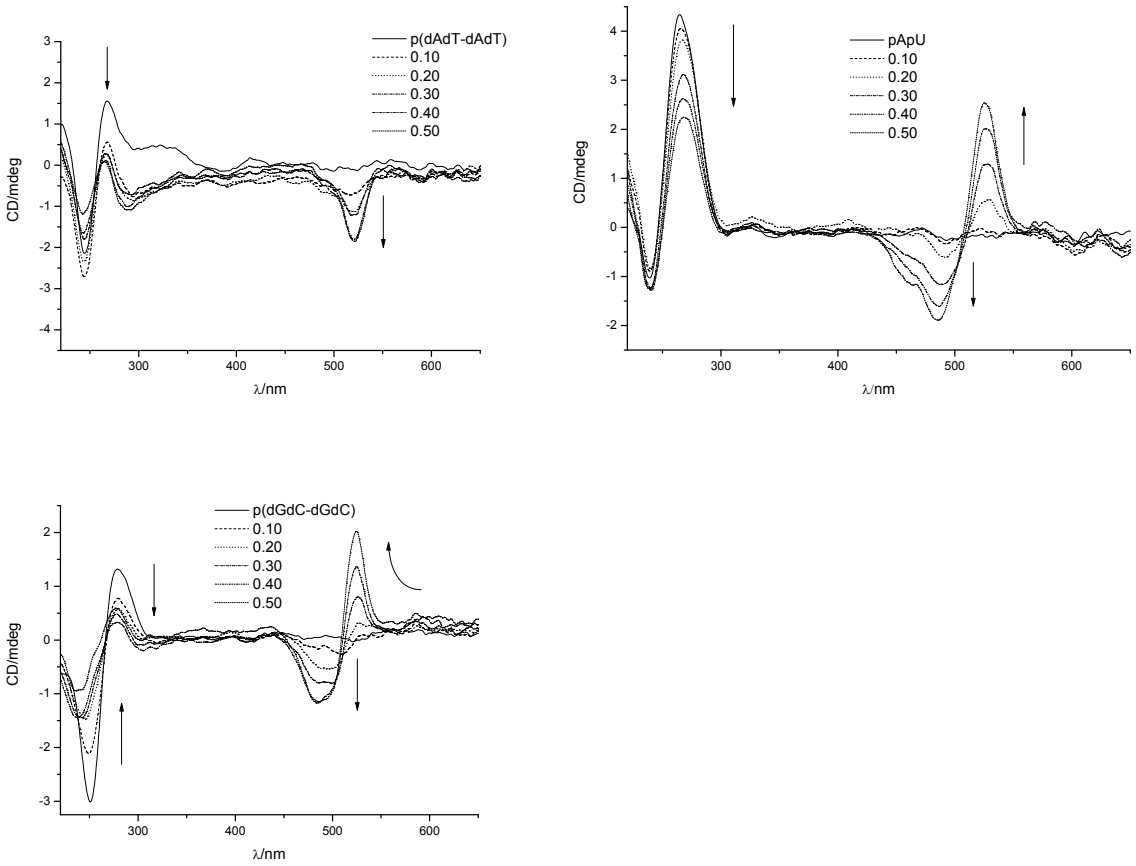

Figure 5. Changes in the CD spectra of $p(dAdT)_2$ upper left; pApU upper right and $p(dGdC)_2$ polynucleotides (c= 2.00×10^{-5} M) upon titration with **A4** ; at pH 7.0, sodium cacodylate buffer, I = 0.05 M.

Intercalative binding mode suggested by CD results not only distorts and decreases CD bands of DNA (230 – 290 nm) but should also strongly stabilise double stranded (ds)-DNA helix against thermal denaturation. On the other side, aggregation of dye could have very different effects on ds-RNA stability, ranging from very strong stabilisation to negligible impact. We performed experiments for mixed sequence DNA (ct-DNA), and well defined polynucleotides: AT-DNA and AU-RNA. All dyes stabilised ds-DNA/RNA against thermal denaturation (Table 2). For ds-DNAs the dye stabilisation effects were within the range expected for classical intercalation [22].

Table 2 The [a]Δ*Tm* values (°C) of studied ds- polynucleotides upon addition[b] of AK-A1, AK-A2, AK-A3, AK-A4 and AK-A7 at pH 7.0 (sodium cacodylate buffer, I = 0.05 M).

	ct-DNA		$p(dAdT)_2$		pApU	
[b]r=	0.2	0.3	0.2	0.3	0.2	0.3
AK2-A1	6.2	7.0	8.7	9.6	6.9	10.7
AK2-A2	4.9	7.2	12.7	13.5	8.7	10.3
AK2-A3	3.6	c	6.8	C	9.6	c
AK2-A4	12.1	c	20.4	C	9.3	c
AK2-A7	c	8.8	9.6	C	c	8.6

[a]Error in Δ*Tm* ± 0.5 °C. [b] r = [dye] / [nucleotide]. [c]Not determined.

However, stabilisation of ds-RNA was also significant and indicated that aggregated dye form strongly interacts with RNA double helix. Since **A1-7** dyes carry only two positive charges, electrostatic interactions along outer RNA surface could be excluded since contribution of about 5kJ/mol for one electrostatic interaction could not yield such strong stabilisation. The minor groove of ds-RNA is too shallow and too broad for small molecule binding [23, 24], thus RNA major groove could be the preferred binding site for **A1-7** dye aggregation.

Calorimetric titration of ds-DNA sequences (mixed sequence-ctDNA, alternating AT and GC sequences) with the studied compounds revealed comparable binding constants (Figure 6) with somewhat higher K_a for **A1** and particularly **A4**. The thermodynamic parameters obtained and calculated from ITC titrations (Figure 7 and Supp. info), as well as stoichiometric ratios of binding (Table 3), indicate that in the case of **A4**, apart from intercalative binding there is a secondary binding mode manifested by considerable entropic contribution and binding ratios that exceed the maximum available intercalative sites (N≥0.25), for $p(dAdT)_2$, $p(dGdC)_2$). Binding **A4** with $p(dAdT)_2$, $p(dGdC)_2$ sequences shows expected enthalpic contributions to the free

energy ΔG, the usual sign of the intercalation [25], however there is a considerable entropic contribution, greatly surpassing unavoidable entropic penalties due to the loss of translational and rotational freedom of motion [26]. Water displacement, non-specific hydrophobic interaction results with an increase of ΔS, meaning that the secondary binding site might be DNA groove, which is normally filled with water molecules [27].

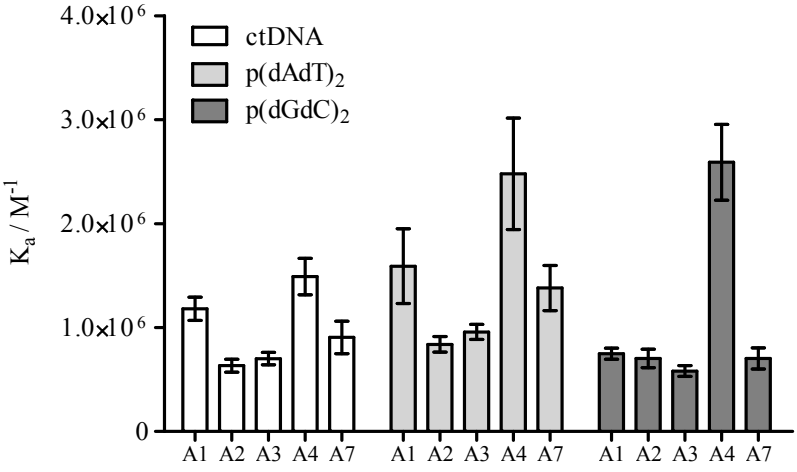

Figure 6 The binding constants (K_a) obtained by ITC, using one set of sites fitting model and Origin 7.5 software

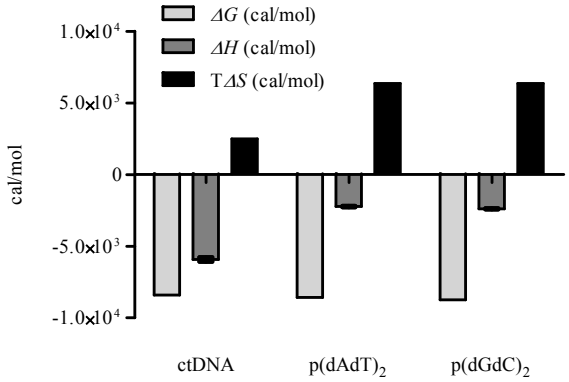

Figure 7 Thermodynamic parameters of the binding with **A4**, obtained/calculated from ITC titrations of ds-DNA sequences**.**

Table 3 Binding ratios N obtained by ITC, using one set of sites fitting model and Origin 7.5 software

	ctDNA	$p(dAdT)_2$	$p(dGdC)_2$
	N	**N**	**N**
A1	0.135 ± 0.0033	0.281 ± 0.00828	0.26 ± 0.0037
A2	0.106 ± 0.0047	0.193 ± 0.00326	0.148 ± 0.0057
A3	0.118 ± 0.0038	0.243 ± 0.00413	0.114 ± 0.004
A4	0.207 ± 0.0042	0.351 ± 0.00714	0.416 ± 0.0049
A7	0.173 ± 0.0063	0.302 ± 0.00843	0.256 ± 0.0066

3.3 Biological activity, cellular uptake and distribution

We assessed **A1-7** dyes for antiproliferative activity against human tumour cell lines **H460**, **MCF7** and studied their subcellular localisation in **H460** and **HeLa** tumour cell line. To further study the uptake and the distribution of the dyes we used confocal microscopy and flow cytometry. All studied dyes have insignificant effect on the cell proliferation at up to 0.1 mM concentrations (Table S2, Supp. Info.). Considering afore determined intercalative binding mode of **A1-7** dyes to ds-DNA and considerable stabilisation effect against thermal denaturation (Table 3), this was a surprising result. Strong stabilisation against thermal denaturation signifies that the dyes are bound in such a way to prevent unwinding of the double helix, which is necessary in the DNA replication process. Similarly, intercalation by definition yields strong antiproliferative effect, usually by inhibition of topoisomerases I/II, subsequently inhibiting the DNA replication [28, 29]. Taking into consideration that the compounds are doubly charged and therefore somewhat incapacitated for the cellular uptake, safe assumption was that the low cytotoxicity could be due to the inefficient permeation across the cellular membrane. For instance, classical DNA intercalator, propidium iodide, also doubly charged compound, is used for cell viability testing since it does not permeate viable cells and thus it is not significantly cytotoxic or antiproliferative. After initial screening of the whole series in **H460**, cells (Figure S63, Supp. Info), which revealed that all the compounds pass the cell membrane and after entering the cell, they occupy mitochondrial space. To further explore subcellular localization, **A1** and **A4** were chosen for colocalization studies in **HEK293**, **HeLa** cells (Figure 9) and uptake rate studies in **HeLa** cells. Rate of the cell permeation by the **A1** and **A4** dyes was established by flow cytometry (Supp info). The observed difference in the time needed to reach maximum

fluorescence intensity between the two dyes was considerable, namely **A1** accumulated in the cells after 90 min while **A4** reached its peak concentration after 20 min (Figure S62, Supp. info.). Colocalization experiments were performed using commercially available mitochondrial fluorescent markers (MitoTracker® Deep Red FM, DiOC6(3), (Figure 10). Further colocalization experiments were done by means of transient transfection of the HeLa cells with pECFP-Mito vector, which is designed for fluorescent labelling of mitochondria in living cells (Supp. Info, Figure S64). The transfected cells were afterwards exposed to the dyes, 1h prior to visualization on confocal microscope. Simple superimposing of the fluorescence photomicrographs, although informational and illustrational, is highly subjective and ambiguous, mainly due to the non-equivalent fluorescence intensity of the two different probes. In order to quantify the colocalization we used Pearson's correlation coefficient (PCC)[14], corrected for noise by Replicate-based noise correction correlation (RBNCC)[15], explained in more detail in the Supporting information. The results, indicating excellent colocalization of the studied dyes with the commercial mitochondrial trackers and the cyan fluorescent protein expressed in the mitochondria are presented in the Table 4.

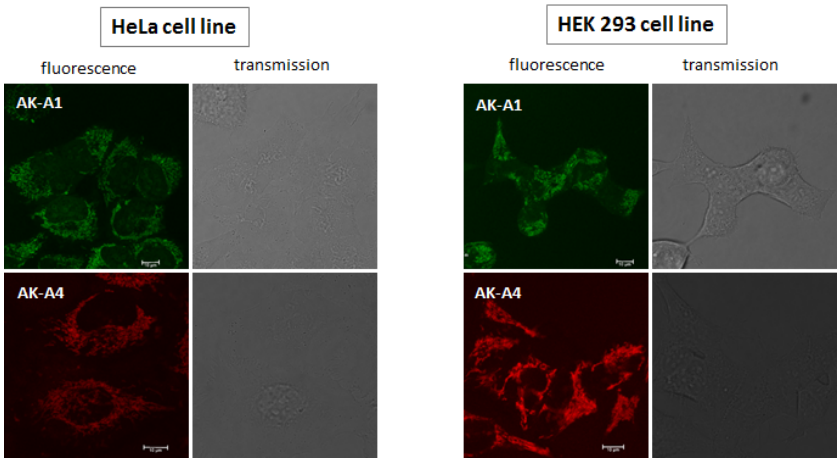

Figure 8: Confocal photofluoromicrographs of HeLa and HEK 293 cell lines after 120 min incubation with **A1** and **A4** cyanine dyes ($c = 2 \times 10^{-5}$ mol dm^{-3}). Fluorescence confocal and transmission images are represented. Scale bars, 10 μm.

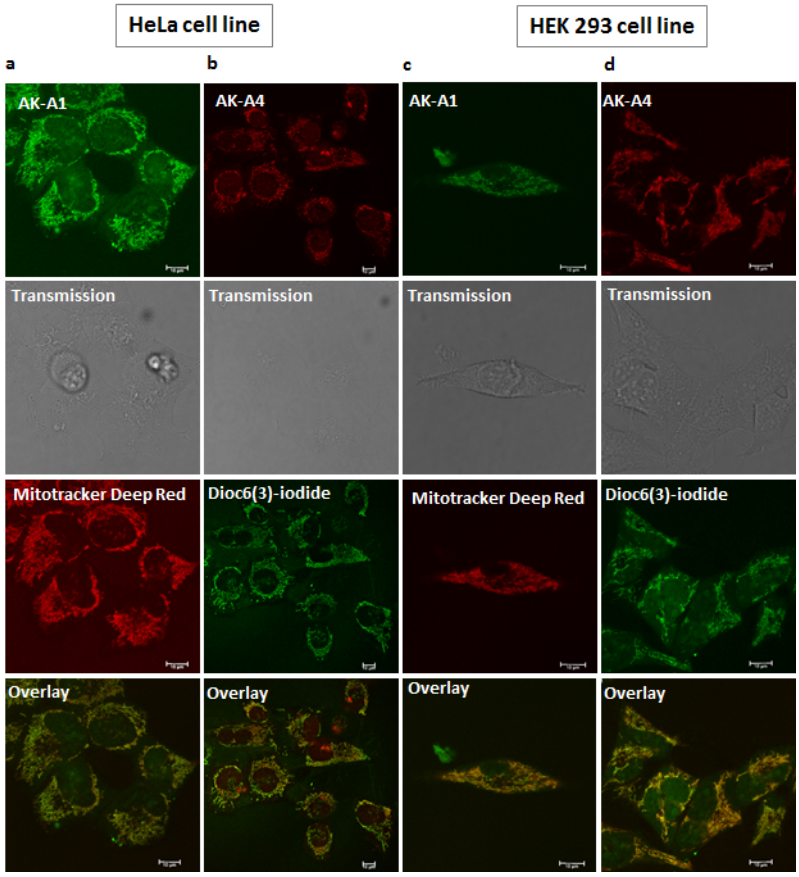

Figure 9 Confocal photofluoromicrographs of HeLa (a), (b) and HEK 293 (c), (d) cell lines after 120 min incubation with **A1** (a), (c) and **A4** (b), (d) dyes ($c = 2 \times 10^{-5}$ mol dm^{-3}). Far red-fluorescent dye MitoTracker Deep Red (a), (c) was used for mitochondrial co-localization study with **A1** dye. Green fluorescent lipophilic dye Dioc6(3)-iodide (b), (d) was used to stain mitochondria live cells and for the co-localization study with **A4** dye. Fluorescence confocal, transmission, and overlaid images are represented. Scale bars, 10 μm.

Table 4 The colocalization correlation, PCC values corrected for noise by RBNCC method.

Probe combination	PCC ± SD
A1:MitoTracker	0.905 ± 0.0737
A4:DiOC6(3)	0.919 ± 0.0347
A1:CFP	0.845 ± 0.0769
A4:CFP	0.952 ± 0.0178

4. Conclusions

The **A1-7** dyes bind with micromolar affinity to all ds-DNA/RNA, strongly stabilising ds-helix against thermal denaturation. The dyes predominantly intercalate into ds-DNAs but also exhibit certain secondary binding event at higher dye/DNA ratios. On the other hand primary

binding site for ds-RNA, seems to be major groove, where dyes form aggregates. Fluorimetric response of the dye-polynucleotide complexes is strongly dependent on a dye structure, indicating that minor differences in heterocyclic atom (oxazole *vs* thiazole) and steric effects of side chains have pronounced influence on fluorimetric recognition. Also, some dyes show fluorimetric selectivity between various ds-DNA and ds-RNA, dependent on a type of polynucleotide secondary structure. Even though the dyes intercalate into DNA and strongly stabilise the double helix against thermal denaturation, their anti-proliferative activity is negligible in relatively high concentrations. Furthermore, despite their di-cationic nature they permeate into the cell relatively quickly and accumulate in the mitochondrial space. Localization within the mitochondrial intermembrane space could explain the low impact on cell proliferation, similar to our previous mitochondrial membrane potential probes [7]. By accumulation in the mitochondrial space the dyes are depleted from the DNA-rich cell nucleus where they could cause more damage and block the cell proliferation process. However their precise localisation within the mitochondrial space and their impact on the mitochondrial homeostasis remains to be further explored. Furthermore, additional future prospect is the design of novel dyes which will take advantage of DNA vs. RNA groove aggregation for the fluorimetric reporting.

Acknowledgment:

AK, NG and TD are grateful for the financial support to "Funding of research projects in support of PhD students"-University of Sofia "St. Kliment Ohridski" – Project No 098/08.05.2014 and IC, IO, ATP and IP gratefully acknowledge financial support of ESF project HR.3.2.01 0254 and Croatian Science Foundation Grant No 1477: DNA/RNA-MolSense.

References

[1] M.J.W. Waring, L.P.G., Small Molecule DNA and RNA Binders: From Synthesis to Nucleic Acid Complexes, Wiley-VCH Verlag GmbH & Co. KGaA, Weinheim, Germany, 2004.

[2] B. Willis, D.P. Arya, Triple Recognition of B-DNA by a Neomycin-Hoechst 33258-Pyrene Conjugate, Biochemistry-Us, 49 (2010) 452-469.

[3] M.P. Murphy, Targeting lipophilic cations to mitochondria, Bba-Bioenergetics, 1777 (2008) 1028-1031.

[4] D.G. Nicholls, M.W. Ward, Mitochondrial membrane potential and neuronal glutamate excitotoxicity: mortality and millivolts, Trends Neurosci, 23 (2000) 166-174.

[5] H. Rottenberg, S.L. Wu, Quantitative assay by flow cytometry of the mitochondrial membrane potential in intact cells, Bba-Mol Cell Res, 1404 (1998) 393-404.

[6] S.W. Perry, J.P. Norman, J. Barbieri, E.B. Brown, H.A. Gelbard, Mitochondrial membrane potential probes and the proton gradient: a practical usage guide, Biotechniques, 50 (2011) 98-115.

[7] I. Crnolatac, L.M. Tumir, N.Y. Lesev, A.A. Vasilev, T.G. Deligeorgiev, K. Miskovic, L. Glavas-Obrovac, O. Vugrek, I. Piantanida, Probing the Structural Properties of DNA/RNA Grooves with Sterically Restricted Phosphonium Dyes: Screening of Dye Cytotoxicity and Uptake, Chemmedchem, 8 (2013) 1093-1103.

[8] A. Saric, I. Crnolatac, S. Sobocanec, Z. Safranko, T. Delgeorgiev, I. Piantanida, P.X. Petit, New water soluble fluorescent phosphonium probes for assessment of mitochondrial functionalities, Eur J Clin Invest, 46 (2016) 59-59.

[9] M.F. Ross, T. Da Ros, F.H. Blaikie, T.A. Prime, C.M. Porteous, I.I. Severina, V.P. Skulachev, H.G. Kjaergaard, R.A.J. Smith, M.P. Murphy, Accumulation of lipophilic dications by mitochondria and cells, Biochem J, 400 (2006) 199-208.

[10] R.A.J. Smith, C.M. Porteous, A.M. Gane, M.P. Murphy, Delivery of bioactive molecules to mitochondria in vivo, Proceedings of the National Academy of Sciences of the United States of America, 100 (2003) 5407-5412.

[11] H.-W. Mewes, J. Rafael, The 2-(dimethylaminostyryl)-1-methylpyridinium cation as indicator of the mitochondrial membrane potential, FEBS Letters, 131 (1981) 7-10.

[12] L. Glavas-Obrovac, I. Piantanida, S. Marczi, L. Masic, I.I. Timcheva, T.G. Deligeorgiev, Minor structural differences of monomethine cyanine derivatives yield strong variation in their interactions with DNA, RNA as well as on their in vitro antiproliferative activity, Bioorgan Med Chem, 17 (2009) 4747-4755.

[13] J.L. Bresloff, D.M. Crothers, Equilibrium Studies of Ethidium-Polynucleotide Interactions, Biochemistry-Us, 20 (1981) 3547-3553.

[14] K.W. Dunn, M.M. Kamocka, J.H. McDonald, A practical guide to evaluating colocalization in biological microscopy, Am J Physiol-Cell Ph, 300 (2011) C723-C742.

[15] J. Adler, S.N. Pagakis, I. Parmryd, Replicate-based noise corrected correlation for accurate measurements of colocalization, J Microsc-Oxford, 230 (2008) 121-133.

[16] J. Gershberg, M.R. Stojkovic, M. Skugor, S. Tomic, T.H. Rehm, S. Rehm, C.R. Saha-Moller, I. Piantanida, F. Wurthner, Sensing of Double-Stranded DNA/RNA Secondary Structures by Water Soluble Homochiral Perylene Bisimide Dyes, Chem-Eur J, 21 (2015) 7886-7895.

[17] T.H. Rehm, M.R. Stojkovic, S. Rehm, M. Skugor, I. Piantanida, F. Wurthner, Interaction of spermine-alanine functionalized perylene bisimide dye aggregates with ds-DNA/RNA secondary structure, Chem Sci, 3 (2012) 3393-3397.

[18] A.N. Rodger, B., Circular Dichroism and Linear Dichroism, Oxford University Press, New York, 1997.

[19] M. Eriksson, B. Norden, Linear and circular dichroism of drug-nucleic acid complexes, Method Enzymol, 340 (2001) 68-98.

[20] J. Cairns, The Application of Autoradiography to the Study of DNA Viruses, in: Cold Spring Harbour Symposia on Quantitative Biology, CSH Press, Cold Spring Harbour, 1962.

[21] B.A. Armitage, Cyanine dye-DNA interactions: Intercalation, groove binding, and aggregation, DNA Binders and Related Subjects, 253 (2005) 55-76.

[22] D.M. Crothers, Calculation of Melting Curves for DNA, Biopolymers, 6 (1968) 1391-&.

[23] W. Saenger, Principles of Nucleic Acid Structure, Springer-Verlag, New York, 1983.

[24] C.R. Cantor, Conformational Studies on 5s Ribosomal Rna, Biophys J, 8 (1968) A63-&.

[25] J.B. Chaires, A thermodynamic signature for drug-DNA binding mode, Arch Biochem Biophys, 453 (2006) 26-31.

[26] L.M. Amzel, Loss of translational entropy in binding, folding, and catalysis, Proteins, 28 (1997) 144-149.

[27] M.L. McDermott, H. Vanselous, S.A. Corcelli, P.B. Petersen, DNA's Chiral Spine of Hydration, Acs Central Sci, 3 (2017) 708-714.

[28] A. Bolognese, G. Correale, M. Manfra, A. Lavecchia, O. Mazzoni, E. Novellino, P. La Colla, G. Sanna, R. Loddo, Antitumor agents. 3. Design, synthesis, and biological evaluation of new pyridoisoquinolindione and dihydrothienoquinolindione derivatives with potent cytotoxic activity, J Med Chem, 47 (2004) 849-858.

[29] M.A. Lynch, O. Duval, A. Sukhanova, J. Devy, S.P. MacKay, R.D. Waigh, I. Nabiev, Synthesis, biological activity and comparative analysis of DNA binding affinities and human DNA topoisomerase I inhibitory activities of novel 12-alkoxy-benzo[c]phenanthridinium salts, Bioorg Med Chem Lett, 11 (2001) 2643-2646.

Supp. Info: New series of non-toxic DNA intercalators, mitochondria targeting fluorescent dyes fluorescent dyes

Atanas Kurutos[a,b*†], Iva Orehovec[c†], Ana Tomašić Paić[c], Ivo Crnolatac[c*], Lucija Horvat[d], Nikolai Gadjev[a], Ivo Piantanida[b*], Todor Deligeorgiev[a]

[a] *Institute of Organic Chemistry with Centre of Phytochemistry, Bulgarian Academy of Sciences, Acad. G. Bonchev str., bl. 9, 1113 Sofia, Bulgaria*

[b] *Department of Pharmaceutical and Applied Organic Chemistry, Faculty of Chemistry, University of Sofia, 1164 Sofia, Bulgaria*

[c] *Laboratory for Biomolecular Interactions and Spectroscopy, Division of Organic Chemistry and Biochemistry, Ruđer Bošković Institute, Bijenička c. 54, 10000 Zagreb, Croatia*

[d] *Laboratory for Molecular Plant Biology and Biotechnology, Division of Molecular Biology, Ruđer Bošković Institute, Bijenička c. 54, 10000 Zagreb, Croatia*

1. Synthesis:

Unless otherwise stated, all starting materials and solvents used in the synthesis of the monomethine cyanine dyes were obtained from Sigma-Aldrich, Organica Feinchemie GmbH Wolfen, Fluka, and Alfa-Aesar as commercial products of analytical grade, and were used without further purification. The synthesis is described in detail in the supporting material. The solvents used for the spectrophotometric and spectrofluorimetric analyses were purchased form Macron Fine Chemicals TM. Deuterated solvents for NMR spectroscopy were purchased from Deutero GmbH.

1.1 Analysis methods and equipment

Analytical samples of all products including dyes **A1-7** and their intermediates, were obtained after purification by recrystallization from methanol. Chemical structures were evaluated by ^{1}H-NMR and APT carbon NMR spectra recorded on Brucker Avance III HD 500 MHz, Bruker Avance 600 MHz, and Bruker Avance 300 MHz in DMSO-d_6 at 25 ^{o}C. Chemical shifts were reported in ppm in δ-values with respect to tetramethylsilane (TMS) as an internal reference. Coupling constants J are expressed in Hz. ESI/MS were obtained on TSQ Quantum Access Max Masspectrometer coupled with triple quadrupole. IR spectra were recorder on Thermo Scientific Fisher Nicolet 6700 (KBr). Melting point temperatures were determined on a Kofler bench and are uncorrected. Absorption spectra of the unbound dyes were recorded on a Cecil Aurius CE 3021 UV-Vis spectrophotometer in methanol solutions

at room temperature. Fluorescence measurements were performed in methanol using 10-mm path-length quartz cuvettes on a Perkin Elmer LS45 fluorescence spectrometer at room temperature.

1.2 Preparation of intermediate 2.

A fivefold excess of 1,3-dibromopropane (10.2 mL, 0.1 mol) was added dropwise to pyridine **1** (1.61 mL , 0.02 mol) and the reaction vessel was stored in a dark place [13, 14] for 24 hours at room temperature (Scheme 1). The precipitated product **2** was collected by filtration and stored in a desiccator. The excess of 1,3-dibromopropane was removed by washing the crude product with diethyl ether. Yield of crude product = 91%. The chemical structure of **2** was evaluated by ^{1}H-NMR and ^{13}C-NMR spectroscopy.

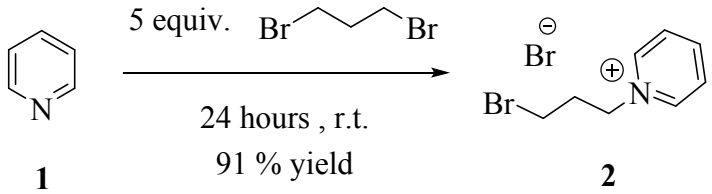

Scheme S 1 Preparation of intermediate **2**.

1-(3-bromopropyl)pyridin-1-ium bromide (**2**); (white solid), yield = 91 %, m.p. = 129-130 ^{o}C, lit. m.p. = 128-129 ^{o}C; ^{1}H-NMR (DMSO-d_6, 500 MHz) δ/ppm: 2.53 (2H, quint., J 6.9, CH_2), 3.60 (2H, t, J 6.6, CH_2), 4.78 (2H, t, J 7.1, CH_2), 8.18-8.21 (2H, m, 2 x ArH), 8.63-8.66 (1H, m, ArH), 9.19-9.21 (2H, m, 2 x ArH); ^{13}C-NMR (DMSO-d_6, 125 MHz): 30.7; 33.6; 59.9; 128.6; 145.5; 146.2;

1.3 Preparation of intermediates 4a, 4b.

1-(3-bromopropyl)pyridin-1-ium bromide (4.50 g, 0.016 mol) **2** was mixed with 4-methylpyridine **3a** (1.56 mL, 0.016 mol) or 4-methylquinoline **3b** (2.12 mL, 0.016 mol), and the reaction mixture was heated at reflux for 15 minutes with stirring in 5 mL 2-methoxyethanol (Scheme 2). After cooling down to room temperature diethyl ether (20 mL) was added, and subsequently the solvent was filtered off. 4-methyl-1-(3-(pyridin-1-ium-1-yl)propyl)pyridin-1-ium bromide **4a** was isolated as white crystals. In the case of 4-methyl-1-(3-(pyridin-1-ium-1-yl)propyl)quinolin-1-ium bromide **4b**, a dark brown oil was formed, which was transferred to a 100 mL beaker of an aqueous potassium hexafluorphosfate yielding pale brown precipitate.

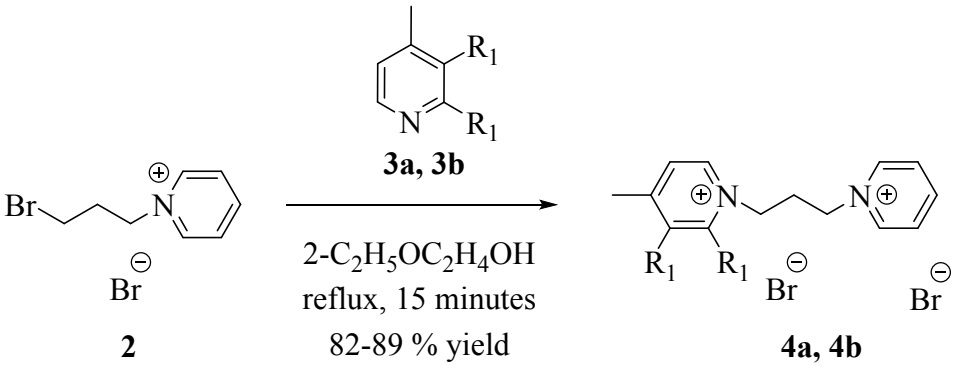

4a: R_1 = H
4b: R_1 = -CH=CH-CH=CH-

Scheme S 2. Preparation of intermediates **4a, 4b**.

4-methyl-1-(3-(pyridin-1-ium-1-yl)propyl)pyridin-1-ium bromide (**4a**): (white crystals), yield 89 %, M.p. = 220-222; ^{1}H-NMR (DMSO-d_6, 500 MHz) δ/ppm: 2.62 (3H, s, $\underline{CH_3}$), 2.68 (2H, quint., J 7.5, CH_2-$\underline{CH_2}$-CH_2), 4.75 (2H, t, J 7.4, CH_2-$\underline{CH_2}$-N), 4.81 (2H, t, J 7.4, CH_2-$\underline{CH_2}$-N), 8.04 (2H, d, J 6.4, 2 x ArH), 8.02-8.24 (2H, m, 2 x ArH), 8.64-8.68 (1H, m, ArH), 9.05 (2H, d, J 6.6, 2 x ArH), 9.22 (2H, dd, J 1.1, 6.7, 2 x ArH); ^{13}C-NMR (DMSO-d_6, 125 MHz): 21.9; 32.2; 57.0; 57.8; 128.6; 128.9; 144.3; 145.4; 146.3; 159.6;

4-methyl-1-(3-(pyridin-1-ium-1-yl)propyl)quinolin-1-ium hexafluorphosfate (**4b**): (pale brown crystals), yield 82 %, M.p. = 225-227; ^{1}H-NMR (DMSO-d_6, 500 MHz) δ/ppm: 2.67 (2H, quint., J 7.4, CH_2-$\underline{CH_2}$-CH_2), 3.04 (3H, s, $\underline{CH_3}$), 4.81 (2H, t, J 7.5, CH_2-$\underline{CH_2}$-N), 5.12 (2H, t, J 7.5, CH_2-$\underline{CH_2}$-N), 8.08 (1H, t, J 7.7, ArH), 8.12 (1H, d, J 6.1, ArH), 8.19 (2H, t, J 6.9, 2 x ArH), 8.28-8.31 (1H, m, ArH), 8.57-8.65 (3H, m, 3 x ArH), 9.06 (2H, d, J 5.9, 2 x ArH), 9.35 (1H, d, J 6.1, ArH); ^{13}C-NMR (DMSO-d_6, 125 MHz): 20.1; 31.0; 54.2; 58.4; 119.6; 123.2; 127.7; 128.6; 129.5; 130.1; 135.7; 137.4; 145.3; 146.2; 149.1; 159.5; ^{19}F-NMR (DMSO-d_6, 470 MHz) δ/ppm: -69.3; -70.8;

1.4 Preparation of intermediates 5a, 5b.

Intermediates **5a** and **5b** were obtained using a method described in the literature [15].

1.5 Preparation of intermediates 6a, 6b [16-18]

2-methylmercaptobenzothiazole **5a** (4.53 g, 0.025 mol) or 2-methylmercaptobenzoxazole **5b** (4.13 g, 0.025 mol) and 1,3-dibromopropane (7.65 mL, 0.075 mol) were mixed in a 50 mL Erlenmeyer flask. The reaction mixture was heated to boiling point with stirring for 30 minutes (Scheme 3). Upon cooling down to room temperature, compound **6** was precipitated with diethyl ether (10 mL), and suction filtered. The product was washed with acetone (10 mL) and dried.

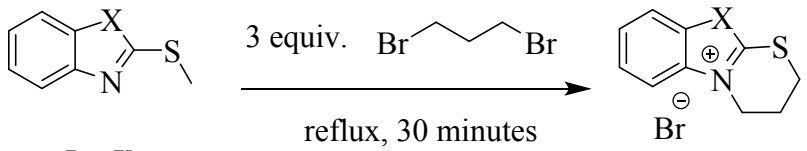

5a, 5b **6a, 6b**

6a: X = S
6b: X = O

Scheme S 3. Preparation of intermediates **6a, 6b**.

3,4-dihydro-2H-benzo[4,5]thiazolo[2,3-b][1,3]thiazin-5-ium bromide (**6a**): (white crystals), yield = 91 %, M.p. = 225 ^{o}C, (lit. m.p. = 226-226.5 ^{o}C as chloride [6]); ^{1}H-NMR (DMSO-d_6, 500 MHz) δ/ppm: 2.53 (2H, quint., J 5.3, CH_2-CH_2-CH_2), 3.62 (2H, t, J 5.5, CH_2), 4.63 (2H, t, J 5.6, CH_2), 7.69-7.72 (1H, m, ArH), 7.77-7.81 (1H, m, ArH), 8.12 (1H, d, J 8.5, ArH), 8.38 (1H, d, J 8.1, ArH); ^{13}C-NMR (DMSO-d_6, 125 MHz): 20.4; 28.1; 47.3; 115.4; 124.4; 127.4; 128.0; 129.0; 142.3; 175.6;

3,4-dihydro-2H-benzo[4,5]oxazolo[2,3-b][1,3]thiazin-5-ium bromide (**6b**): (white crystals), yield = 78 %; Product is highly hygroscopic and unstable. It is used without further purification in the dye synthesis. It's chemical structure is evaluated on the target cyanine dyes AK-A1 and AK-A7.

1.6 Synthesis of cyanine dyes A1-7.

In a reaction vessel equipped with magnetic stirrer, equimolar amounts of intermediates **4a** or **4b** (0.005 mol) and **6a** or **6b** (0.005 mol) were mixed in 1,2-dimethoxyethane (10 mL). A fivefold excess (0.025 mol) of the corresponding anhydride and N-Ethyldiisopropylamine (1.74 mL, 0.010 mol) were added, and the reaction mixture was heated to boiling point for 15 minutes. The reaction mixture was further stirred for 5 hours at room temperature (Scheme 4), followed by addition of diethyl ether (20 mL).

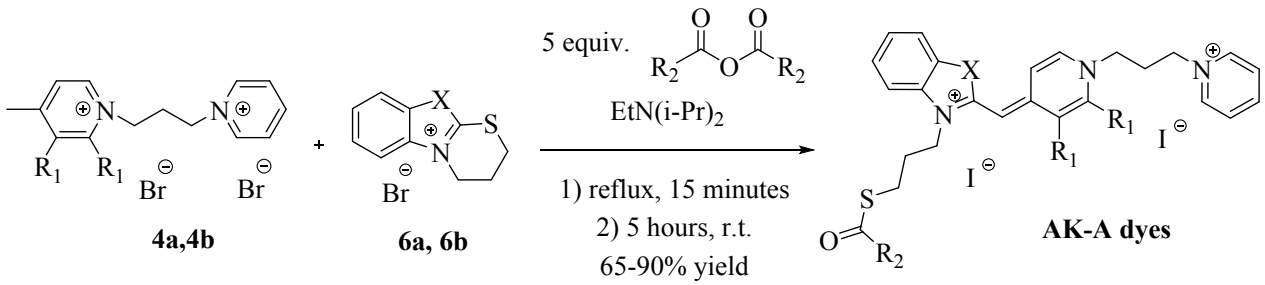

4a,4b **6a, 6b** **AK-A dyes**

X = O, S
R_1 = H, -CH=CH-CH=CH-
R_2 = CH_3, C_2H_5, $(CH_3)_2CH$, C_5H_{11}

Scheme S 4. Synthesis of monomethine cyanine dyes **A1-7**.

Anions were exchanged by dissolving the crude dyes in methanol, and transferring to an aqueous solution of potassium iodide (1.66 g, 0.01 mol). Upon precipitation the dyes were filtered off and dried. Yields and melting point temperatures are given in Table 1**.**

Table S 1. Chemical structures of monomethine cyanine dyes **A1-7**.

Dye	X	R_1	R_2	yield (%)	m.p. (^oC)
A1	O	-CH=CH-CH=CH-	$(CH_3)_2CH$	85	142-145
A2	S	H	CH_3	70	237-240
A3	S	H	$(CH_3)_2CH$	65	249-252
A4	S	-CH=CH-CH=CH-	C_2H_5	90	137-140
A7	O	-CH=CH-CH=CH-	C_5H_{11}	66	140-142

(E)-3-(3-(isobutyrylthio)propyl)-2-((4-(3-(pyridin-1-ium-1-yl)propyl)naphthalen-1(4H)-ylidene)methyl)benzo[d]oxazol-3-ium iodide **(A1)**; (yellow crystals), yield = 85 %, M.p. = 142-145 ^{o}C; FTIR (KBr, cm^{-1}): 422; 546; 682; 705; 759; 823; 865; 922; 978; 1009; 1050; 1090; 1120; 1159; 1221; 1254; 1300; 1329; 1389; 1399; 1478; 1538; 1563; 1620; 1639; 1679; 2256; 2870; 2930; 2965; 3022; ^{1}H NMR (DMSO-d_6, 600 MHz) δ/ppm: 1.05 (6H, d, J 6.9, 2 x CH_3-CH), 2.09 (2H, quint., J 7.1, CH_2-CH_2-CH_2), 2.57 (2H, t, J 7.2, CH_2-CH_2), 2.71 (1H, quint., J 6.9, CH-$(CH_3)_2$), 3.00 (2H, t, J 7.3, CH_2-CH_2-S), 4.51 (2H, t, J 6.8, CH_2-CH_2-N), 4.72 (2H, t, J 7.2, CH_2-CH_2-N), 4.79 (2H, t, J 7.5, CH_2-CH_2-N), 6.34 (1H, s, CH), 7.41-7.44 (1H, m, ArH), 7.49-7.52 (1H, m, ArH), 7.68 (1H, d, J 8.0, ArH), 7.75-7.78 (1H, m, ArH), 7.82 (1H, d, J 8.2, ArH), 7.98 (1H, d, J 7.3, ArH), 7.99-8.02 (1H, m, ArH), 8.15-8.17 (3H, m, 3 x ArH), 8.46 (1H, d, J 7.3, ArH), 8.59-8.62 (1H, m, ArH), 8.79 (1H, dd, J 0.9, 8.7, ArH), 9.07-9.09 (2H, m, ArH); APT-NMR (DMSO-d_6, 75 MHz) δ/ppm: 18.9; 25.0; 27.3; 30.1; 42.3; 42.5; 50.8; 58.0; 74.1; 109.4; 110.7; 110.9; 117.9; 123.4; 124.5; 126.0; 126.1; 126.5; 128.1; 130.6; 133.3; 137.2; 143.5; 144.8; 145.6; 146.1; 150.2; 161.0; ESI: m/z: Found [M+] 652.1 $C_{32}H_{35}IN_3O_2S^+$ requires [M+] 652.15; UV/VIS (methanol): λ_{max} = 481 nm, ε = 80.200 $l.mol^{-1}.cm^{-1}$, λ_{fl} = 533 nm**;**

3-(3-(acetylthio)propyl)-2-((4-(3-(pyridin-1-ium-1-yl)propyl)cyclohexa-2,5-dien-1-ylidene)methyl)benzo[d]thiazol-3-ium iodide (**A2**) [19]; (orange crystals), yield = 70 %, M.p. = 237-240 ^{o}C; FTIR (KBr, cm^{-1}): 416; 514; 581; 628; 679; 716; 743; 765; 775; 814; 857; 903; 951; 996; 1018; 1039; 1059; 1110; 1138; 1159; 1189; 1218; 1308; 1330; 1349; 1368; 1389; 1469; 1521; 1581; 1641; 1680; 2362; 2950; 3000; 3011; 3037; ^{1}H NMR (DMSO-d_6,

600 MHz) δ/ppm: 1.98 (2H, quint., J 7.4, CH_2-$\underline{CH_2}$-CH_2), 2.33 (3H, s, $\underline{CH_3}$-CO), 2.52-2.57 (2H, m, $\underline{CH_2}$), 2.99 (2H, t, J 7.3, CH_2-$\underline{CH_2}$-S), 4.33-4.36 (4H, m, 2 x $\underline{CH_2}$), 4.69 (2H, t, J 7.2, CH_2-$\underline{CH_2}$-N), 6.35 (1H, s, $\underline{CH}$), 7.32-7.35 (1H, m, $\underline{ArH}$), 7.44 (2H, d, J 7.3, $\underline{ArH}$), 7.53-7.56 (1H, m, $\underline{ArH}$), 7.62 (1H, d, J 8.2, $\underline{ArH}$), 7.95 (1H, dd, 0.9, 7.9, $\underline{ArH}$), 8.19-8.22 (2H, m, 2 x $\underline{ArH}$), 8.35-8.37 (2H, m, $\underline{ArH}$), 8.62-8.66 (1H, m, $\underline{ArH}$), 9.08-9.10 (2H, m, $\underline{ArH}$); APT-NMR (DMSO-d_6, 75 MHz) δ/ppm: 25.5; 26.6; 30.5; 31.3; 44.1; 54.4; 57.7; 89.4; 111.9; 122.7; 123.4; 123.7; 127.9; 128.1; 139.8; 141.2; 144.9; 145.7; 150.5; 156.8; ESI: m/z: Found [M+] 590.1 $C_{26}H_{29}IN_3OS_2^+$ requires [M+] 590.08; UV/VIS (methanol): λ_{max} = 453 nm, ε = 92.300 $l.mol^{-1}.cm^{-1}$, λ_{fl} = 489 nm**;**

3-(3-(isobutyrylthio)propyl)-2-((4-(3-(pyridin-1-ium-1-yl)propyl)cyclohexa-2,5-dien-1-ylidene)methyl)benzo[d]thiazol-3-ium iodide (**A3**); (orange crystals), yield = 65 %, M.p. = 249-252 ^oC; FTIR (KBr, cm^{-1}): 433; 484; 506; 680; 712; 742; 766; 816; 859; 904; 979; 1039; 1059; 1189; 1220; 1309; 1330; 1349; 1369; 1389; 1469; 1520; 1589; 1637; 1680; 2355; 2870; 2930; 2970; 3013; 3035; ^1H NMR (DMSO-d_6, 600 MHz) δ/ppm: 1.08 (6H, d, J 6.9, 2 x $\underline{CH_3}$-CH), 1.98 (2H, quint., J 7.3, CH_2-$\underline{CH_2}$-CH_2), 2.55 (2H, quint., J 7.3, CH_2-$\underline{CH_2}$-CH_2), 2.74 (2H, quint., J 7.0, CH_2-$\underline{CH_2}$-CH_2), 2.99 (2H, t, J 7.4, CH_2-CH_2), 4.34 (2H, t, J 7.1, $\underline{CH_2}$), 4.35 (2H, t, J 7.1, $\underline{CH_2}$), 4.69 (2H, t, J 7.2, CH_2-$\underline{CH_2}$-N), 6.35 (1H, s, $\underline{CH}$), 7.32-7.35 (1H, m, $\underline{ArH}$), 7.43-7.45 (2H, m, $\underline{ArH}$), 7.52-7.55 (1H, m, $\underline{ArH}$), 7.60 (1H, d, J 8.2, $\underline{ArH}$), 7.94 (1H, dd, J 0.9, 8.1, $\underline{ArH}$), 8.18-8.21 (2H, m, 3 x $\underline{ArH}$), 8.36 (2H, d, J 7.0, $\underline{ArH}$), 8.62-8.65 (1H, m, $\underline{ArH}$), 9.07-9.09 (2H, m, $\underline{ArH}$); APT-NMR (DMSO-d_6, 75 MHz) δ/ppm: 19.0; 25.0; 26.5; 31.3; 42.3; 44.2; 54.4; 57.7; 89.4; 111.9; 122.7; 123.4; 123.7; 127.9; 128.1; 139.8; 141.2; 144.9; 145.7; 150.6; 156.9; ESI: m/z: Found [M+] 618.1 $C_{28}H_{33}IN_3OS_2^+$ requires [M+] 618.11; UV/VIS (methanol): λ_{max} = 453 nm, ε = 75.300 $l.mol^{-1}.cm^{-1}$, λ_{fl} = 489 nm**;**

(E)-3-(3-(propionylthio)propyl)-2-((4-(3-(pyridin-1-ium-1-yl)propyl)naphthalen-1(4H)-ylidene)methyl)benzo[d]thiazol-3-ium iodide (**A4**); (red crystals), yield = 90 %, M.p. = 137-140 ^oC; FTIR (KBr, cm^{-1}): 417; 473; 508; 545; 597; 639; 680; 715; 750; 791; 817; 888; 925; 942; 1008; 1019; 1050; 1086; 1130; 1161; 1228; 1260; 1301; 1340; 1388; 1469; 1508; 1539; 1609; 1637; 1649; 1669; 1697; 2941; 2970; 3018; 3041; ^1H NMR (DMSO-d_6, 600 MHz) δ/ppm: 1.00 (3H, d, J 7.4, $\underline{CH_3}$-CH), 2.06 (2H, quint., J 7.3, CH_2-$\underline{CH_2}$-CH_2), 2.57 (2H, q, J 7.4, $\underline{CH_2}$-CH_3), 3.05 (2H, t, J 7.2, $\underline{CH_2}$-CH_2), 4.71 (2H, t, 7.4, CH_2-$\underline{CH_2}$-N), 4.72 (2H, t, J 7.2, CH_2-$\underline{CH_2}$-N), 4.79 (2H, t, J 7.5, CH_2-$\underline{CH_2}$-N), 6.96 (1H, s, $\underline{CH}$), 7.42 (1H, d, J 7.3, $\underline{ArH}$), 7.44-7.47 (1H, m, $\underline{ArH}$), 7.63-7.66 (1H, m, $\underline{ArH}$), 7.78-7.81 (1H, m, $\underline{ArH}$), 7.83 (1H, d, J 8.4, $\underline{ArH}$), 8.01-8.04 (1H, m, $\underline{ArH}$), 8.08 (1H, d, J 8.0, $\underline{ArH}$), 8.15-8.18 (2H, m, 2 x $\underline{ArH}$), 8.20 (1H, d, J 8.8, $\underline{ArH}$), 8.59 (1H, d, J 7.2, $\underline{ArH}$), 8.59-8.62 (1H, m, $\underline{ArH}$), 8.80 (1H, dd, J 0.9, 8.7, $\underline{ArH}$), 9.07-9.09 (2H, m, $\underline{ArH}$); APT-NMR (DMSO-d_6, 75 MHz) δ/ppm: 9.3; 25.1; 27.1; 30.1;

36.8; 44.6; 51.0; 58.0; 87.9; 108.1; 112.9; 118.0; 123.0; 124.0; 124.2; 124.7; 125.7; 126.8; 128.1; 128.3; 133.3; 137.0; 139.8; 144.2; 144.8; 145.6; 148.7; 159.8; 199.3; ESI: m/z: Found [M+] 654.1 $C_{31}H_{33}IN_3OS_2^+$ requires [M+] 654.11; UV/VIS (methanol): λ_{max} = 508 nm, ε = 88.900 $l.mol^{-1}.cm^{-1}$, λ_{fl} = 553 nm**;**

(E)-3-(3-(hexanoylthio)propyl)-2-((4-(3-(pyridin-1-ium-1-yl)propyl)naphthalen-1(4H)-ylidene)methyl)benzo[d]oxazol-3-ium iodide (**A7**); (orange crystals), yield = 66 %, M.p. = 140-142 ^oC; FTIR (KBr, cm^{-1}): 419; 463; 478; 519; 546; 581; 616; 647; 681; 703; 765; 809; 821; 861; 885; 923; 962; 1009; 1050; 1090; 1118; 1158; 1180; 1219; 1250; 1300; 1329; 1389; 1401; 1480; 1538; 1560; 1618; 1639; 1681; 2858; 2930; 2950; 3022; ^1H NMR (DMSO-d_6, 600 MHz) δ/ppm: 0.78 (3H, t, J 6.9, $\underline{CH_3}$-CH_2), 1.15-1.21 (4H, m, 2 x $\underline{CH_2}$), 1.47 (2H, quint., J 7.4, CH_2-$\underline{CH_2}$- CH_2), 2.08 (2H, quint., J 7.2, CH_2-$\underline{CH_2}$- CH_2), 2.51-2.58 (4H, m, 2 x $\underline{CH_2}$), 3.00 (2H, t, J 7.0, $\underline{CH_2}$- CH_2), 4.51 (2H, t, J 6.8, $\underline{CH_2}$- CH_2), 4.71 (2H, t, J 7.2, $\underline{CH_2}$- CH_2), 4.78 (2H, t, J 7.6, $\underline{CH_2}$- CH_2), 6.34 (1H, s, $\underline{CH}$), 7.41-7.44 (1H, m, $\underline{ArH}$), 7.49-7.52 (1H, m, $\underline{ArH}$), 7.68 (1H, d, J 7.9, $\underline{ArH}$), 7.75-7.78 (1H, m, $\underline{ArH}$), 7.83 (1H, d, J 8.1, $\underline{ArH}$), 7.98 (1H, d, J 7.3, $\underline{ArH}$), 7.99-8.02 (1H, m, $\underline{ArH}$), 8.15-8.18 (3H, m, $\underline{ArH}$), 8.46 (1H, d, J 7.3, $\underline{ArH}$), 8.59-8.62 (1H, m, $\underline{ArH}$), 8.79 (1H, d, J 8.5, $\underline{ArH}$), 9.09 (1H, d, J 5.9, $\underline{ArH}$), APT-NMR (DMSO-d_6, 75 MHz) δ/ppm: 13.6; 21.6; 24.6; 25.1; 27.4; 30.1; 30.2; 42.5; 43.2; 50.8; 58.0; 74.1; 109.4; 110.7; 110.9; 117.9; 123.4; 124.5; 126.0; 126.1; 126.5; 128.1; 130.6; 133.3; 137.1; 143.5; 144.8; 145.6; 146.1; 150.2; 161.0; 198.6; ESI: m/z: Found [M+] 680.2 $C_{34}H_{39}IN_3O_2S^+$ requires [M+] 680.18; UV/VIS (methanol): λ_{max} = 481 nm, ε = 57.200 $l.mol^{-1}.cm^{-1}$, λ_{fl} = 542 nm**;**

2. **Spectroscopy:**

a)

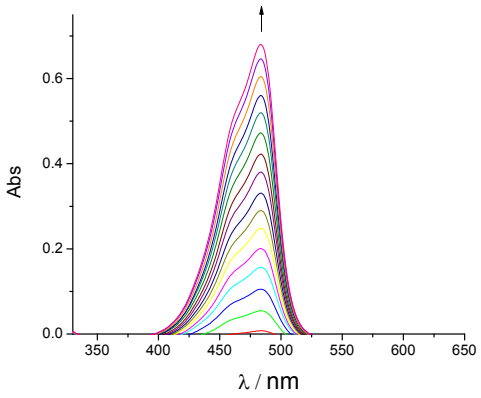

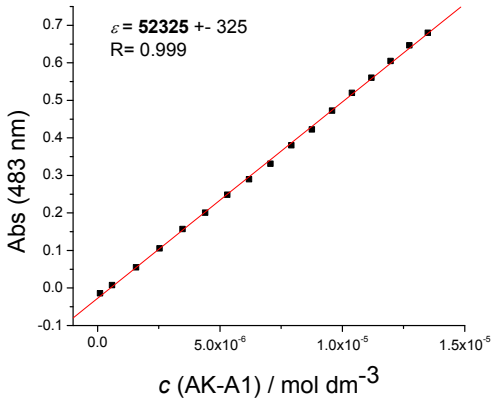

b)

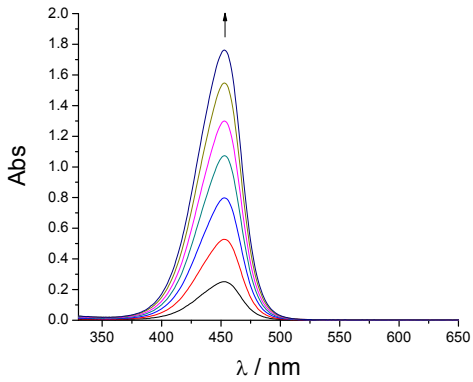

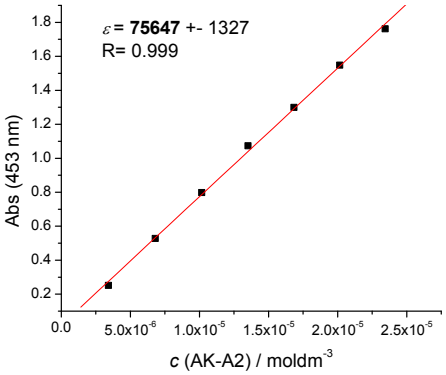

c)

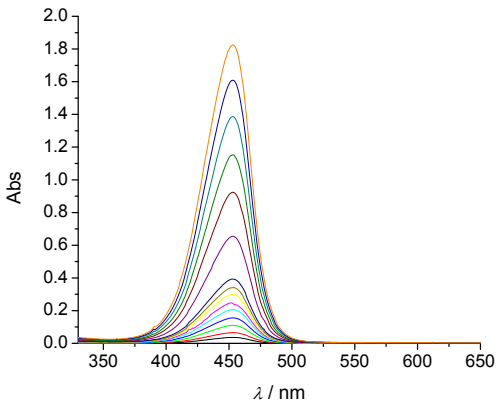

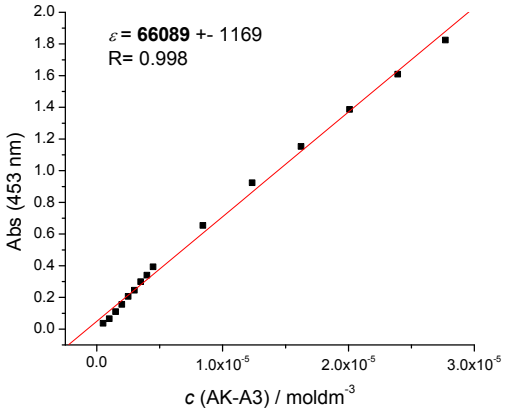

d)

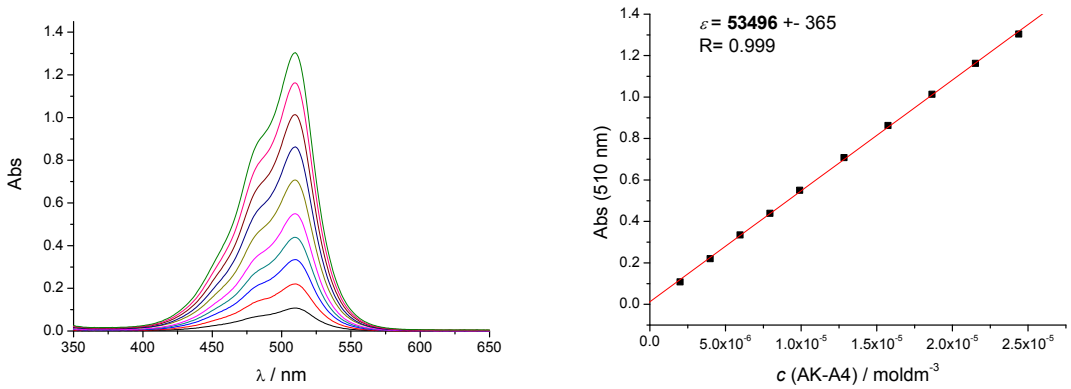

e)

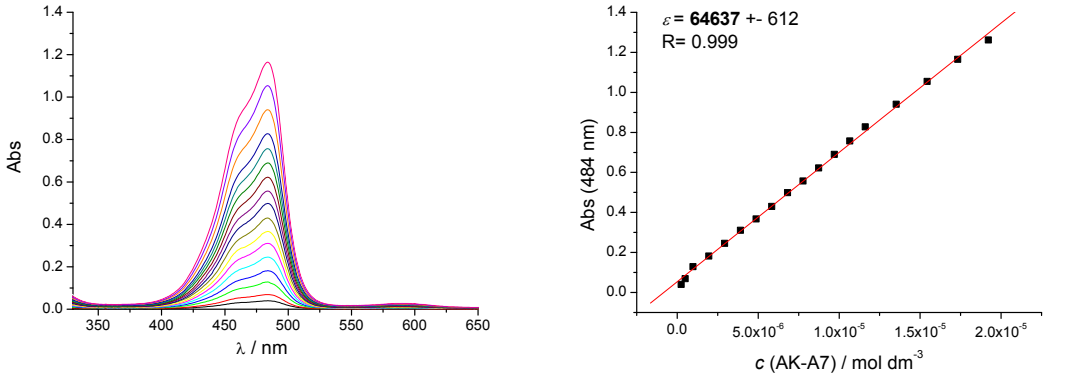

Figure S 1: Dependence of UV/Vis spectra on concentration of a) **A1, b) A2, c) A3, d) A4, e) A7** at pH 7.0, sodium cacodylate buffer, *I* = 50 mM.

3. Study of interactions of AK2-A1, AK2-A2, AK2-A3, AK2-A4 and AK2-A7 with double-stranded DNA/RNA in aqueous medium

3.1 UV/vis Spectrophotometric titrations

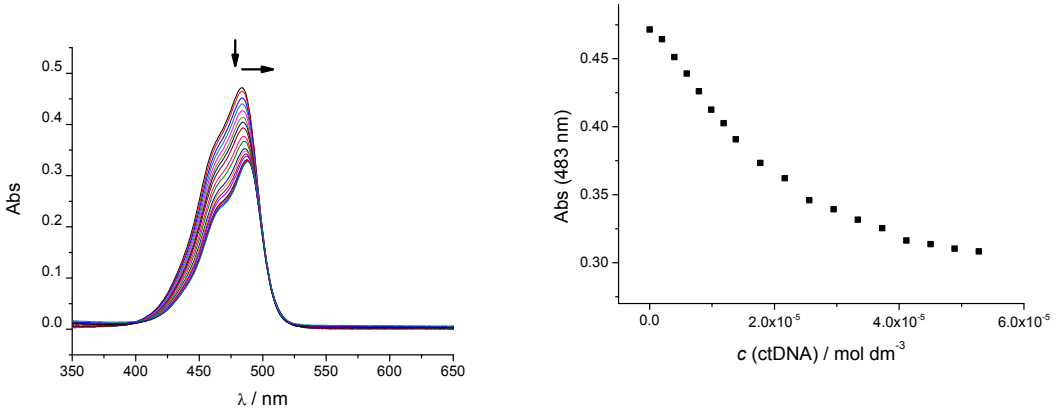

Figure S 2 LEFT Changes in UV/Vis spectrum of **A1** (c = 1.00 × 10^{-5} M) upon titration with ctDNA; **RIGHT** Dependence of **A1** absorbance at λ_{max} = 483 nm on c(ctDNA), at pH 7.0, sodium cacodylate buffer, I = 0.05 M.

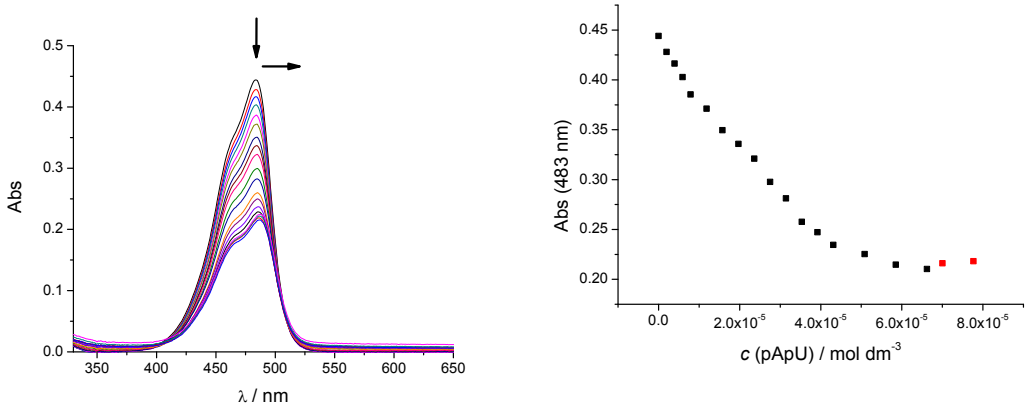

Figure S 3 LEFT Changes in UV/Vis spectrum of **A1** (c = 1.00 × 10^{-5} M) upon titration with pApU; **RIGHT** Dependence of **AK2-A1** absorbance at λ_{max} = 483 nm on c(pApU), at pH 7.0, sodium cacodylate buffer, I = 0.05 M.

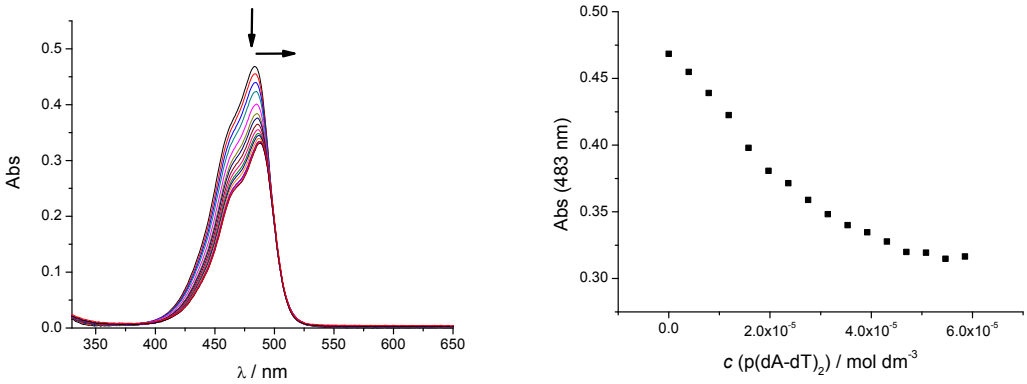

Figure S 4 LEFT Changes in UV/Vis spectrum of **A1** (c = 1.00 × 10-5 M) upon titration with p(dA-dT)2; RIGHT Dependence of **A1** absorbance at λ_{max} = 483 nm on c(p(dA-dT)$_2$), at pH 7.0, sodium cacodylate buffer, I = 0.05 M.

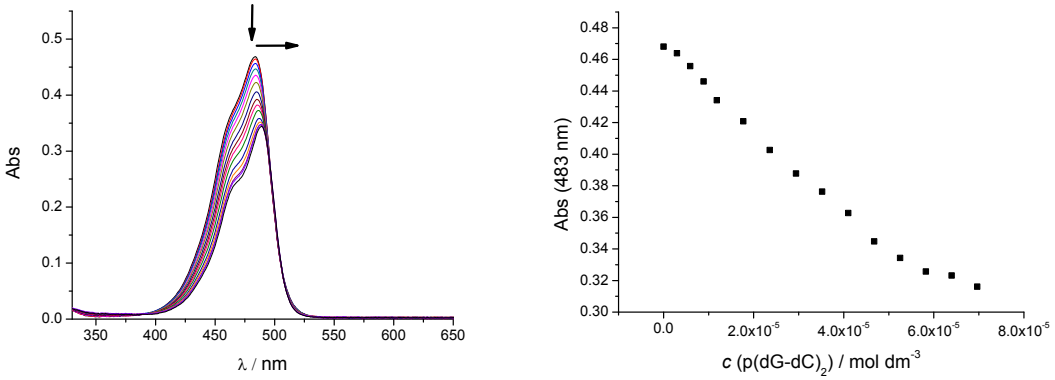

Figure S 5. LEFT Changes in UV/Vis spectrum of **A1** (c = 1.00 × 10^{-5} M) upon titration with p(dGdC)$_2$; **RIGHT** Dependence of **AK2-A1** absorbance at λ_{max} = 483 nm on c(p(dG-dC)$_2$), at pH 7.0, sodium cacodylate buffer, I = 0.05 M.

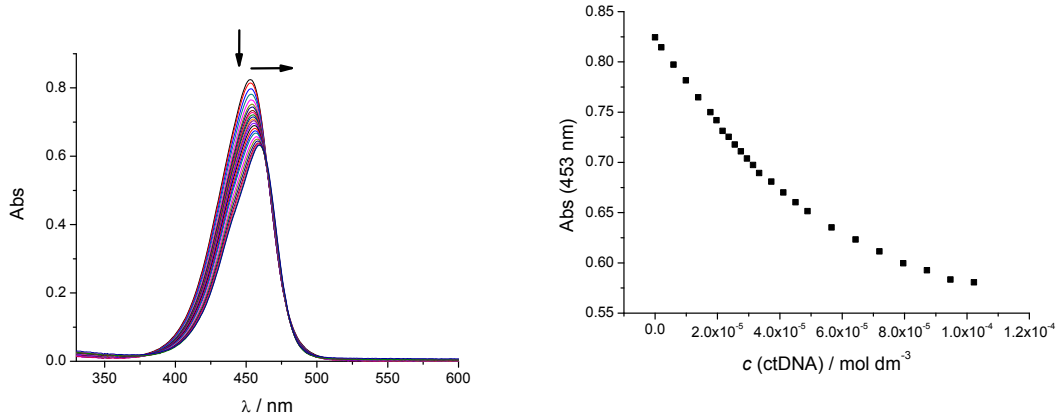

Figure S 6 LEFT Changes in UV/Vis spectrum of **A2** (c = 1.00 × 10^{-5} M) upon titration with ctDNA; **RIGHT** Dependence of **A2** absorbance at λ_{max} = 453 nm on c(ctDNA), at pH 7.0, sodium cacodylate buffer, I = 0.05 M.

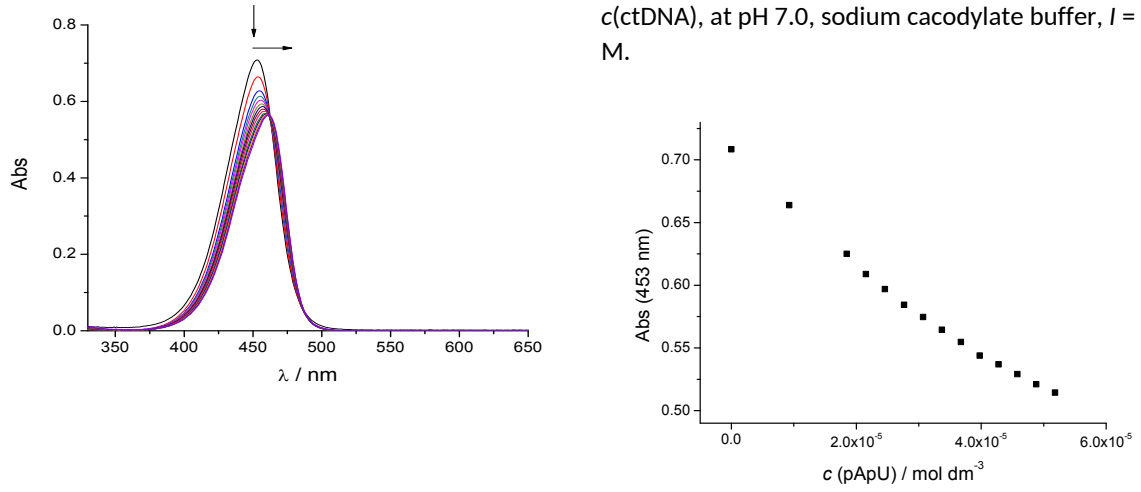

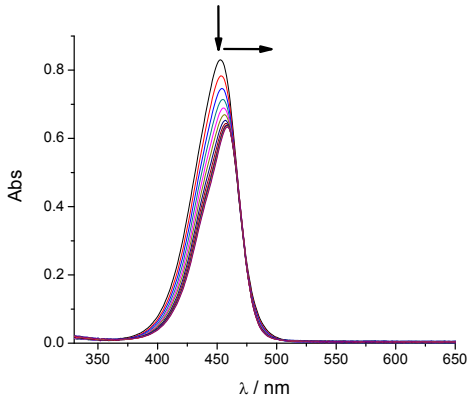

Figure S 7 LEFT Changes in UV/Vis spectrum of **A2** (c = 1.00 × 10^{-5} M) upon titration with pApU; **RIGHT** Dependence of **A2** absorbance at λ_{max} = 453 nm on c(pApU), at pH 7.0, sodium cacodylate buffer, I = 0.05 M.

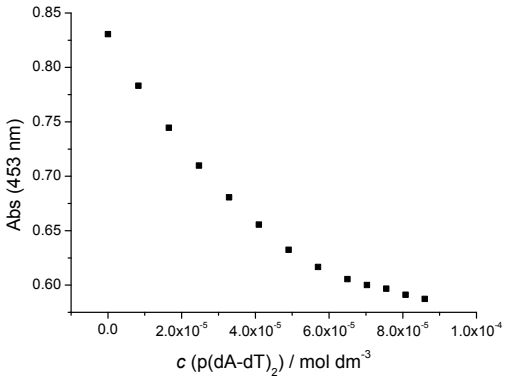

Figure S 8 LEFT Changes in UV/Vis spectrum of **A2** (c = 1.00 × 10^{-5} M) upon titration with p(dA-dT)$_2$; **RIGHT** Dependence of **A2** absorbance at λ_{max} = 453 nm on c(p(dA-dT)$_2$), at pH 7.0, sodium cacodylate buffer, I = 0.05 M.

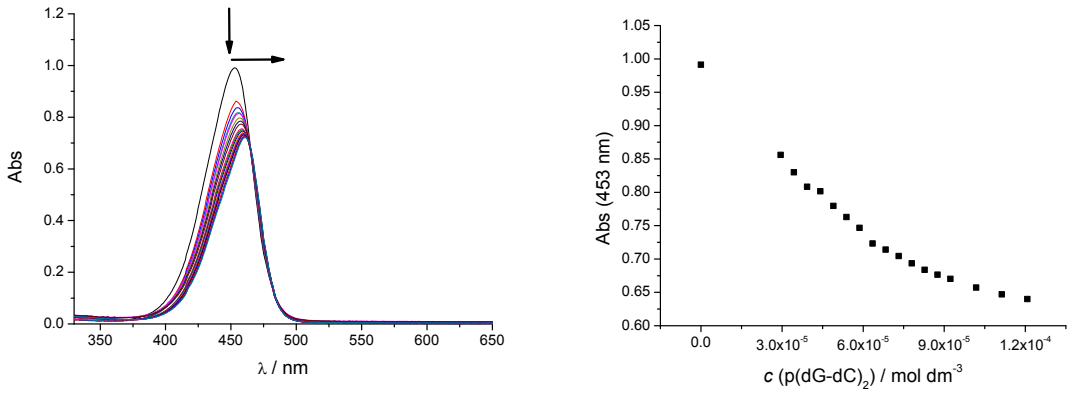

Figure S 9 LEFT Changes in UV/Vis spectrum of **A2** (c = 1.00 × 10^{-5} M) upon titration with p(dG-dC)$_2$; **RIGHT** Dependence of **AK2-A2** absorbance at λ_{max} = 453 nm on c(p(dG-dC)$_2$), at pH 7.0, sodium cacodylate buffer, I = 0.05 M.

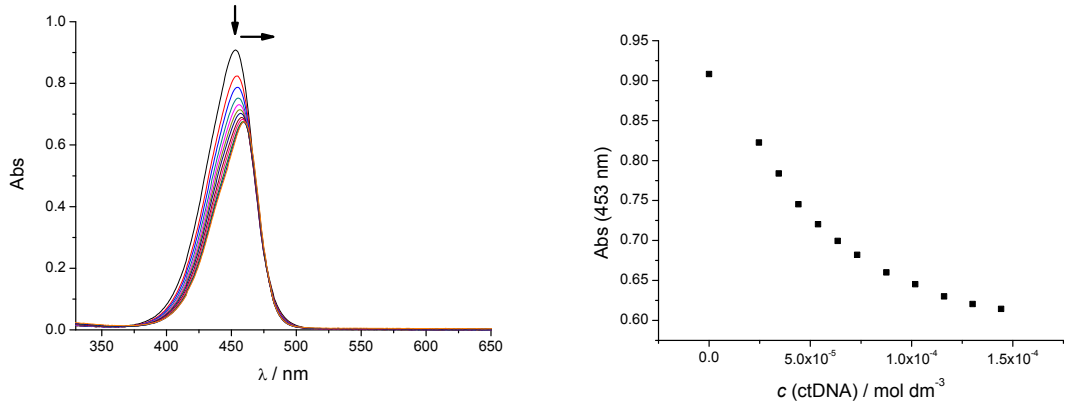

Figure S 10 LEFT Changes in UV/Vis spectrum of **A3** (c = 1.00 × 10^{-5} M) upon titration with ctDNA; **RIGHT** Dependence of **AK2-A3** absorbance at λ_{max} = 453 nm on c(ctDNA), at pH 7.0, sodium cacodylate buffer, I = 0.05 M.

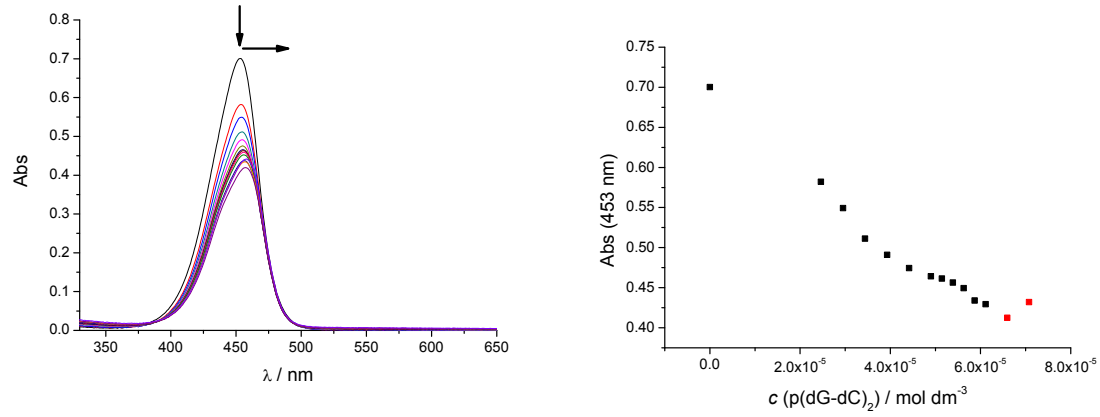

Figure S 11 LEFT Changes in UV/Vis spectrum of **A3** (c = 1.00 × 10^{-5} M) upon titration with p(dG-dC)$_2$; **RIGHT** Dependence of **AK2-A3** absorbance at λ_{max} = 453 nm on c(p(dG-dC)$_2$), at pH 7.0, sodium cacodylate buffer, I = 0.05 M.

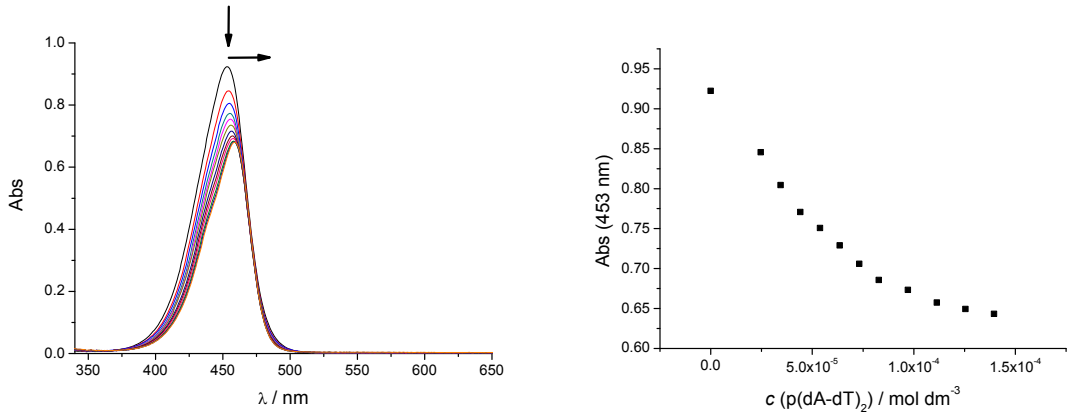

Figure S 12 LEFT Changes in UV/Vis spectrum of **A3** (c = 1.00 × 10^{-5} M) upon titration with p(dA-dT)$_2$; **RIGHT** Dependence of **A3** absorbance at λ_{max} = 453 nm on c(p(dA-dT)$_2$), at pH 7.0, sodium cacodylate buffer, I = 0.05 M.

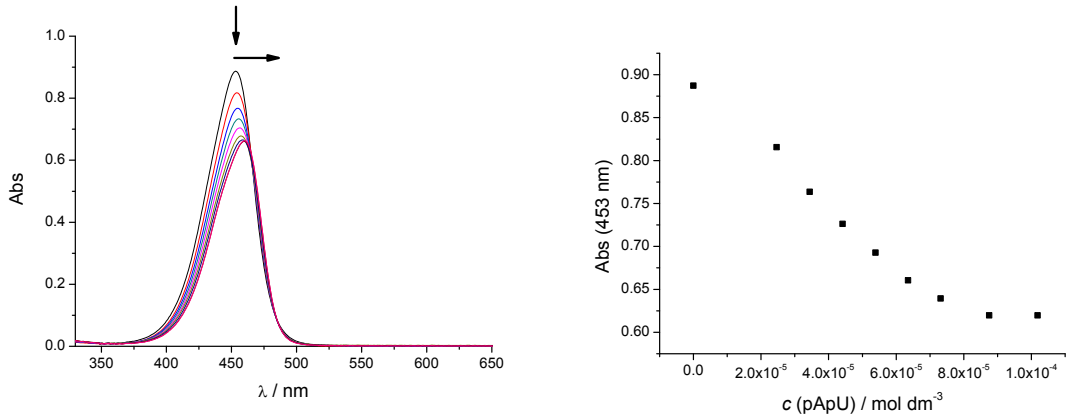

Figure S 13 LEFT Changes in UV/Vis spectrum of **A3** (c = 1.00 × 10^{-5} M) upon titration with pApU; **RIGHT** Dependence of **A3** absorbance at λ_{max} = 453 nm on c(pApU), at pH 7.0, sodium cacodylate buffer, I = 0.05 M.

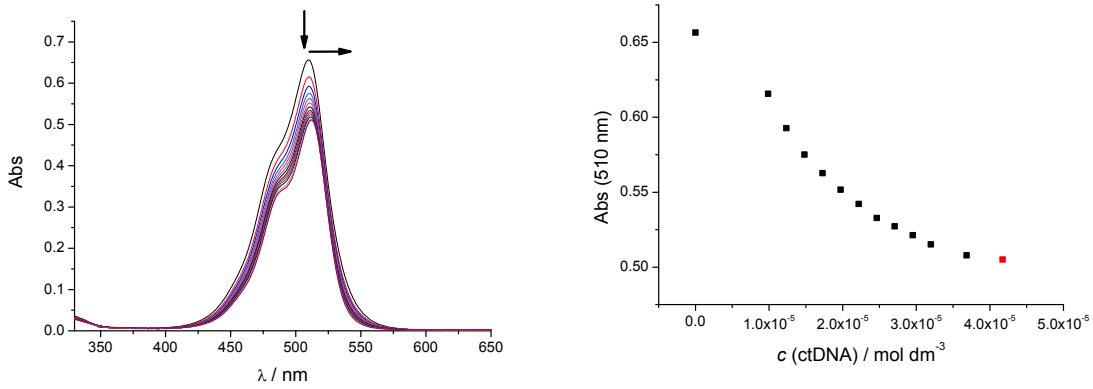

Figure S 14 LEFT Changes in UV/Vis spectrum of **A4** (c = 1.00 × 10^{-5} M) upon titration with ctDNA; **RIGHT** Dependence of **A4** absorbance at λ_{max} = 510 nm on c(ctDNA), at pH 7.0, sodium cacodylate buffer, I = 0.05 M.

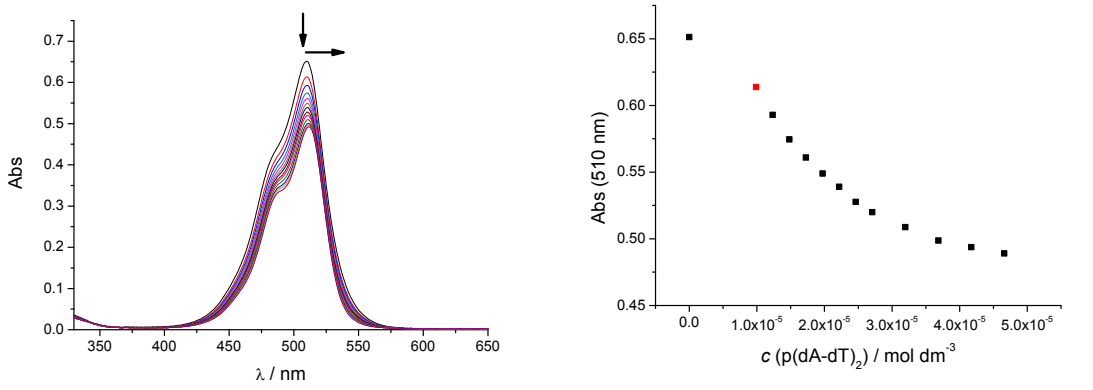

Figure S 15 LEFT Changes in UV/Vis spectrum of **A4** (c = 1.00 × 10^{-5} M) upon titration with p(dA-dT)$_2$; **RIGHT** Dependence of **A4** absorbance at λ_{max} = 510 nm on c(p(dA-dT)$_2$), at pH 7.0, sodium cacodylate buffer, I = 0.05 M.

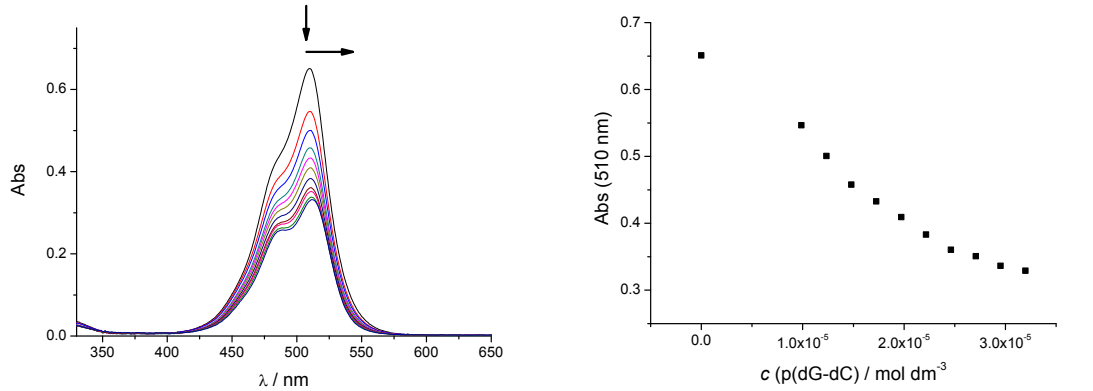

Figure S 16 LEFT Changes in UV/Vis spectrum of **A4** (c = 1.00 × 10^{-5} M) upon titration with p(dG-dC)$_2$; **RIGHT** Dependence of **A4** absorbance at λ_{max} = 510 nm on c(p(dG-dC)$_2$), at pH 7.0, sodium cacodylate buffer, I = 0.05 M.

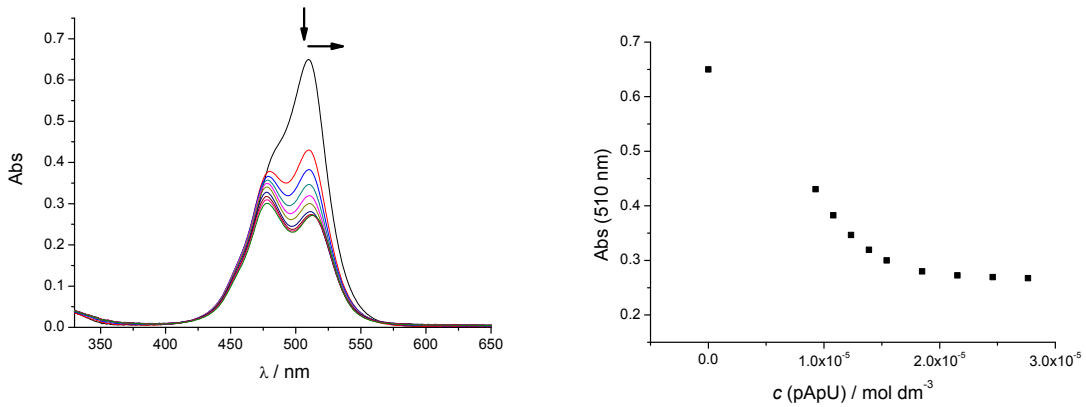

Figure S 17 LEFT Changes in UV/Vis spectrum of **A4** (c = 1.00 × 10^{-5} M) upon titration with pApU; **RIGHT** Dependence of **A4** absorbance at λ_{max} = 510 nm on c(pApU), at pH 7.0, sodium cacodylate buffer, I = 0.05 M.

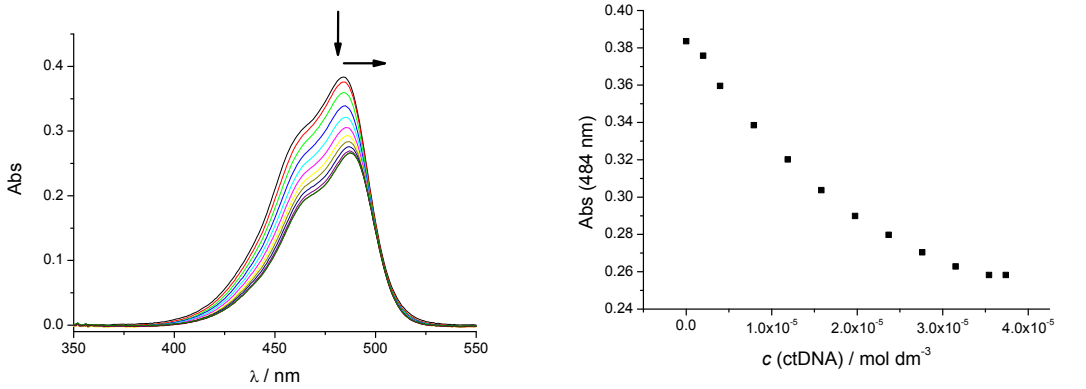

Figure S 18 LEFT Changes in UV/Vis spectrum of **A7** (c = 6.81 × 10^{-6} M) upon titration with ctDNA; **RIGHT** Dependence of **AK2-A7** absorbance at λ_{max} = 484 nm on c(ctDNA), at pH 7.0, sodium cacodylate buffer, I = 0.05 M.

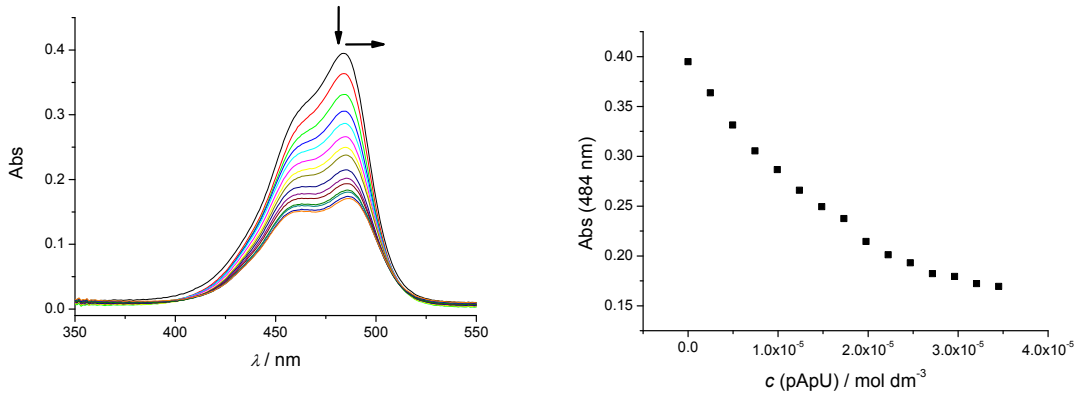

Figure S 19 LEFT Changes in UV/Vis spectrum of **A7** (c = 6.81 × 10^{-6} M) upon titration with pApU; **RIGHT** Dependence of **AK2-A7** absorbance at λ_{max} = 484 nm on c(pApU), at pH 7.0, sodium cacodylate buffer, I = 0.05 M.

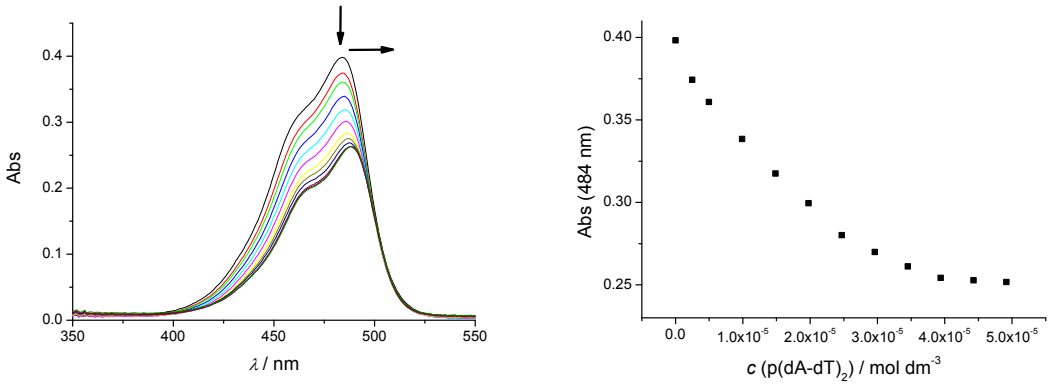

Figure S 20 LEFT Changes in UV/Vis spectrum of **A7** (c = 6.81 × 10^{-6} M) upon titration with p(dA-dT)$_2$; **RIGHT** Dependence of **AK2-A7** absorbance at λ_{max} = 484 nm on c(p(dA-dT)$_2$), at pH 7.0, sodium cacodylate buffer, I = 0.05 M.

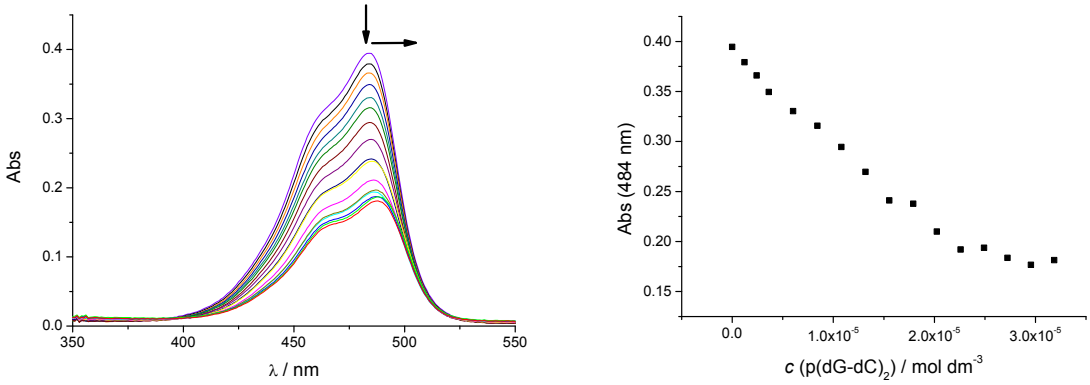

Figure S 21 LEFT Changes in UV/Vis spectrum of **A7** (c = 6.81 × 10^{-6} M) upon titration with p(dG-dC); **RIGHT** Dependence of **AK2-A7** absorbance at λ_{max} = 484 nm on c(p(dG-dC)$_2$), at pH 7.0, sodium cacodylate buffer, I = 0.05 M.

3.2 Fluorescence spectrophotometric titrations

General conditions: slits 2.5-5; emission at 508 nm; excitation: 483 nm

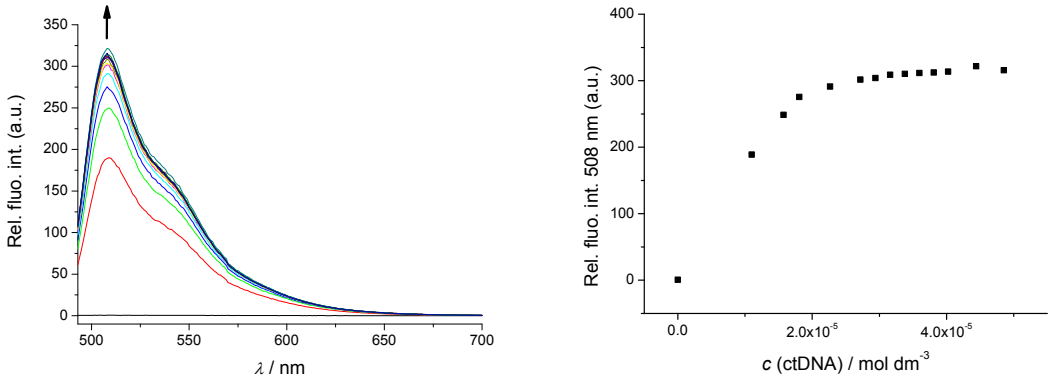

Figure S 22 LEFT Changes in fluorescence spectrum of **A1** (c = 1.00 × 10^{-6} M) upon titration with ctDNA **RIGHT** Dependence of **A1** intensity at λ_{max} = 508 nm on c(ctDNA), at pH 7.0, sodium cacodylate buffer, I = 0.05 M.

General conditions: slits 5-5; emission at 513 nm; excitation: 483 nm

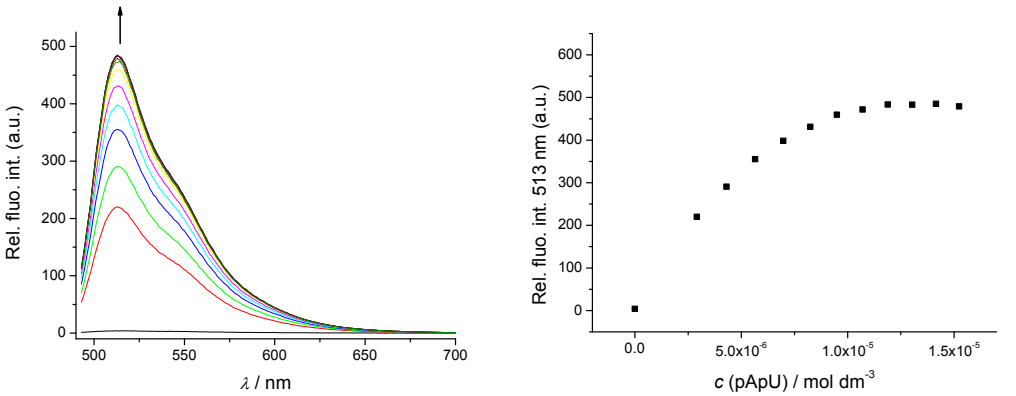

Figure S 23 LEFT Changes in fluorescence spectrum of **A1** (c = 1.00 × 10^{-6} M) upon titration with pApU **RIGHT** Dependence of **A1** intensity at λ_{max} = 513 nm on c(pApU), at pH 7.0, sodium cacodylate buffer, I = 0.05 M.

General conditions: slits 5-5; emission at 508 nm; excitation: 483 nm

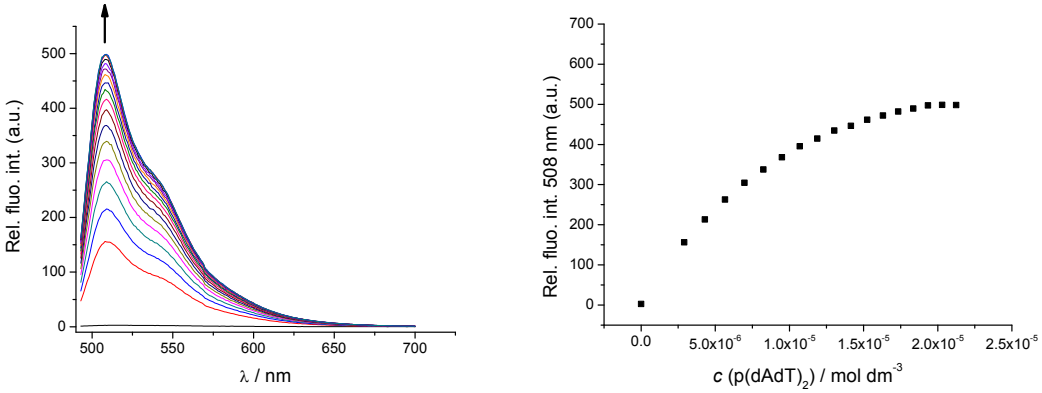

Figure S 24 LEFT Changes in fluorescence spectrum of **A1** (c = 1.00 × 10^{-6} M) upon titration with p(dA-dT)$_2$ **RIGHT** Dependence of **A1** intensity at λ_{max} = 508 nm on c(p(dA-dT)$_2$), at pH 7.0, sodium cacodylate buffer, I = 0.05 M.

General conditions: slits 5-5; emission at 508 nm; excitation: 483 nm

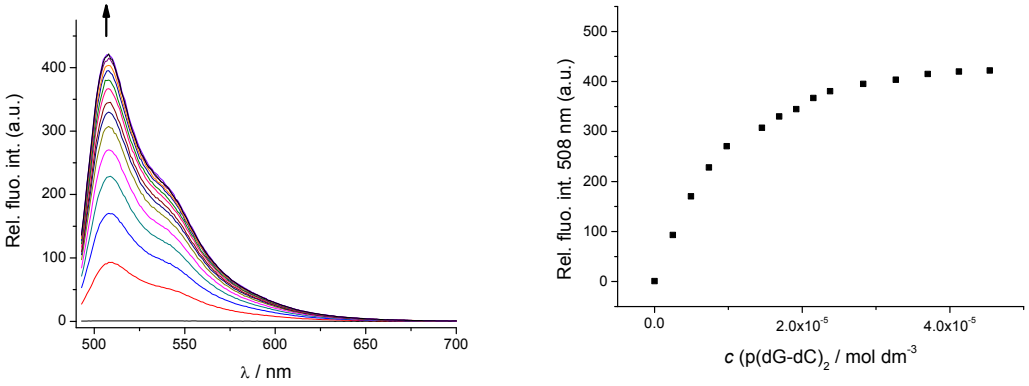

Figure S 25 LEFT Changes in fluorescence spectrum of **A1** (c = 1.00 × 10^{-6} M) upon titration with p(dG-dC)$_2$; **RIGHT** Dependence of **A1** intensity at λ_{max} = 508 nm on c(p(dG-dC)$_2$), at pH 7.0, sodium cacodylate buffer, I = 0.05 M.

General conditions: slits 5-5; emission at 485 nm; excitation: 453

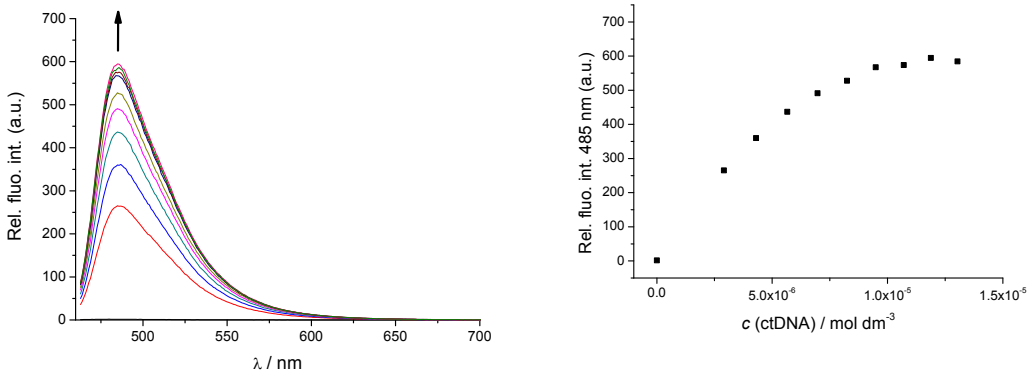

Figure S 26 LEFT Changes in fluorescence spectrum of **A2** (c = 1.00 × 10^{-6} M) upon titration with ctDNA; **RIGHT** Dependence of **A2** intensity at λ_{max} = 485 nm on c(ctDNA), at pH 7.0, sodium cacodylate buffer, I = 0.05 M.

General conditions: slits 2.5-5; emission at 488 nm; excitation: 453 nm

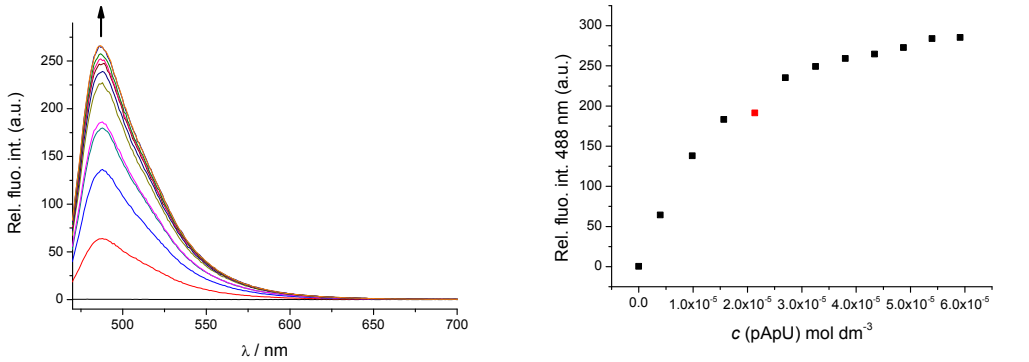

Figure S 27 LEFT Changes in fluorescence spectrum of **A2** (c = 1.00 × 10^{-6} M) upon titration with pApU; **RIGHT** Dependence of **A2** intensity at λ_{max} = 488 nm on c(pApU), at pH 7.0, sodium cacodylate buffer, I = 0.05 M.

General conditions: slits 2.5-5; emission at 485 nm; excitation: 453 nm

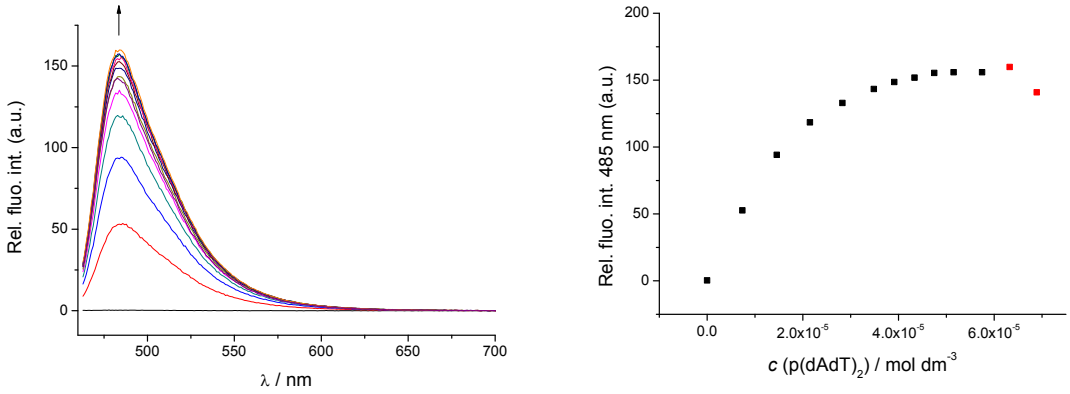

Figure S 28 LEFT Changes in fluorescence spectrum of **A2** (c = 1.00 × 10^{-6} M) upon titration with p(dA-dT)$_2$; **RIGHT** Dependence of **A2** intensity at λ_{max} = 485 nm on c(p(dA-dT)$_2$), at pH 7.0, sodium cacodylate buffer, I = 0.05 M.

General conditions: slits 5-5; emission at 488 nm; excitation: 453 nm

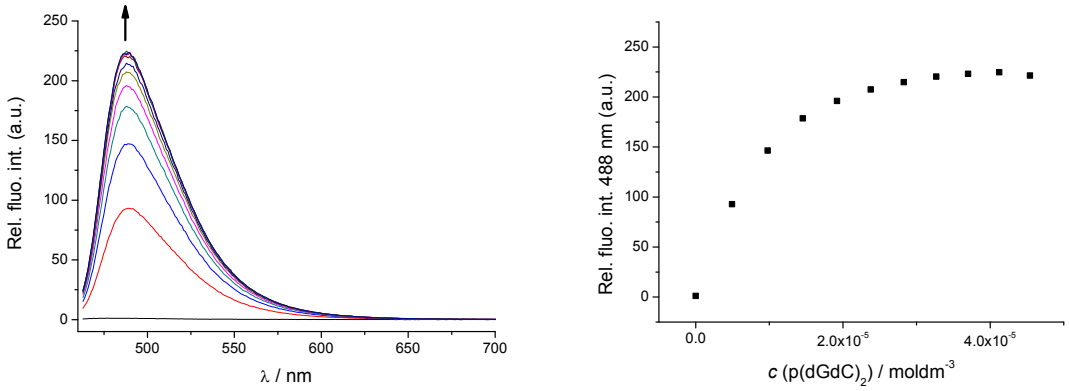

Figure S 29 LEFT Changes in fluorescence spectrum of **A2** (c = 1.00 × 10^{-6} M) upon titration with p(dG-dC)$_2$; **RIGHT** Dependence of **A2** intensity at λ_{max} = 488 nm on c(p(dG-dC)$_2$), at pH 7.0, sodium cacodylate buffer, I = 0.05 M.

General conditions: slits 5-5; emission at 484 nm; excitation: 453 nm

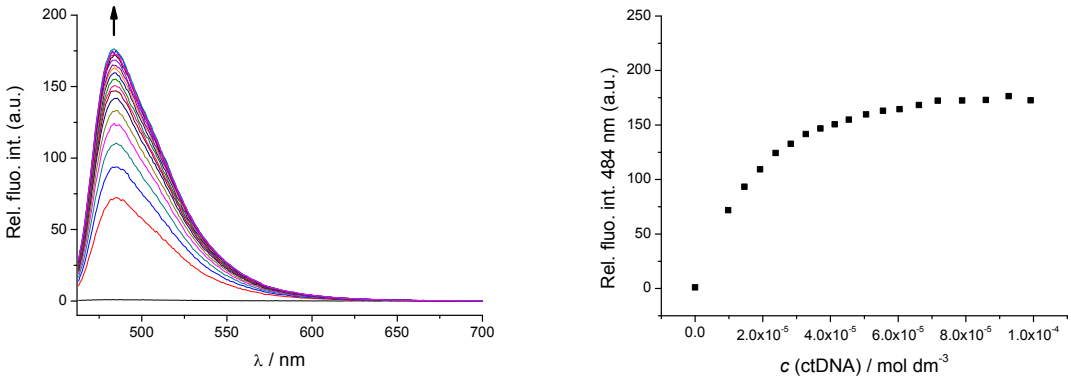

Figure S 30 LEFT Changes in fluorescence spectrum of **A3** (c = 1.00 × 10^{-6} M) upon titration with ctDNA; **RIGHT** Dependence of **A3** intensity at λ_{max} = 484 nm on c(ctDNA), at pH 7.0, sodium cacodylate buffer, I = 0.05 M.

General conditions: slits 5-5; emission at 487 nm; excitation: 453 nm

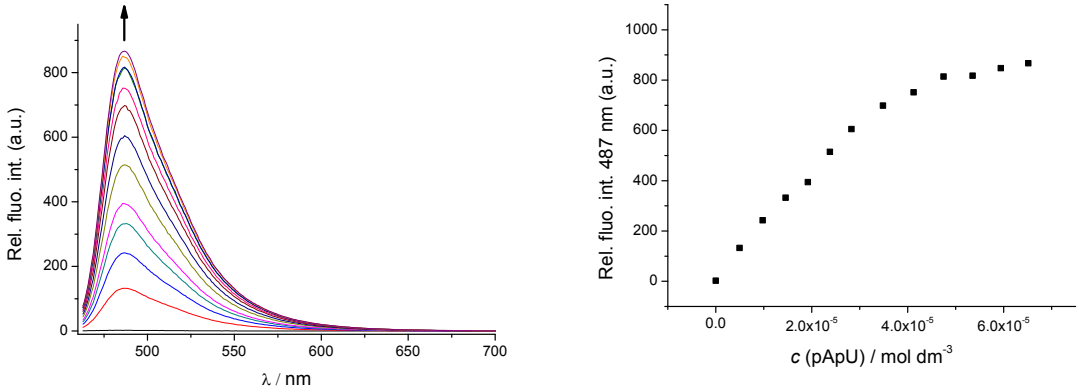

Figure S 31 LEFT Changes in fluorescence spectrum of **A3** (c = 1.00 × 10^{-6} M) upon titration with pApU; **RIGHT** Dependence of **A3** intensity at λ_{max} = 487 nm on c(pApU), at pH 7.0, sodium cacodylate buffer, I = 0.05 M.

General conditions: slits 5-5; emission at 484 nm; excitation: 453 nm

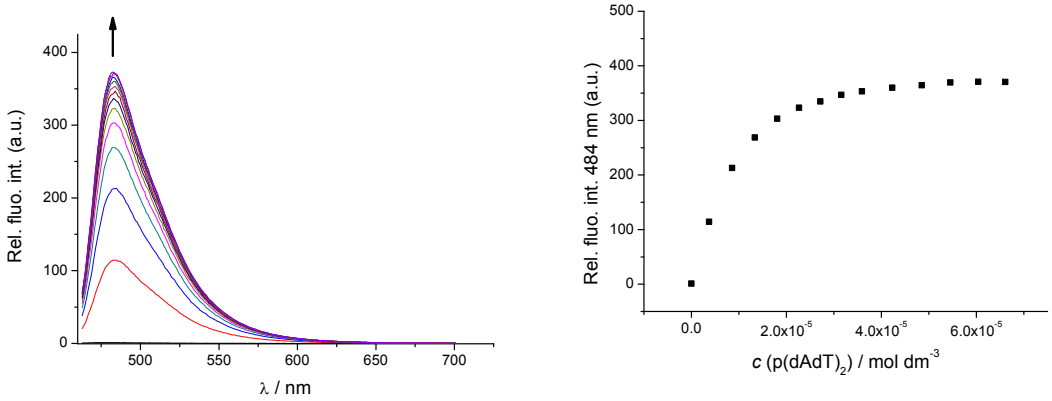

Figure S 32 LEFT Changes in fluorescence spectrum of **A3** (c = 1.00 × 10^{-6} M) upon titration with p(dA-dT)$_2$; **RIGHT** Dependence of **A3** intensity at λ_{max} = 484 nm on c(p(dA-dT)$_2$), at pH 7.0, sodium cacodylate buffer, I = 0.05 M.

General conditions: slits 5-5; emission at 489 nm; excitation: 453 nm

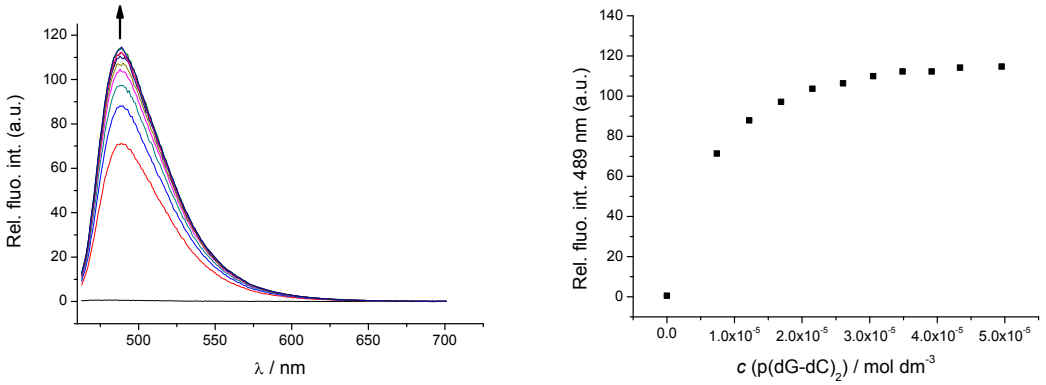

Figure S 33 LEFT Changes in fluorescence spectrum of **A3** (c= 1.00 × 10^{-6} M) upon titration with p(dG-dC)$_2$; **RIGHT** Dependence of **A3** intensity at λ_{max} = 489 nm on c(p(dG-dC)$_2$), at pH 7.0, sodium cacodylate buffer, I = 0.05 M.

General conditions: slits 5-5; emission at 533 nm; excitation: 510 nm

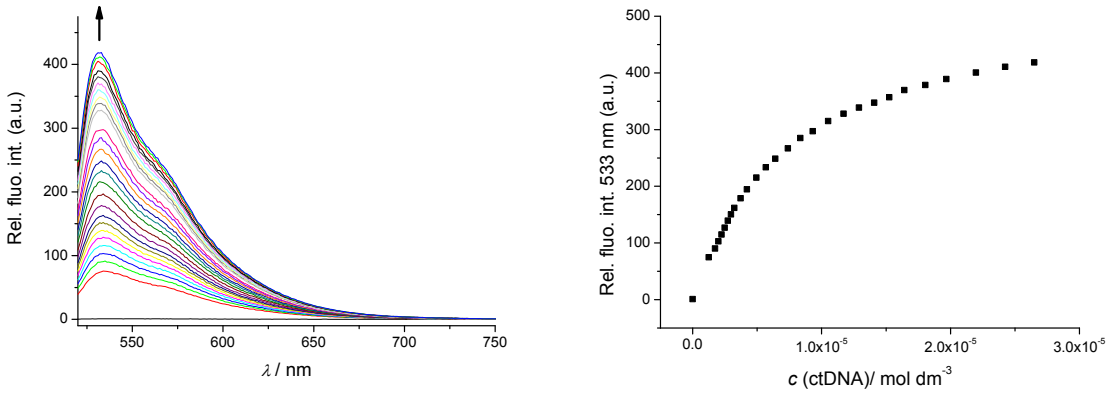

Figure S 34 LEFT Changes in fluorescence spectrum of **A4** (c = 1.00 × 10^{-6} M) upon titration with ctDNA; **RIGHT** Dependence of **A4** intensity at λ_{max} = 533 nm on c(ctDNA), at pH 7.0, sodium cacodylate buffer, I = 0.05 M.

General conditions: slits 5-5; emission at 539 nm; excitation: 510 nm

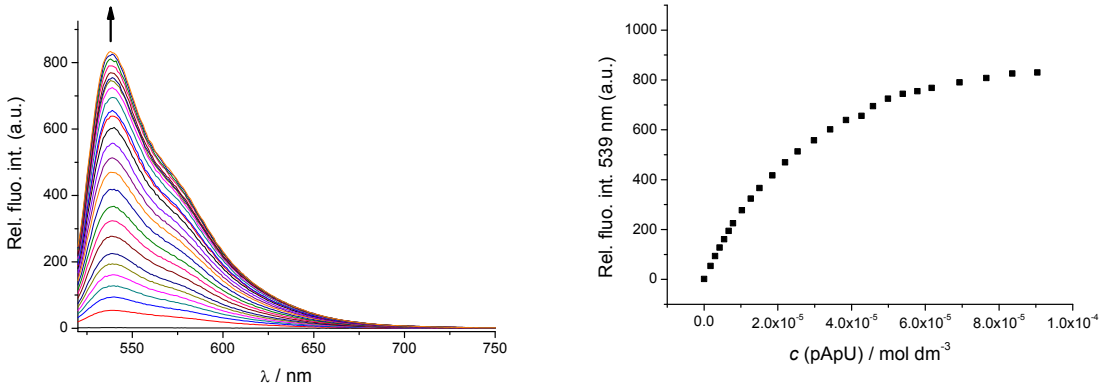

Figure S 35 LEFT Changes in fluorescence spectrum of **A4** (c = 1.00 × 10^{-6} M) upon titration with pApU; **RIGHT** Dependence of **A4** intensity at λ_{max} = 539 nm on c(pApU), at pH 7.0, sodium cacodylate buffer, I = 0.05 M.

General conditions: slits 5-5; emission at 532 nm; excitation: 510 nm

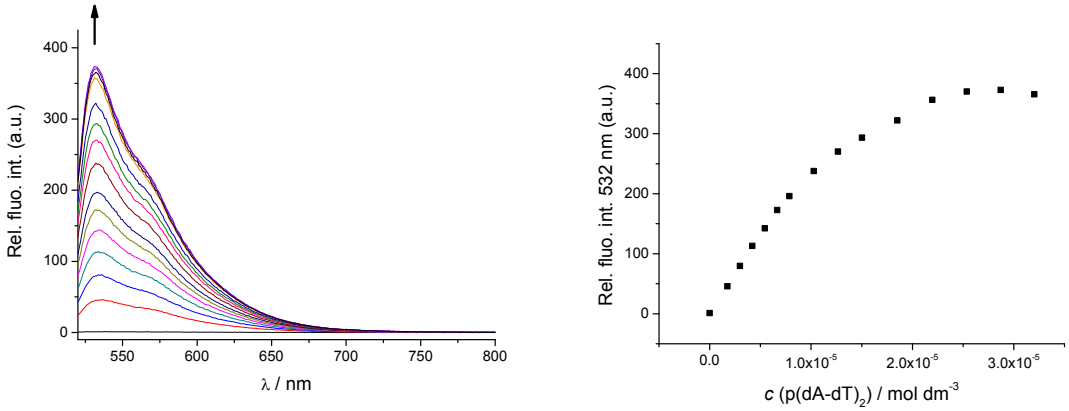

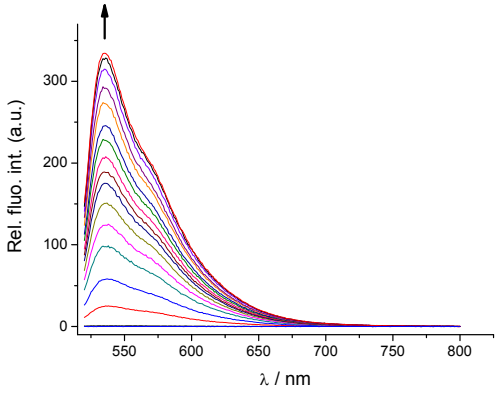

Figure S 36 LEFT Changes in fluorescence spectrum of **A4** (c = 1.00 × 10^{-6} M) upon titration with p(dA-dT)$_2$; **RIGHT** Dependence of**A4** intensity at λ_{max} = 532 nm on c(p(dA-dT)$_2$), at pH 7.0, sodium cacodylate buffer, I = 0.05 M.

General conditions: slits 5-5; emission at 535 nm; excitation: 510 nm

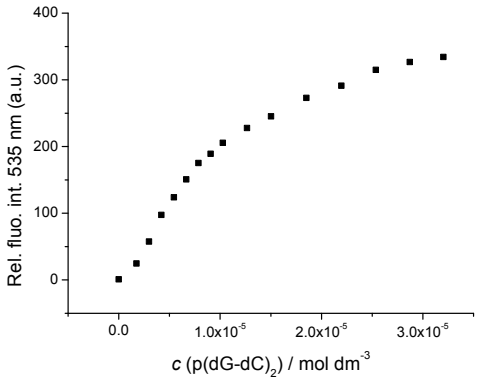

Figure S 37 LEFT Changes in fluorescence spectrum of **A4** (c = 1.00 × 10^{-6} M) upon titration with p(dG-dC)$_2$; **RIGHT** Dependence of **A4** intensity at λ_{max} = 535 nm on c(p(dG-dC)$_2$), at pH 7.0, sodium cacodylate buffer, I = 0.05 M.

General conditions: slits 5-5; emission at 537 nm; excitation: 484 nm

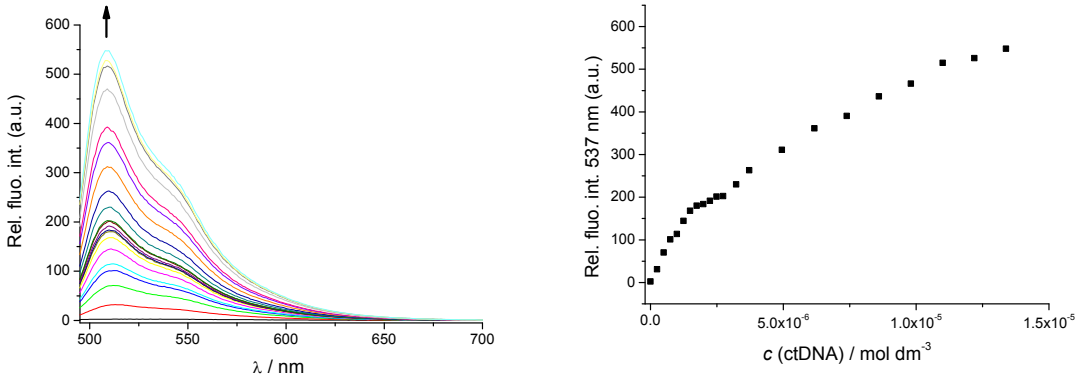

Figure S 38 LEFT Changes in fluorescence spectrum of **A7** (c = 9.80 × 10^{-7} M) upon titration with ctDNA; **RIGHT** Dependence of **A7** intensity at λ_{max} = 537 nm on c(ctDNA), at pH 7.0, sodium cacodylate buffer, I = 0.05 M.

General conditions: slits 5-5; emission at 514 nm; excitation: 484 nm

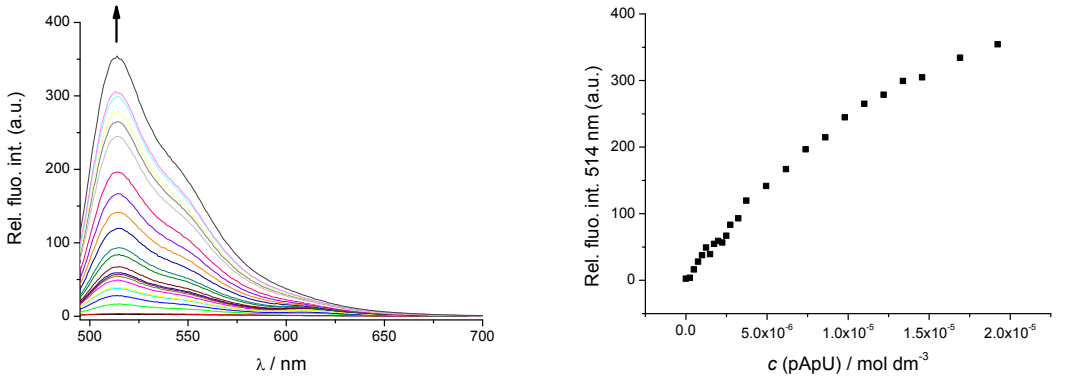

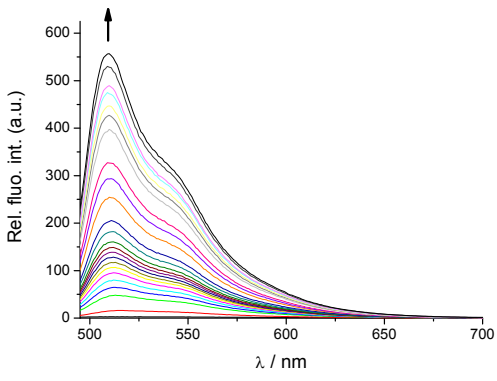

Figure S 39 LEFT Changes in fluorescence spectrum of **A7** (c = 9.80 × 10^{-7} M) upon titration with pApU; **RIGHT** Dependence of **A7** intensity at λ_{max} = 514 nm on c(pApU), at pH 7.0, sodium cacodylate buffer, I = 0.05 M.

General conditions: slits 5-5; emission at 510 nm; excitation: 484 nm

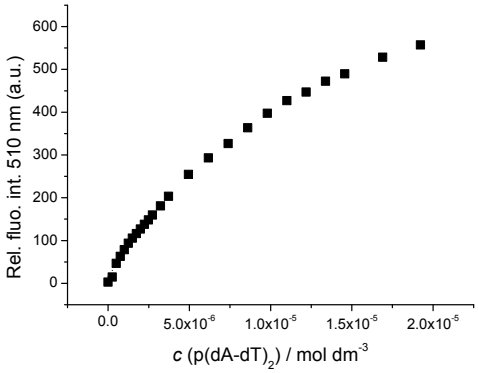

Figure S 40 LEFT Changes in fluorescence spectrum of **A7** (c = 9.80 × 10^{-7} M) upon titration with p(dA-dT)$_2$; **RIGHT** Dependence of **A7** intensity at λ_{max} = 510 nm on c(p(dA-dT)$_2$), at pH 7.0, sodium cacodylate buffer, I = 0.05 M.

General conditions: slits 5-5; emission at 510 nm; excitation: 484 nm

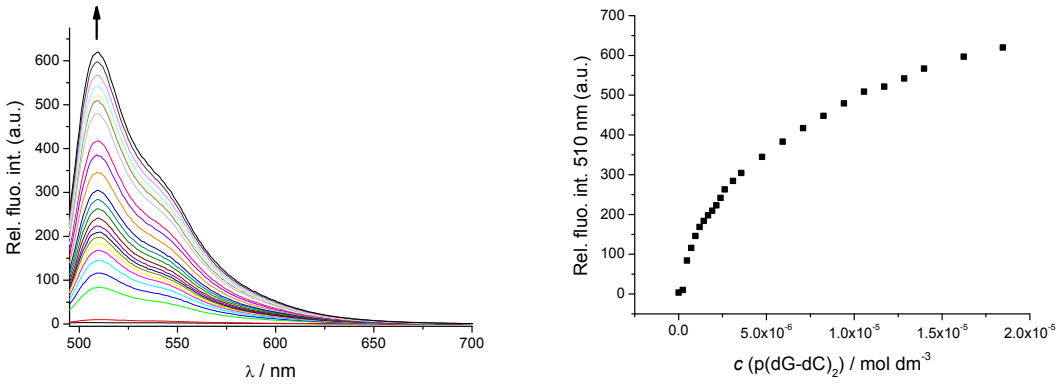

Figure S 41 LEFT Changes in fluorescence spectrum of **A7** (c = 9.80 × 10^{-7} M) upon titration with p(dG-dC)$_2$; **RIGHT** Dependence of **A7** intensity at λ_{max} = 510 nm on c(p(dG-dC)$_2$), at pH 7.0, sodium cacodylate buffer, I = 0.05 M.

3.3 CD Spectroscopy

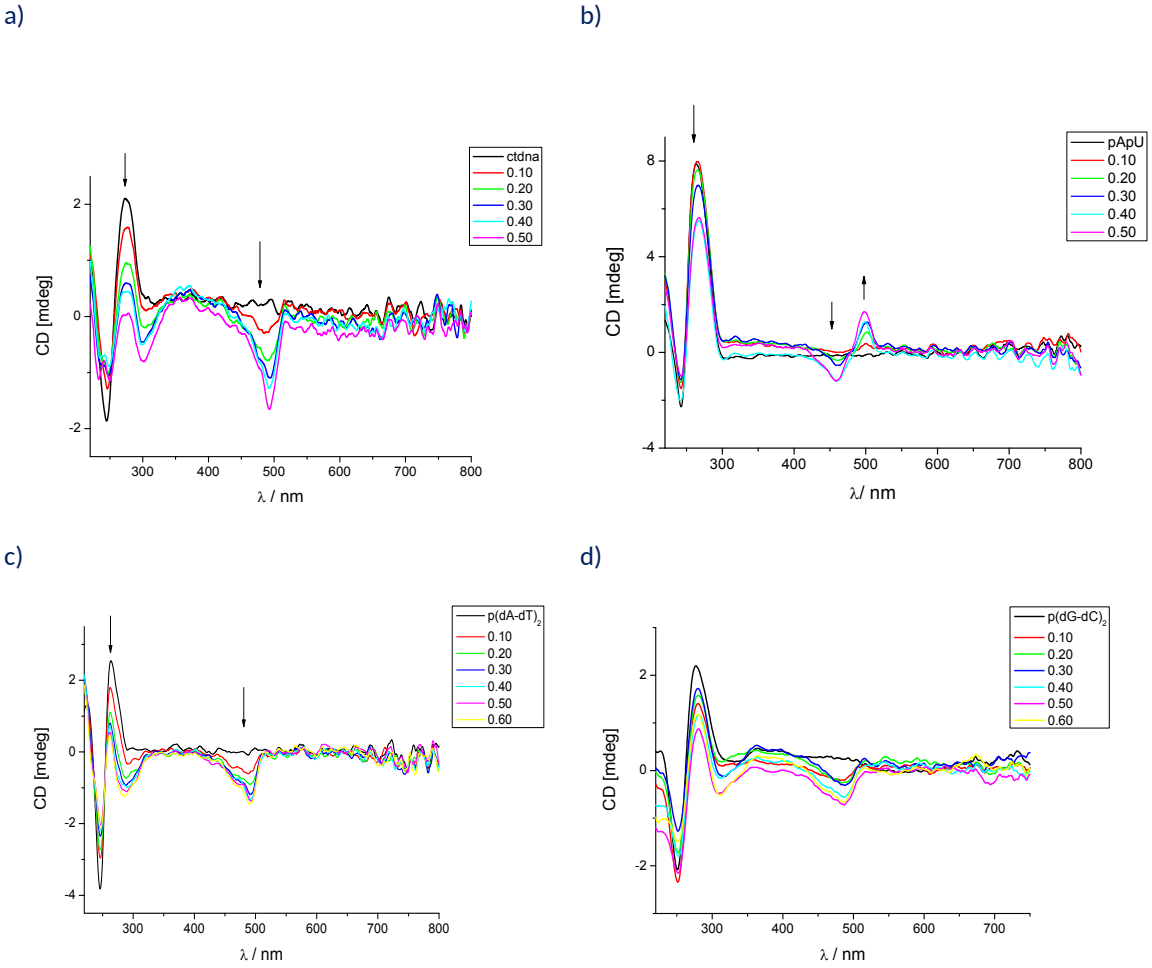

Figure S 42. CD titration of a) ctDNA (c = $2*10^{-5}$ M), b) pApU (c = $2*10^{-5}$ M), c) $p(dA\text{-}dT)_2$(c =$2*10^{-5}$ M), d) $p(dG\text{-}dC)_2$ (c = $2*10^{-5}$ M) with **A1** at molar ratios r = [compound] / [nucleotide] (pH 7.0, buffer sodium cacodylate, *I* = 0.05 M).

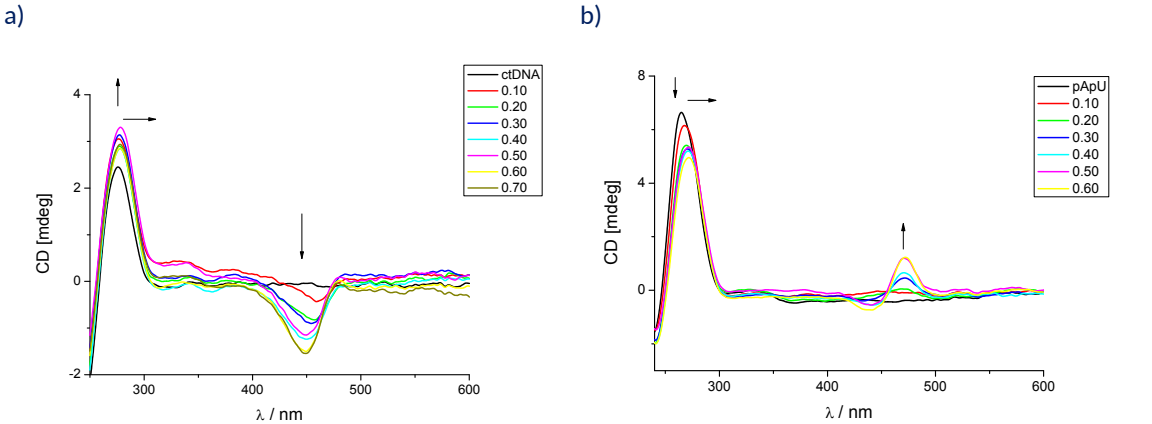

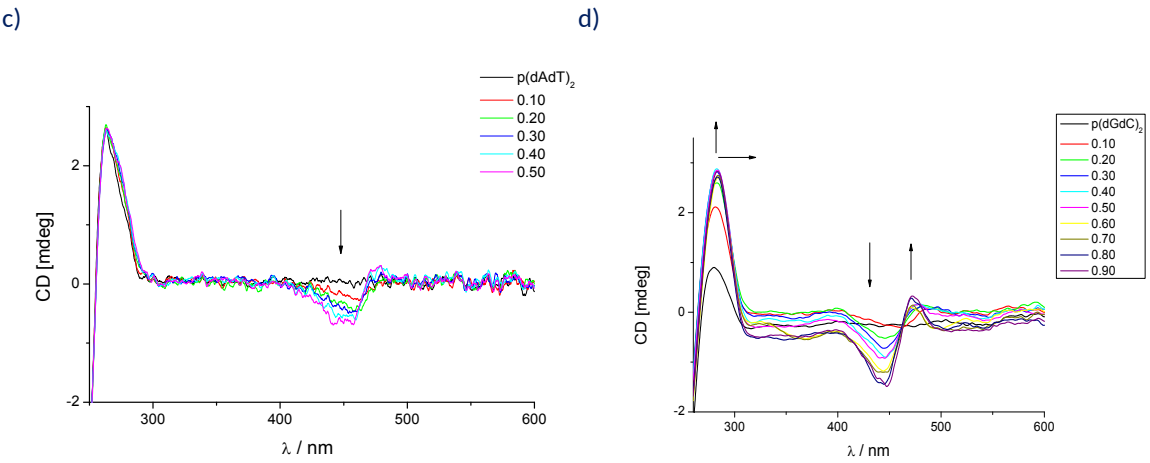

Figure S 43 CD titration of a) ctDNA (c = 2*10^{-5} M), b) pApU (c = 2*10^{-5} M), c) p(dA-dT)$_2$(c =2*10^{-5} M), d) p(dG-dC)$_2$ (c = 2*10^{-5} M) with **A2** at molar ratios r = [compound] / [nucleotide] (pH 7.0, buffer sodium cacodylate, *I* = 0.05 M).

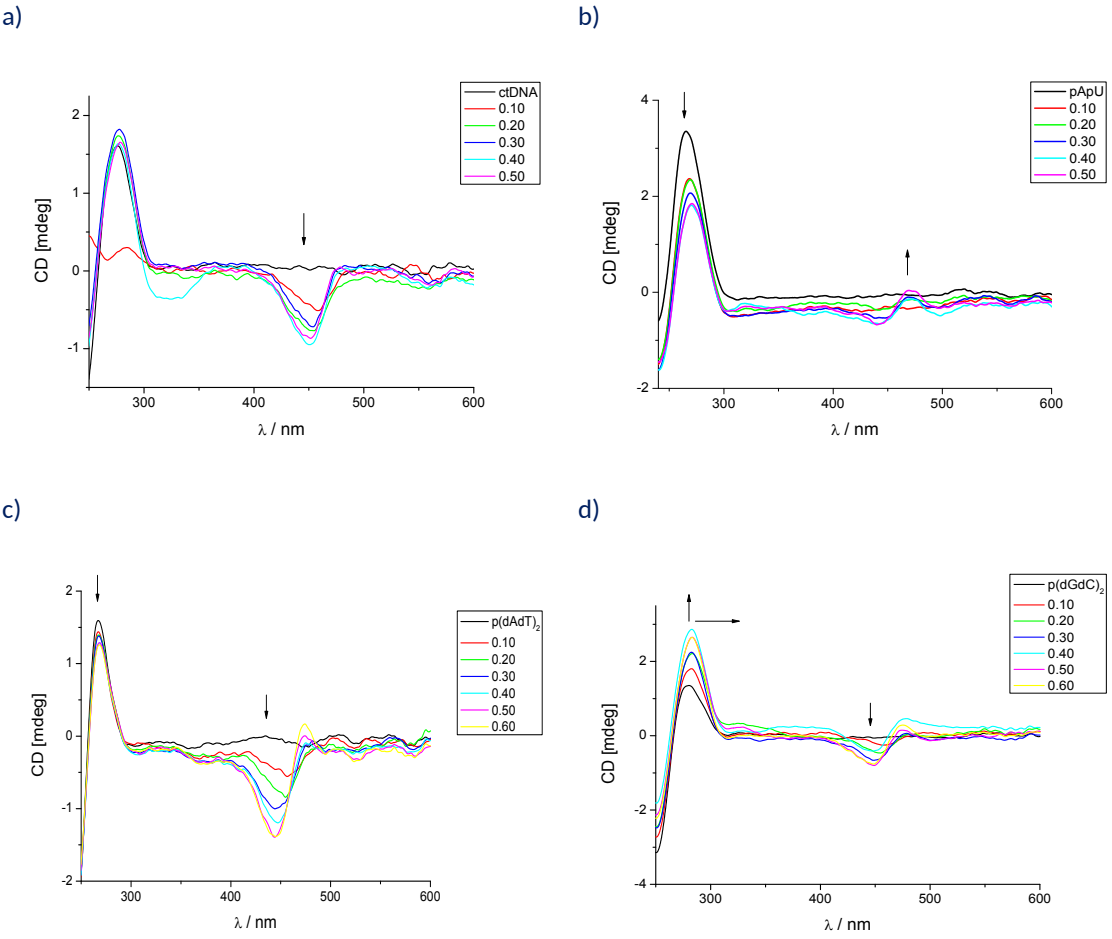

Figure S 44. CD titration of a) ctDNA (c = 2*10^{-5} M), b) pApU (c = 2*10^{-5} M), c) p(dA-dT)$_2$(c =2*10^{-5} M), d) p(dG-dC)$_2$ (c = 2*10^{-5} M) with **A3** at molar ratios r = [compound] / [nucleotide] (pH 7.0, buffer sodium cacodylate, *I* = 0.05 M).

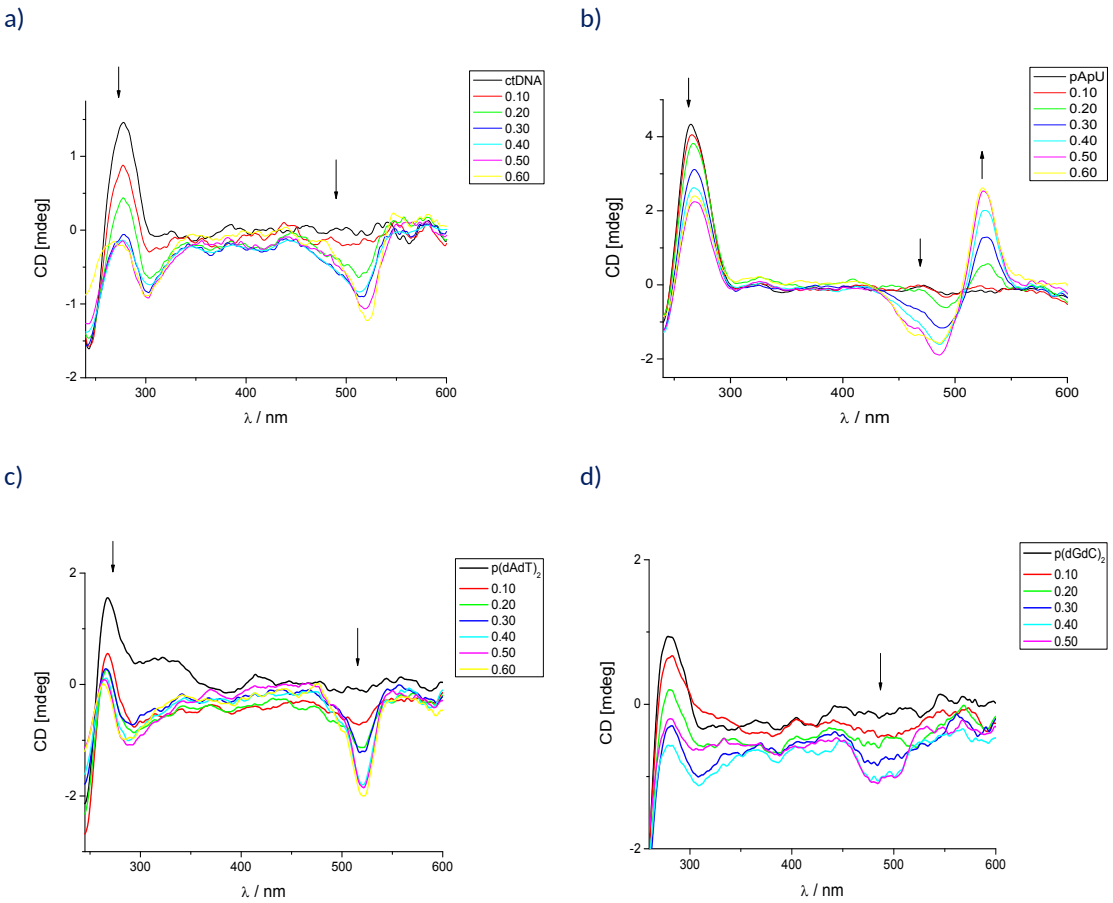

Figure S 45. CD titration of a) ctDNA (c = 2*10^{-5} M), b) pApU (c = 2*10^{-5} M), c) p(dA-dT)$_2$ (c =2*10^{-5} M), d) p(dG-dC)$_2$ (c = 2*10^{-5} M) with **A4** at molar ratios r = [compound] / [nucleotide] (pH 7.0, buffer sodium cacodylate, *I* = 0.05 M).

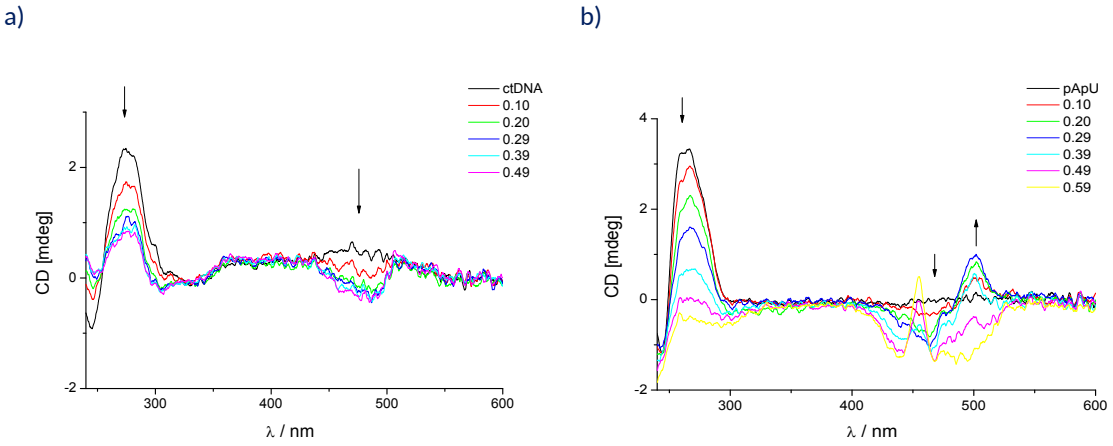

c) d)

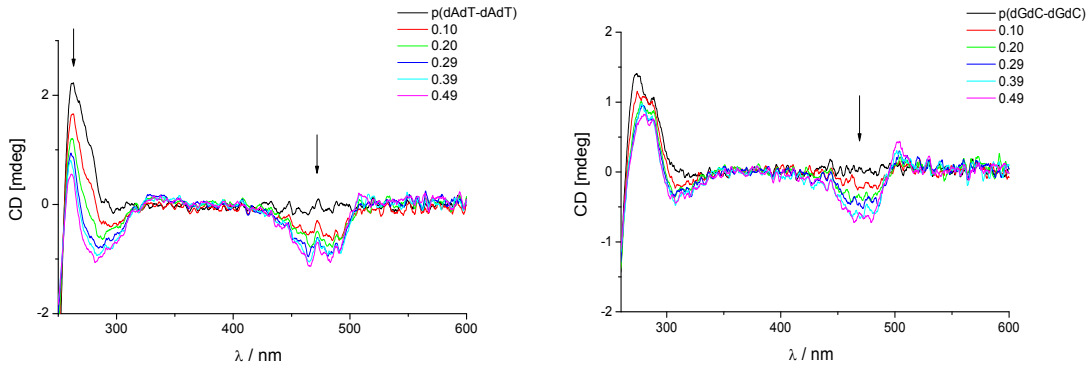

Figure S 46. CD titration of a) ctDNA (c = $2*10^{-5}$ M), b) pApU (c = $2*10^{-5}$ M), c) $p(dA\text{-}dT)_2$(c =$2*10^{-5}$ M), d) $p(dG\text{-}dC)_2$ (c = $2*10^{-5}$ M) with **A7** at molar ratios r = [compound] / [nucleotide] (pH 7.0, buffer sodium cacodylate, *I* = 0.05 M).

3.4 Isothermal titration calorimetry

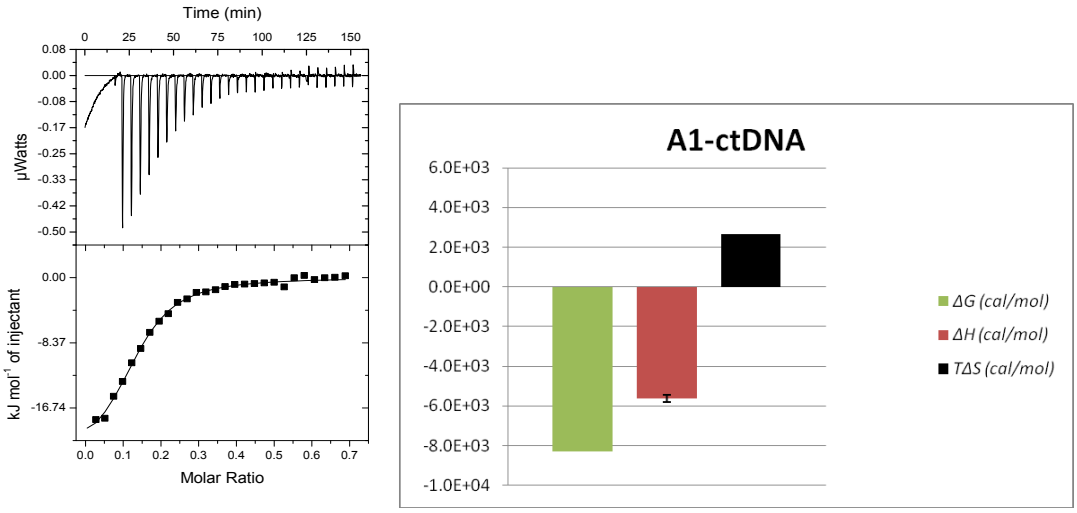

Figure S 47. left) ITC titration of ctDNA (c=28.8 µM) with **A1** (c=100 µM); right) Thermodynamic parameters of the binding.

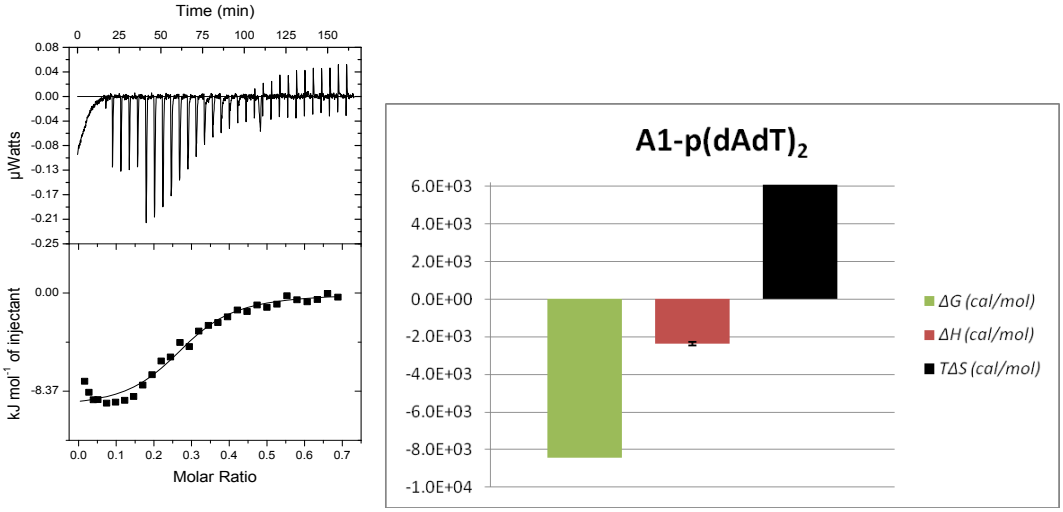

Figure S 48. left) ITC titration of $p(dAdT)_2$ (c=33.5 µM) with **A1** (c=100 µM); right) Thermodynamic parameters of the binding.

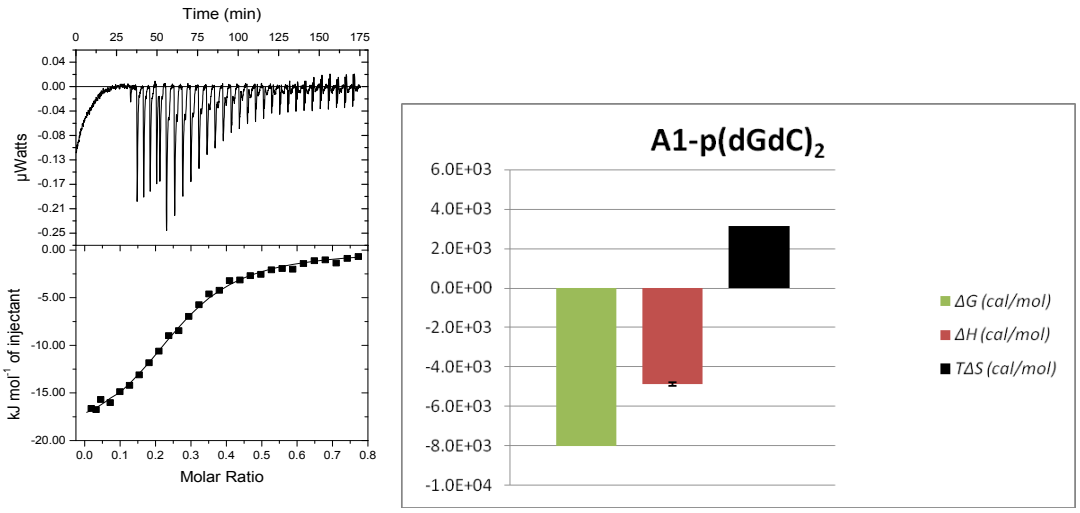

Figure S 49. left) ITC titration of $p(dGdC)_2$ (c=26.2 µM) with **A1** (c=100 µM); right) Thermodynamic parameters of the binding.

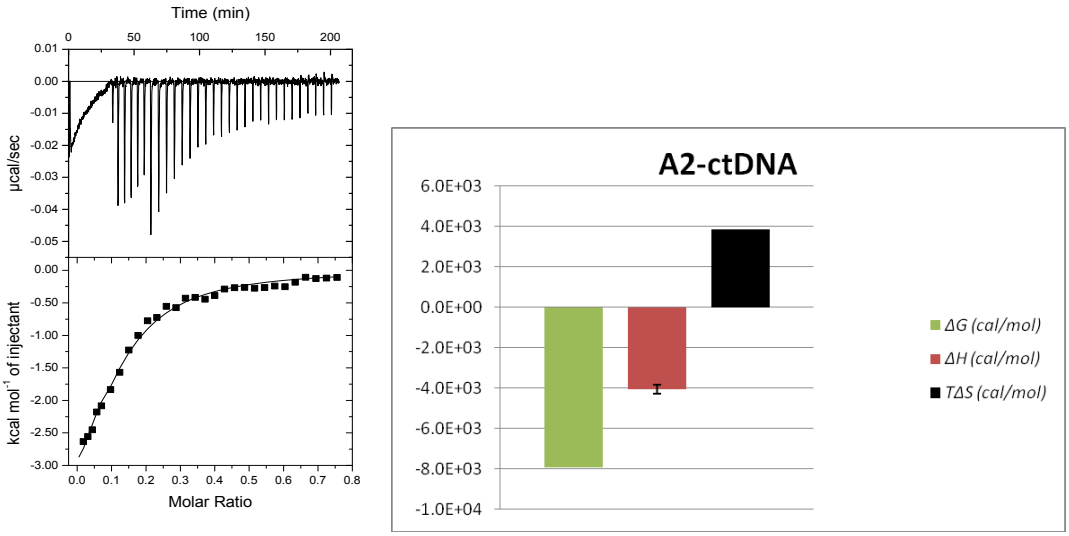

Figure S 50. left) ITC titration of ctDNA (c=26.82 µM) with **A2** (c=100 µM); right) Thermodynamic parameters of the binding.

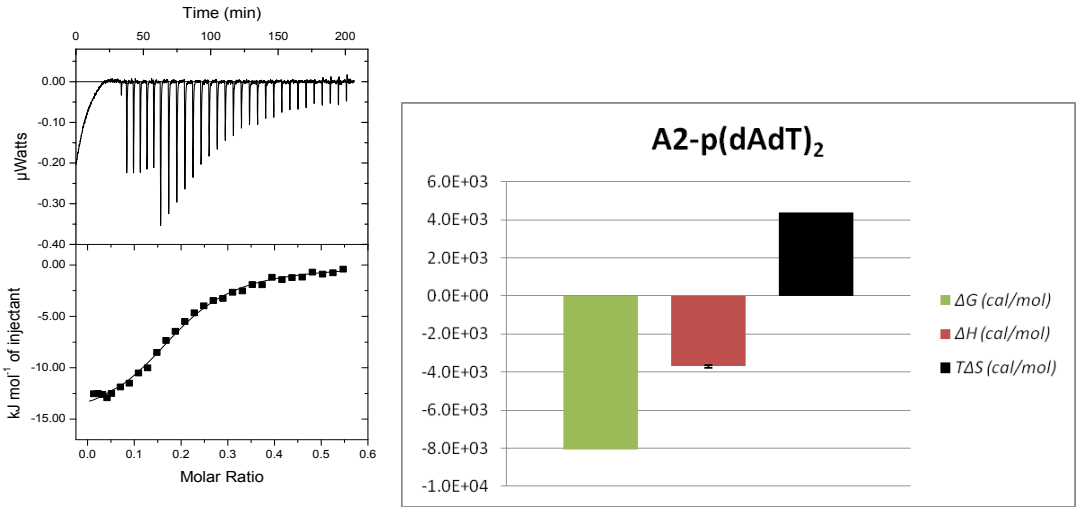

Figure S 51. left) ITC titration of $p(dAdT)_2$ (c=37 µM) with **A2** (c=100 µM); right) Thermodynamic parameters of the binding.

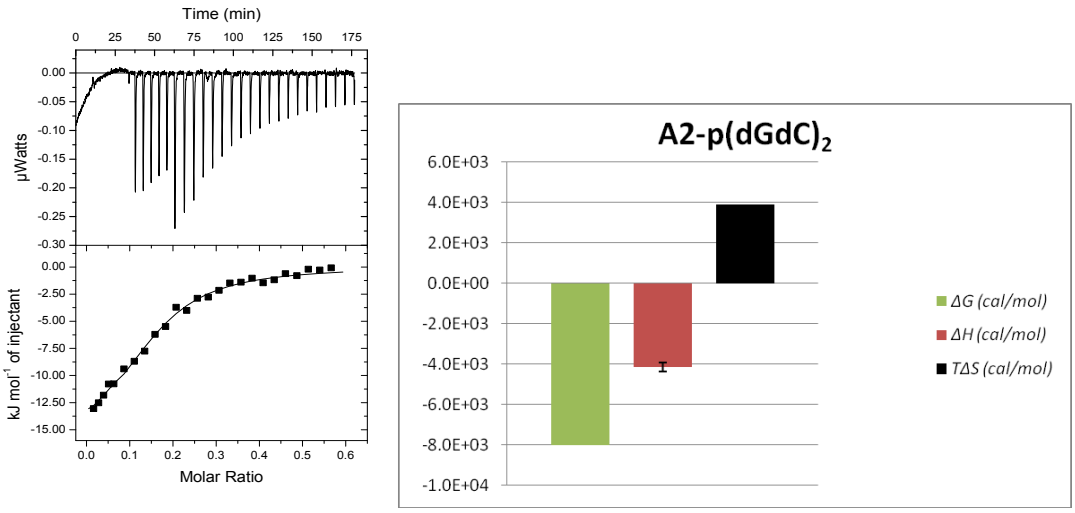

Figure S 52 left) ITC titration of $p(dGdC)_2$ (c=34.4 µM) with **A2** (c=100 µM); right) Thermodynamic parameters of the binding.

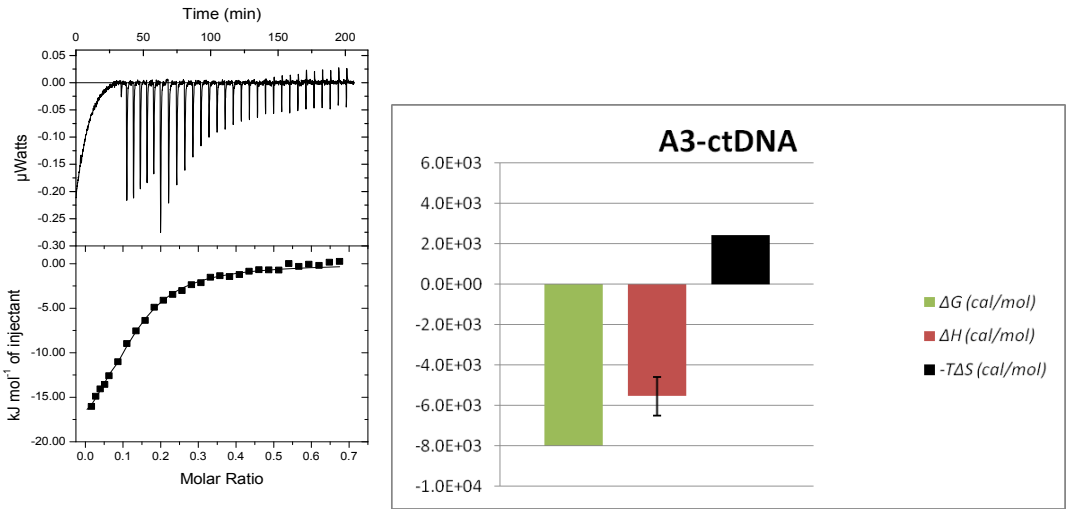

Figure S 53 . left) ITC titration of ctDNA (c=19.8 µM) with **A3** (c=100 µM); right) Thermodynamic parameters of the binding.

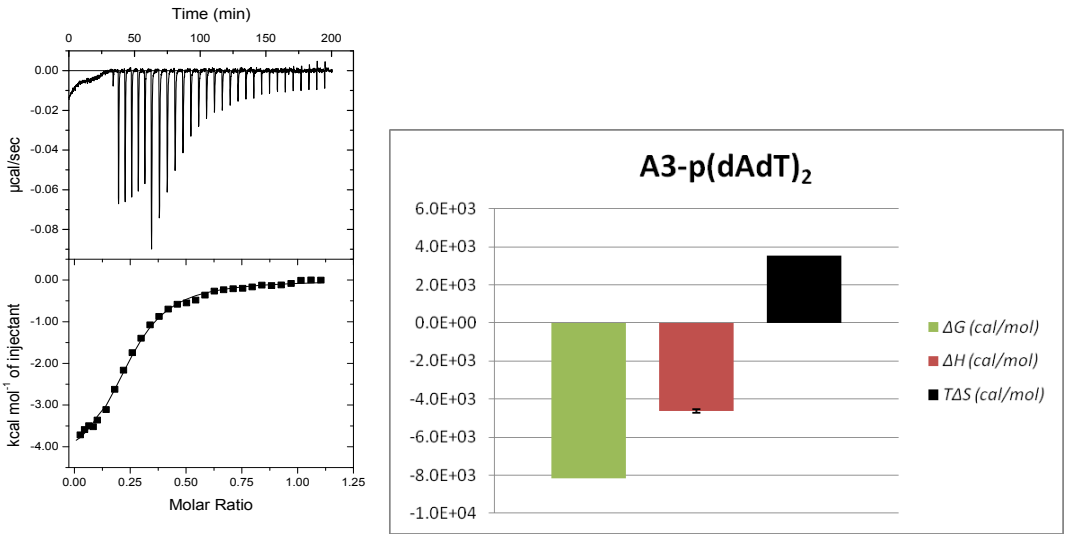

Figure S 54 . left) ITC titration of $p(dAdT)_2$ (c=22.1 µM) with **A3** (c=120 µM); right) Thermodynamic parameters of the binding.

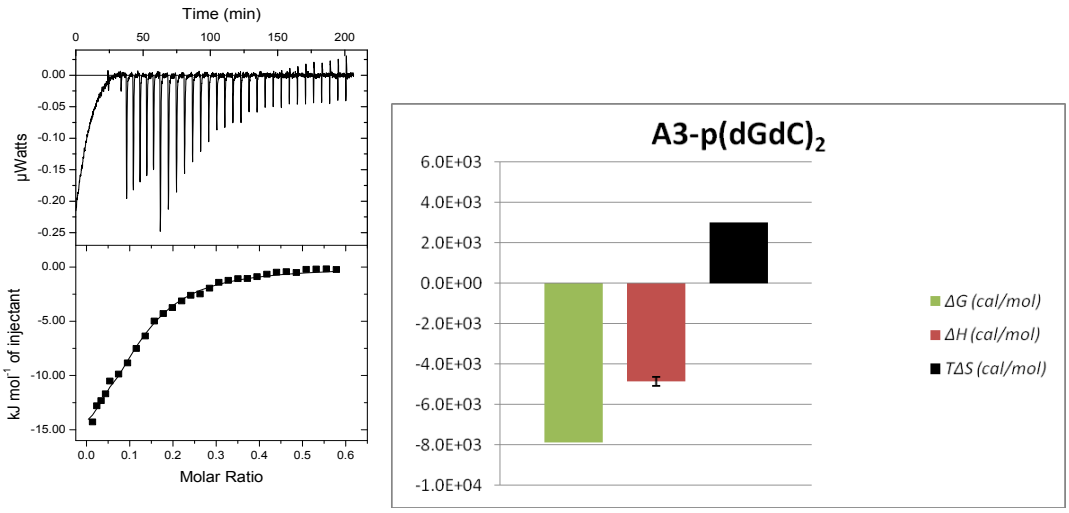

Figure S 55 left) ITC titration of $p(dGdC)_2$ (c=35 µM) with **A3** (c=100 µM); right) Thermodynamic parameters of the binding.

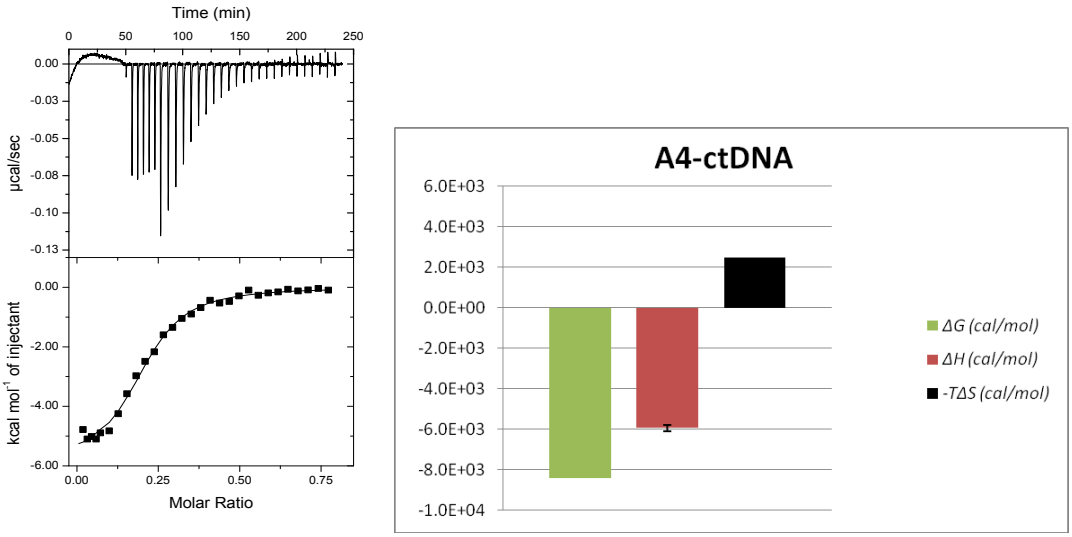

Figure S 56 left) ITC titration of ctDNA (c=26.2 µM) with **A4** (c=100 µM); right) Thermodynamic parameters of the binding.

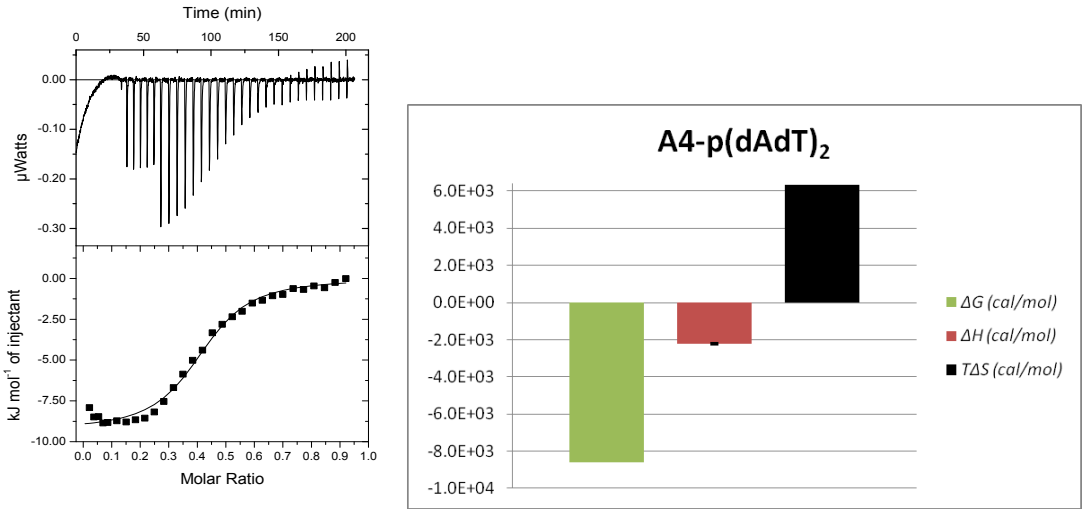

Figure S 57 left) ITC titration of $p(dAdT)_2$ (c=26.4 µM) with **A4** (c=120 µM); right) Thermodynamic parameters of the binding.

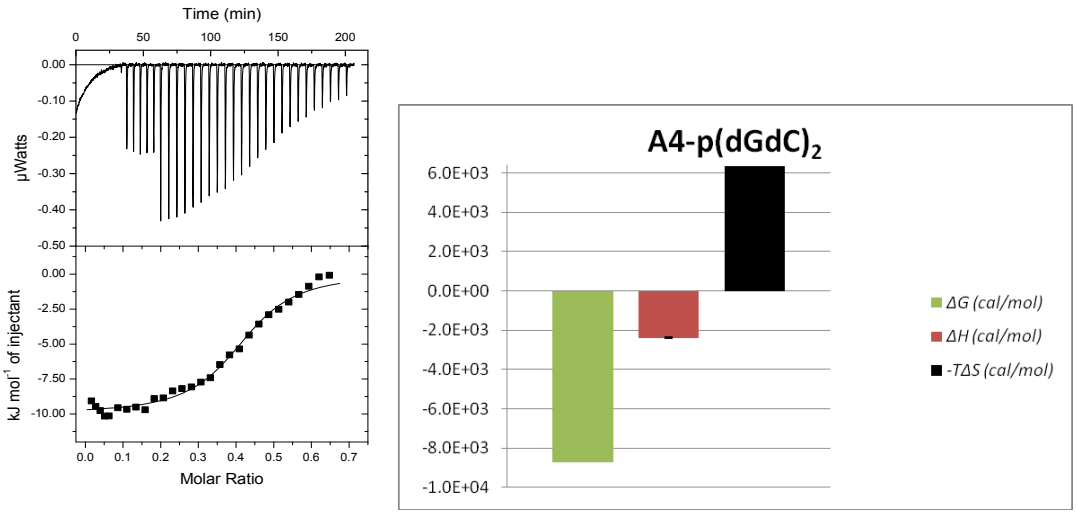

Figure S 58 left) ITC titration of $p(dGdC)_2$ (c=30 µM) with **A4** (c=100 µM); right) Thermodynamic parameters of the binding.

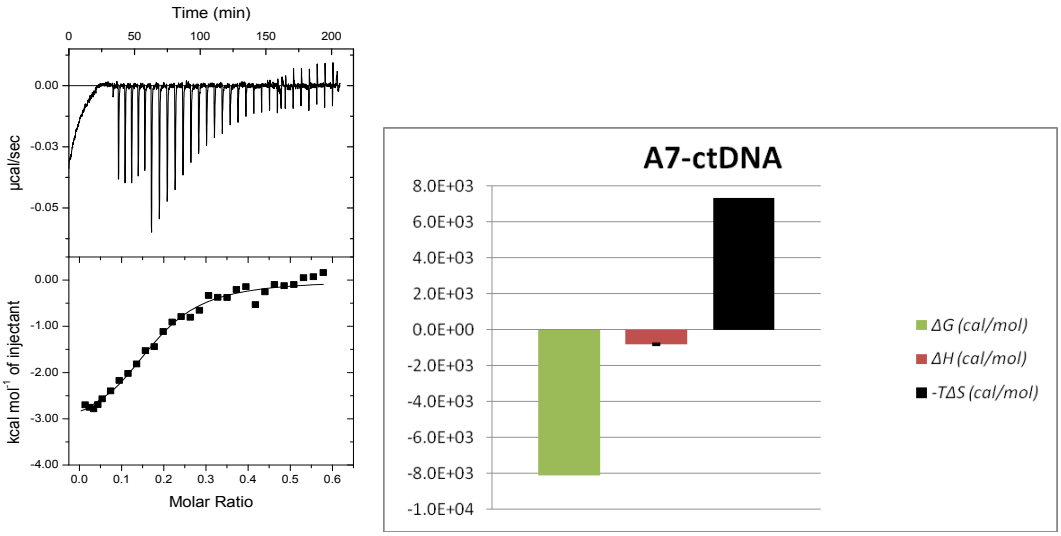

Figure S 59 left) ITC titration of ctDNA (c=35 µM) with **A7** (c=100 µM); right) Thermodynamic parameters of the binding.

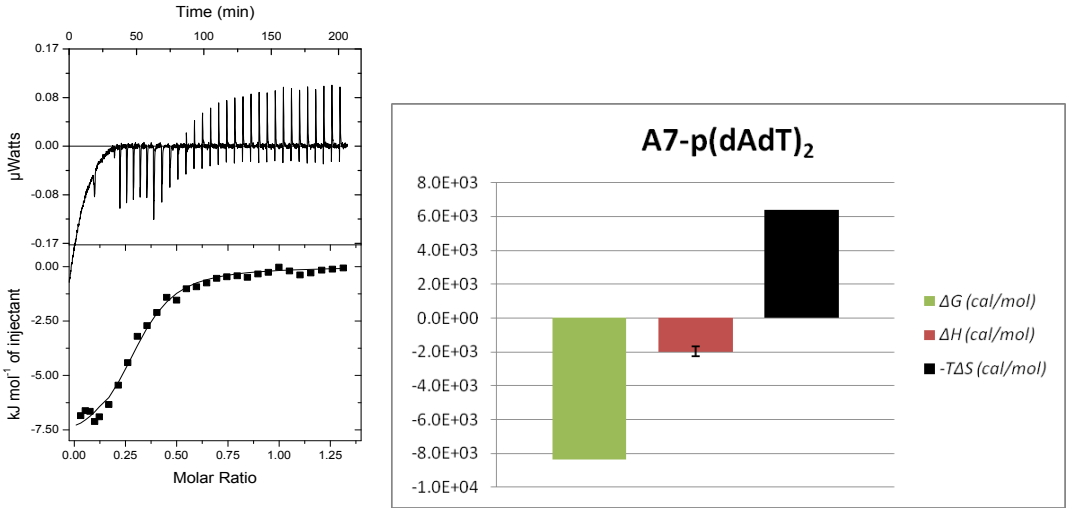

Figure S 60 left) ITC titration of $p(dAdT)_2$ (c=18.5 µM) with **A7** (c=120 µM); right) Thermodynamic parameters of the binding.

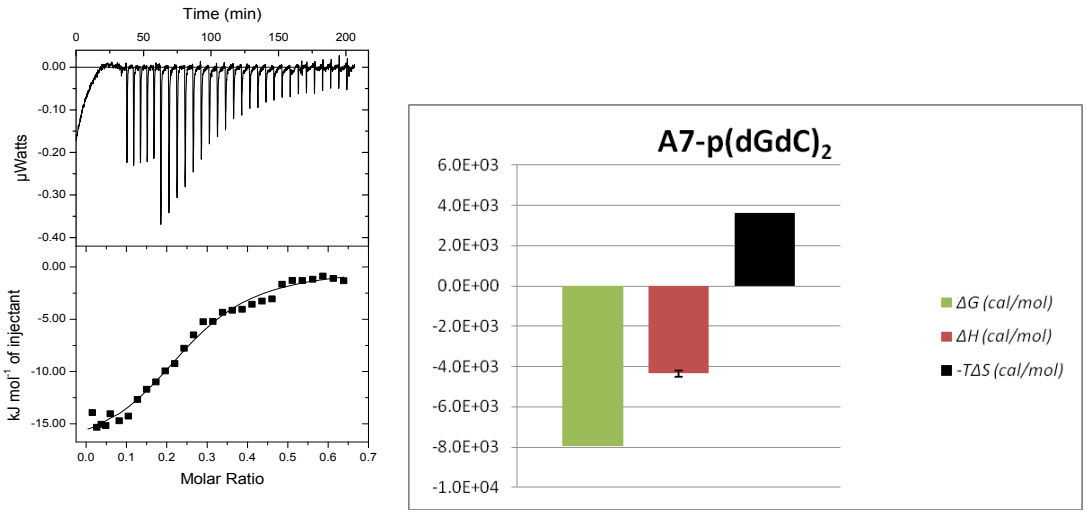

Figure S 61 left) ITC titration of $p(dGdC)_2$ (c=31.7 µM) with **A7** (c=100 µM); right) Thermodynamic parameters of the binding.

4. Biological assays:

4.1 Subculturing of cells

Adherent cell lines (MCF-7, H460, HEK293 and HeLa) growing as monolayers on the surface of T-25 flasks (Sigma) were used. Dulbecco's Modified Eagle's medium (DMEM) (Sigma-Aldrich) containing amino acids and vitamins, as well as additional supplementary components were used for cell growth. The primary cell culture media spent was removed and discarded from the culture flask. Cells were rinsed with 5 ml of the pre-warmed phosphate-buffered saline (PBS) to remove protease inhibitors, and 0.1% trypsin solution to detach the cells from the substrate. Flask was further placed back in an incubator at 37ºC. The progress of the enzyme treatment was checked with an inverted phase contrast microscope. As the cells have rounded up and detach from the surface, 5 ml of growth medium was added to the cell suspension and cells were vigorously washed. Suspended cells were further centrifuged (100xg for 5 minutes) and trypsin containing medium was replaced with the fresh one. Cells were further counted using Neubauer chamber under inverted phase contrast microscope. In line with the required dilutions, the correct amount of the cells in fresh medium was transferred to new flasks.

4.2 Anti-proliferative activity evaluation by MTT assay

This test was performed with MCF-7 and H460 cells. Tested compounds, (AK-A1, AK-A2, AK-A3, AK-A4 and AK-A7) were prepared as stock solutons (4×10^{-2}M moldm^{-3}) in dimethylsulfoxide (DMSO), and working solutions (10^{-4}-10^{-8} moldm^{-3}) were prepared in DMEM medium accordingly. Cells were seeded in a 96 micro well flat bottom plates at the concentration 1×10^4 cells/l and incubated overnight allowing them to attach to the plate surface. 72 h after incubation with tested compounds, growth medium was discarded and 5 mgml^{-1} of MTT was added. After 4h incubation at 37°C water insoluble MTT-formazan crystals were dissolved in DMSO. Absorbance was measured at 570 nm on a microplate reader (Multiskan EX, ThermoFisher Scientific). Control cells were grown under the same conditions. The experiments were performed in tetraplicates. The IC_{50} value, defined as compound concentration leading to cellular viability reduction by 50%, was calculated and used as a comparison parameter.

Table S 2 IC50 values for the tested compounds

Compound	MCF7	H460
AK2-A1	$>10^{-4}$	$>10^{-4}$
AK2-A2	$>10^{-4}$	$>10^{-4}$
AK2-A3	$>10^{-4}$	$>10^{-4}$
AK2-A4	$>10^{-4}$	$>10^{-4}$
AK2-A7	$>10^{-4}$	7.74×10^{-5}

4.3 Flow cytometry analysis of the AKA-dyes kinetics

The cells ($1x10^6$/ml) were incubated in 1 ml culture medium containing respective dyes for indicated amount of time in the dark at 37°C. Flow cytometry was carried out on a Becton Dickinson FACSCalibur model equipped with a 488 nm Argon laser and a 635 nm red diode laser. The collected data was analysed using BD CellQuest or FlowJo software version 7.2.5 for Microsoft (TreeStar, San Carlos, CA, USA). The cells were gated and discriminated from background based on light scattering properties and PI exclusion.

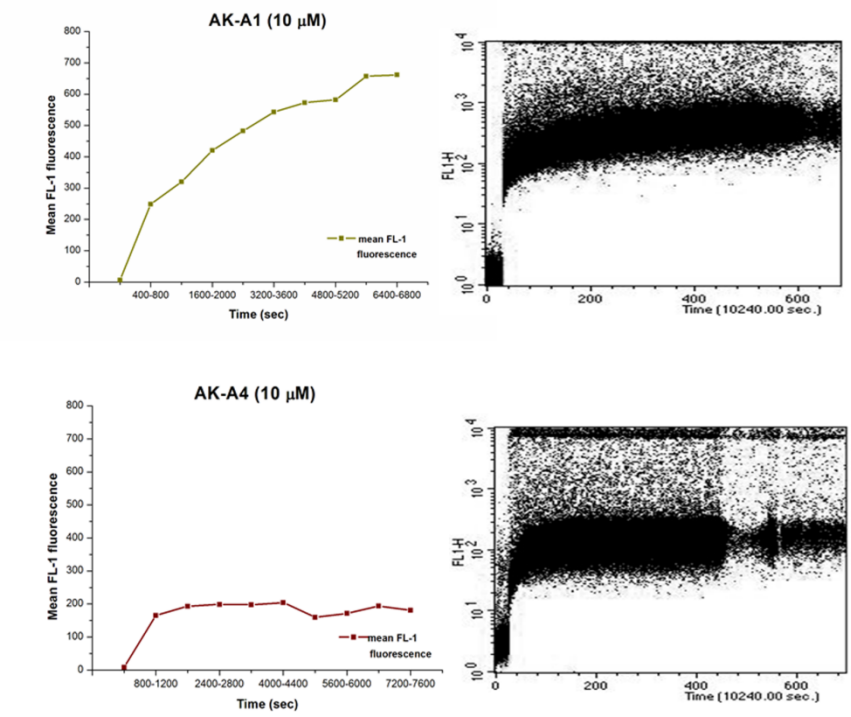

Figure S 62. Kinetics of the **AK2-A1** (A) and **AK2-A4** (B) dyes uptake in mammalian HeLa cells. HeLa cells ($0.5x10^6$/ml) were loaded with 10 µM AKA-dyes in PBS. The uptake kinetics was recorded continuously using FACSCalibur flow cytometer. First 3 min baseline was acquired followed by 120 min acquisition after treatment. At the indicated time points, cells were gated for FL-1 fluorescence intensity and AKA-dyes calibration curves were shown (RIGHT). Intensity of fluorescent signal depending on dye concentration (0-1000 nM) the optimal loading time of 30 min was applied.

4.4 Expression vector

pECFP-Mito vector is designed for fluorescent labeling of mitochondria in living cells and for co-localization experiments. Expression vector encodes monomeric enhanced cyan fluorescent protein (ECFP) fused to mitochondrial leader sequence (ECFP-Mito) derived from the subunit VIII of human cytochrome C oxidase. The resulting CFP has an absorption maximum at 458 nm and emits cyan fluorescence centered at 480 nm. Vector pECFP-Mito was purified from *E. coli* with Plasmid Midi Kit (Promega) according to manufacturer's

protocol and stored at -20ºC in water. pECFP-Mito vector was transiently transfected into the mammalian HeLa cells and the signal was received 24 hours after transfection. A pECFP-Mito vector containing CFP gene was provided by Dr. Oliver Vugrek (Rudjer Boskovic Institute, Zagreb, Croatia).

4.5 Transient transfection of HeLa cells with pECFP-Mito vector by lipofectamine 2000 method

For each transfection with Lipofectamine 2000, 8 x 10^4 cells/ml were distributed in glass bottom petri dish molds (35 mm dish with 20 mm bottom well, In Vitro Scientific, USA) and incubated for 16-24 h in 5% CO_2 at 37°C. Transfections were performed according to manufacturer′s instructions with 7,5 µl lipofectamine 2000 and 3 µg of pECFP-Mito vector. Reagent/DNA was incubated within the cells for minimum 24 h at 37°C, and the wells were then washed and replenished with fresh DMEM medium.

4.6 Confocal Laser Scanning Microscopy (CLSM)

Leica SP8X FLIM was used for complex fluorescence experiments in live-cell imaging. The images were processed in LAS X Leica Microsystems software packages.

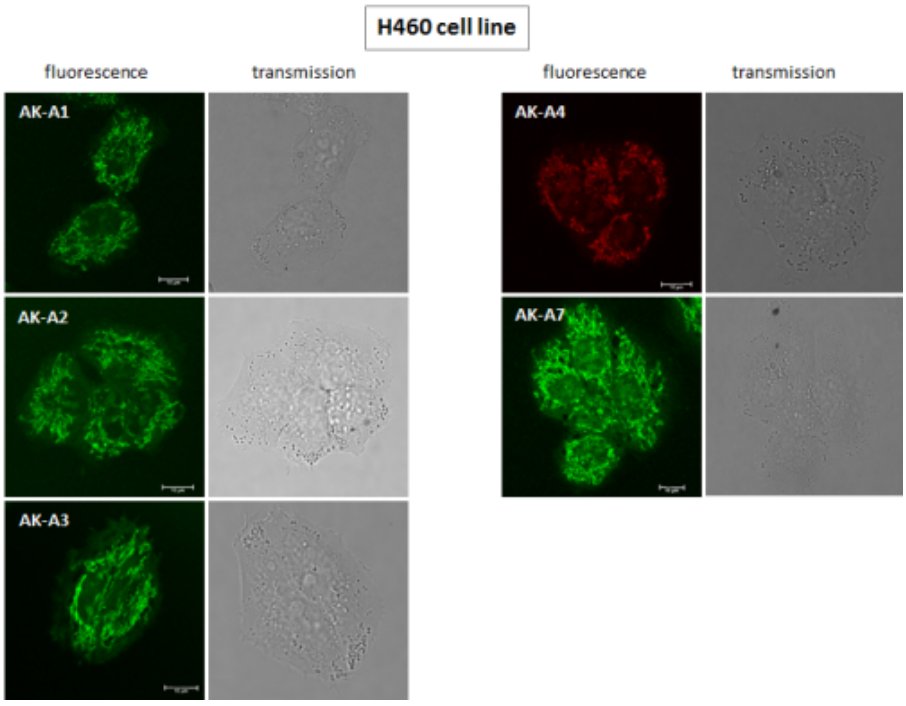

Figure S 63: Confocal photofluoromicrographs of H460 cells stained with **AK-A1, AK-A2, AK-A3, AK-A4 and AK-A7** dyes ($c = 2 \times 10^{-5}$ mol dm^{-3}) and incubated for 120 min. Fluorescence confocal and transmission images are represented. Scale bars, 10 µm.

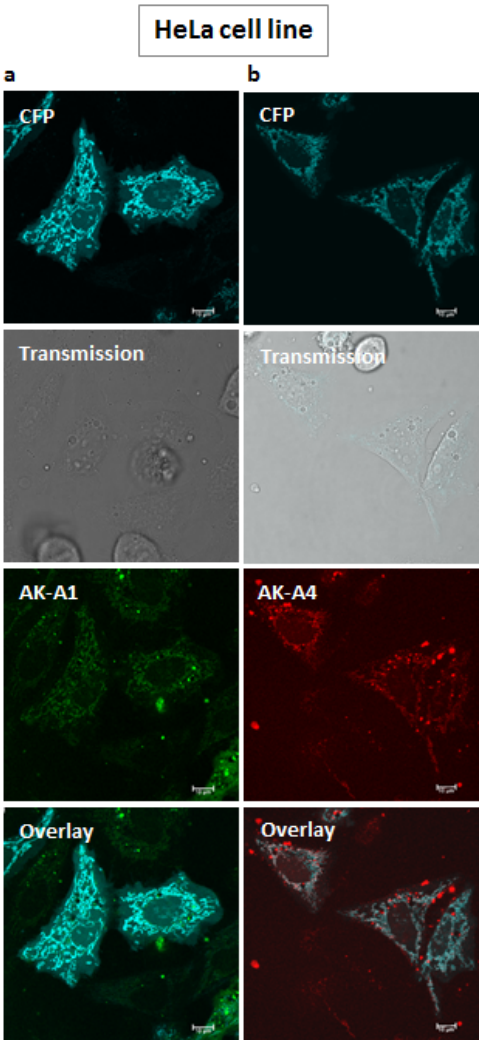

Figure S 64 Confocal photofluoromicrographs of HeLa cells expressing mitochondria-targeted CFP are shown. Transfected cells were incubated with cyanine dyes **AK-A1** (a) and **AK-A4** (b) ($c = 2 \times 10^{-5}$ mol dm^{-3}) for 120 min. Fluorescence confocal, transmission, and overlaid images are represented. Scale bars, 10 µm.

4.7 Colocalization study

Specialised software (ImageJ, Wayne Rasband NIH, US)for colocalization studies that gives the Pearson correlation coefficients (PCC) (JACoP plugin for ImageJ) based on pixel-by-pixel summation of the products of the intensities of two fluorophores, so in case of green pixels G_i and red pixels R_i :

$$r = \frac{\sum (Ri - Rav) * (Gi - Gav)}{\sqrt{\sum (Ri - Rav)^2 * \sum (Gi - Gav)^2}}$$

G_{av} i R_{av} are mean values over the whole dataset. To correct for noise we use the replicate based noise corrected correlation, as suggested by Adler & coworkers, in short, the two identical consecutive fluoromicrographs are taken and the correlation between two consecutive green and red pics is calculated. From those two, correction factor is calculated C_{GR}, using the equation bellow.

$$Corr.f; C_{GR} = \frac{1}{\sqrt{(c_{G1G2} * c_{R1R2})}}$$

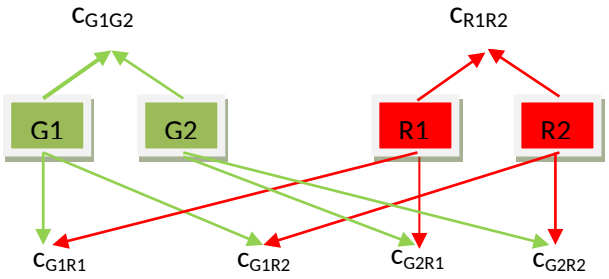

Then the correlation coefficients between the different fluorophores are measured (four combinations, c_{G1R1}, c_{G1R2}, c_{G2R1}, c_{G2R2}), and their mean value is corrected by the correction factor, so the final, corrected correlation coefficient equals

$$PCC = C_{GR} * (c_{G1R1} + c_{G1R2} + c_{G2R1} + c_{G2R2})/4$$